

PONTIFICIA UNIVERSIDAD CATÓLICA DEL PERÚ



**SYNTHESIS, CHARACTERIZATION AND CORROSION  
RESISTANCE OF ELECTROLESS Ni-P AND Ni-P-SiC  
COATINGS: A COMPARATIVE STUDY**

A thesis submitted to the Graduate School of the Pontificia Universidad Católica del Perú in partial fulfillment of the requirements for the degree of Master of Materials Science and Engineering

by

**MAGALI KARINA CAMARGO LEÓN**

Advisor: Dr. Santiago Flores Merino

Co-advisor: Lic. Isabel Díaz Tang

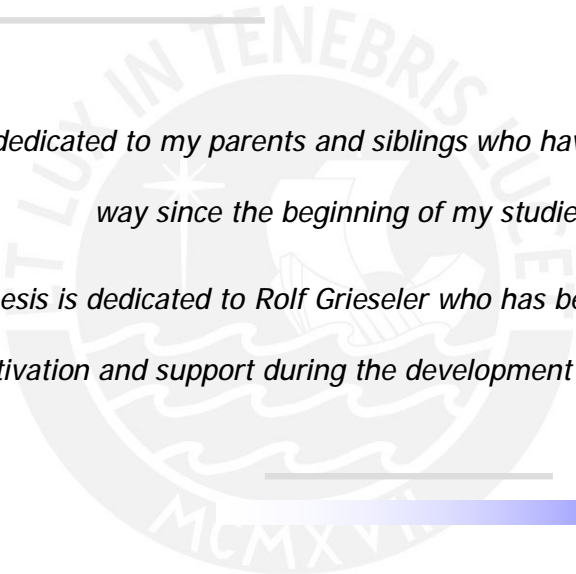
LIMA-PERÚ

2010



*This thesis is dedicated to my parents and siblings who have supported me all the way since the beginning of my studies.*

*Also, this thesis is dedicated to Rolf Grieseler who has been a great source of motivation and support during the development of this work.*



## Abstract

Electroless Ni-P coatings have been widely used due to their good combination of properties such as hardness, wear resistance and corrosion resistance. The addition of dispersed hard micro-particles into the Ni-P matrix has led to the development of composite coatings. Ni-P composite coatings exhibit an improved hardness and wear resistance properties; however, there is still a disagreement among researches on the corrosion behavior of composite Ni-P coatings. The present investigation involves the synthesis, characterization and a comparative study of the corrosion resistance in NaCl 3,5% of electroless Ni-P and Ni-P-SiC deposits obtained by either prepared or commercial electrolytic nickel/hypophosphite based baths.

The characterization of deposits involved studies about morphology by SEM, chemical composition by energy-dispersive X-ray spectroscopy (EDX) and glow discharge optical emission spectroscopy (GDOS), microstructure by X-ray diffraction (XRD) and hardness. All deposits showed an amorphous micro-structure and high phosphorus content (10-14 wt%). Ni-P-SiC deposits showed an increased hardness (802 HV-815 HV) in comparison with Ni-P deposits (469 HV-626 HV).

The techniques used to study the corrosion resistance in NaCl 3,5% were linear polarization resistance (LPR), Tafel plots and electrochemical impedance spectroscopy (EIS). These techniques agreed to show the better corrosion resistance of Ni-P-SiC coatings over the Ni-P coatings. This fact can be ascribed to the decrease in the effective metallic area available for corrosion. Ni-P-SiC deposits exhibited higher polarization resistance ( $R_p$ ) values (103-66  $k\Omega \cdot cm^2$ ) in comparison with Ni-P deposits (46-55  $k\Omega \cdot cm^2$ ). Also, the corrosion current density values of Ni-P-SiC deposits (0,17-0,65  $\mu A/cm^2$ ) were lower than Ni-P deposits (0,71-1,08  $\mu A/cm^2$ ). Concerning to the mechanism by which the Ni-P and Ni-P-SiC become corroded, EIS experiments demonstrated that the corrosion process involved a charge transfer mechanism in all the cases. Tafel plots also corroborated this mechanism since of all deposits showed a Tafel behavior.

## Resumen

Los recubrimientos de aleaciones de Ni-P obtenidos por proceso de reducción autocatalítica (*electroless-plating*) han sido ampliamente utilizados debido sus propiedades de dureza, resistencia al desgaste y resistencia a la corrosión. La adición de micro-partículas duras dispersas en la matriz de Ni-P ha conducido al desarrollo de recubrimientos compuestos de Ni-P. Dichos recubrimientos presentan una mayor dureza y resistencia al desgaste; sin embargo, todavía existen diversas opiniones en cuanto al comportamiento frente a la corrosión de los recubrimientos compuestos de Ni-P. La presente investigación consiste en la síntesis, caracterización y estudio comparativo de la resistencia a la corrosión en NaCl 3,5% de recubrimientos de Ni-P y Ni-P-SiC obtenidos a partir de baños (preparados en laboratorio y comerciales) que contienen sulfato de níquel e hipofosfito de sodio como base de su composición.

La caracterización de los recubrimientos involucró estudios de morfología por microscopía electrónica de barrido (SEM), composición química mediante espectroscopía de dispersión de energía con rayos X (EDX) y espectroscopía de emisión óptica por descarga luminiscente (GDOS); microestructura por difracción de rayos X (XRD) y ensayos de dureza. Todos los recubrimientos mostraron micro-estructura amorfa y alto contenido de fósforo (10-14% en peso). Los recubrimientos de Ni-P-SiC fueron más duros (802 HV-815 HV) en comparación a los recubrimientos de Ni-P (469HV-626HV).

Las técnicas utilizadas para estudiar la resistencia a la corrosión en NaCl 3,5% fueron: resistencia de polarización lineal (LPR), curvas de Tafel y espectroscopía de impedancia electroquímica (EIS). Estas técnicas concordaron en demostrar la mejor resistencia a la corrosión de los depósitos de Ni-P-SiC en relación a los depósitos de Ni-P. Este hecho se atribuye a la disminución del área metálica efectiva expuesta.

Los valores de resistencia a la polarización ( $R_p$ ) fueron mayores para los recubrimientos de Ni-P-SiC (103-66  $k\Omega \cdot cm^2$ ) en relación a los depósitos de Ni-P (46-55  $k\Omega \cdot cm^2$ ). Además, los valores de densidad de corriente de corrosión de los depósitos de Ni-P-SiC (0,17-0,65  $\mu A/cm^2$ ) fueron inferiores a los depósitos de Ni-P (0,71-1,08  $\mu A/cm^2$ ). En cuanto al mecanismo de corrosión, los estudios de EIS demostraron que el proceso de corrosión involucra un mecanismo de transferencia de carga en todos los casos. Las curvas de polarización también corroboraron dicho mecanismo ya que de todos los depósitos mostraron un comportamiento de Tafel.

## Acknowledgements

I would like to express my sincere gratitude to my research advisors Lic. Isabel Díaz Tang and Dr. Santiago Flores Merino from the *Pontificia Universidad Católica del Perú* for their support, advice and guidance.

I would like to acknowledge the research advice, support and guidance of Dr. rer. nat. Udo Schmidt and Prof. Dr.-Ing. Christine Jakob during my academic exchange semester in the *Institut für Werkstofftechnik* from the *Technische Universität Ilmenau* in Germany.

My gratitude to Prof. Francisco de Zela and Dr. Bernd Halbedel for their support in order to make my academic exchange semester in the Technische Universität Ilmenau in Germany through the ISAP-DAAD exchange program possible.

Also, I would like to express my gratitude to all of the members of the *Elektrochemie und Galvanotechnik* group from the *Technische Universität Ilmenau* for their support during the development of the first experimental part of this work.

I also express my gratitude to my colleagues and friends from the Institute of Corrosion and Protection of the *Pontificia Universidad Católica del Perú* for their support during the development of the experimental second part of this work.

Finally I would like to express my gratitude to my family and friends for supporting and encouraging me during the development of this work.

## Table of Contents

Abstract .....	3
Resumen .....	4
Acknowledgements .....	5
Table of Contents .....	6
List of Figures .....	10
List of Tables.....	13
List of Abbreviations .....	15
<b>1. INTRODUCTION.....</b>	<b>18</b>
1.1 Background .....	18
1.2 Research Purpose.....	21
<b>2. LITERATURE REVIEW</b>	
2.1 The Nickel-Phosphorus alloy system.....	22
2.2 Electroless deposition process .....	25
2.2.1 Mechanism of electroless Ni-P deposition process .....	27
2.2.1.1 The atomic hydrogen mechanism .....	27
2.2.1.2 The hydride transfer mechanism.....	28
2.2.1.3 The electrochemical mechanism .....	29
2.2.2 Electroless Ni-P plating bath.....	29
2.2.3 Factors affecting the electroless plating process.....	30
2.2.3.1 Influence of temperature .....	31
2.2.3.2 Influence of pH.....	31
2.2.3.3 Influence of Nickel and Hypophosphite ion concentration .	32
2.3 Electroless Ni-P composite deposition process.....	33
2.4 Structure of electroless Ni-P coatings .....	37
2.5 Properties of electroless Ni-P coatings .....	38
2.5.1 Hardness .....	39
2.5.2 Corrosion resistance .....	41
2.6 Electrochemical techniques for corrosion resistance evaluation .....	44
2.6.1 DC electrochemical test methods .....	44

2.6.1.1 Linear Polarization Resistance (LPR).....	44
2.6.1.2 Tafel Plots .....	45
2.6.2 AC electrochemical test method: Electrochemical Impedance Spectroscopy (EIS) .....	47
<b>3. EXPERIMENTAL PART.....</b>	<b>51</b>
3.1 Synthesis of electroless Ni-P and Ni-P-SiC coatings .....	51
3.1.1 Electroless Ni-P bath preparation .....	51
3.1.1.1 Laboratory materials, equipment and reagents.....	52
3.1.1.2 Procedure .....	53
3.1.1.2.1 Electroless simple bath (S1).....	53
3.1.1.2.2 Electroless composite bath (C1).....	53
3.1.1.2.3 Electroless comercial simple bath (S2) .....	53
3.1.1.2.4 Electroless comercial composite bath (C2) .....	53
3.1.2 Chemical Analysis of electroless of Ni-P Baths .....	54
3.1.2.1 Nickel Determination .....	54
3.1.2.1.1 Laboratory materials and reagents.....	54
3.1.2.1.2 Analysis .....	55
3.1.2.1.3 Calculation .....	56
3.1.2.2 Hypophosphite Determination .....	56
3.1.2.2.1 Laboratory materials, equipment and reagents.....	56
3.1.2.2.2 Analysis .....	57
3.1.2.2.3 Calculation .....	58
3.1.2.3 pH Determination .....	58
3.1.2.3.1 Laboratory materials, equipment and reagents.....	59
3.1.2.3.2 Analysis .....	59
3.1.3 Electroless deposition process of Ni-P and composite Ni-P-SiC coatings.....	60
3.1.3.1 Substrate pre-treatment.....	60
3.1.3.1.1 Laboratory materials, equipment and reagents.....	61
3.1.3.1.2 Procedure .....	62





<b>4. RESULTS AND DISCUSSION</b> .....	<b>76</b>
4.1 Synthesis of electroless Ni-P and Ni-P-SiC coatings.....	76
4.2 Chemical analysis of electroless Ni-P baths .....	78
4.3 Characterization of electroless Ni-P and Ni-P-SiC coatings .....	82
4.3.1 Surface Morphology .....	82
4.3.2 Chemical composition of Ni-P and Ni-P-SiC deposits .....	85
4.3.2.1 Energy dispersive X-ray spectroscopy (EDX) .....	85
4.3.2.2 Glow discharge optical emission spectroscopy (GDOS).....	87
4.3.3 Microstructure .....	90
4.3.4 Thickness .....	91
4.3.5 Hardness .....	93
4.4 Electrochemical tests in NaCl 3,5 % .....	94
4.4.1 Test of equipment .....	94
4.4.2 Open circuit potential (OCP) measurement .....	94
4.4.3 Potentiodynamic anodic polarization.....	96
4.4.4 Cathodic and anodic polarization (Tafel plots) .....	99
4.4.5 Linear polarization resistance (LPR).....	101
4.4.6 Electrochemical impedance spectroscopy (EIS) .....	103
4.4.7 Comparison of results among the different electrochemical techniques .....	106
<b>5. CONCLUSIONS AND RECOMMENDATIONS</b> .....	<b>109</b>
5.1 Conclusions .....	109
5.2 Recommendations.....	111
<b>References</b> .....	<b>112</b>

## Appendices

## List of Figures

Figure 1. Ni-P equilibrium phase diagram.....	23
Figure 2. Non- equilibrium electroless Ni- Ni <sub>3</sub> P phase diagram .....	24
Figure 3. Electroless Ni-P deposition process.....	27
Figure 4. Effect of temperature on plating rate.....	31
Figure 5. Effect of pH on the rate of deposition .....	32
Figure 6. Effect of the pH on phosphorus content.....	32
Figure 7. Effect of nickel concentration on Ni-P alloy composition .....	33
Figure 8. Effect of the hypophosphite concentration on Ni-P alloy composition .....	33
Figure 9. Ideal structure of a composite Ni-P coating.....	35
Figure 10. Effect of the SiC concentration in the incorporation rate of a Ni-P-SiC composite coating .....	37
Figure 11. Comparison of change in hardness with heat treatment temperature for electroless Ni-P-SiC, Ni-P and Ni-P-PTFE .....	41
Figure 12. Typical lineal polarization resistance curve .....	45
Figure 13. Tafel plot .....	46
Figure 14. Model for a simple charge transfer .....	50
Figure 15. Model for a simple charge transfer process in presence of diffusion .....	50
Figure 16. Nickel determination by volumetric titration method .....	55
Figure 17. Hypophosphite determination by titration with Cerium (IV) .....	58
Figure 18. Electroless Ni-P/Ni-P-SiC deposition process.....	60
Figure 19. Low carbon steel panel for electroless deposition of Ni-P coatings .....	61
Figure 20. Electrolytic degreasing of the substrate .....	62
Figure 21. Experimental setup for electroless deposition of Ni-P coatings	64

<b>Figure 22.</b> Top view schema of the bath setting.....	65
<b>Figure 23.</b> Two-bladed glass stirring element .....	66
<b>Figure 24.</b> Experimental setup for electroless deposition of Ni-P-SiC composite coatings.....	66
<b>Figure 25.</b> Area of the sample after GDOS analysis.....	68
<b>Figure 26.</b> The experimental setup for thickness measurements by induction magnetic method .....	69
<b>Figure 27.</b> Vickers hardness measurement.....	70
<b>Figure 28.</b> Electrochemical cell setup.....	71
<b>Figure 29.</b> Dummy cell circuit .....	72
<b>Figure 30.</b> Experimental electrochemical cell connected to the potentiostat/galvanostat equipment .....	73
<b>Figure 31.</b> Ni-P and Ni-P-SiC deposits plated on low carbon steel panels obtained according the type of plating bath used .....	77
<b>Figure 32.</b> Back side of a substrate after Ni-P-SiC electroless deposition.....	77
<b>Figure 33.</b> Nickel concentration before and after electroless plating process .....	80
<b>Figure 34.</b> Hypophospite concentration before and after electroless plating process.....	80
<b>Figure 35.</b> pH before and after electroless plating process .....	81
<b>Figure 36.</b> SEM micrographs in top view of Ni-P and Ni-P-SiC coatings obtained according the type of plating bath used .....	82
<b>Figure 37.</b> Detailed SEM micrographs in top view of Ni-P and Ni-P-SiC coatings obtained according the type of plating bath .....	83
<b>Figure 38.</b> SEM micrographs in cross sectional view of Ni-P and Ni-P-SiC coatings obtained according the type of plating bath.....	84
<b>Figure 39.</b> SEM micrograph of composite deposit C1 showing the line scan on the specimen surface.....	85
<b>Figure 40.</b> Chemical composition of deposit S1 obtained by EDX line scan .....	86
<b>Figure 41.</b> Chemical composition of deposit S2 obtained by EDX line scan.....	86

<b>Figure 42.</b> Chemical composition of deposit C1 obtained by EDX line scan.....	86
<b>Figure 43.</b> Chemical composition of deposit C2 obtained by EDX line scan.....	86
<b>Figure 44.</b> Depth-profile analysis of deposit S1.....	88
<b>Figure 45.</b> Depth-profile analysis of deposit S2.....	88
<b>Figure 46.</b> Depth-profile analysis of deposit C1.....	89
<b>Figure 47.</b> Depth-profile analysis of deposit C2 .....	89
<b>Figure 48.</b> Comparison between EDX and GDOS in chemical analysis of deposits S1, S2, C1 and C2 .....	90
<b>Figure 49.</b> XRD patterns of Ni-P and Ni-P-SiC coatings: C1, C2, S2 and S1.....	91
<b>Figure 50.</b> Nyquist plot of dummy cell circuit.....	94
<b>Figure 51.</b> OCP versus time of deposits S1, S2, C1 and C2 in NaCl 3,5% .....	95
<b>Figure 52.</b> Potentiodynamic anodic polarization plots of deposits S1, S2, C1 and C2 in NaCl 3,5% .....	96
<b>Figure 53.</b> Potentiodynamic anodic polarization plots in lineal scale of deposits S1, S2, C1 and C2 in NaCl 3,5% .....	98
<b>Figure 54.</b> Deposit S2 after a potentyodinamic anodic polarization test.....	98
<b>Figure 55.</b> Tafel plots of deposits S1, S2, C1 and C2 in NaCl 3,5%.....	100
<b>Figure 56.</b> Linear polarization resistance plots of deposits S1, S2, C1 and C2 in NaCl 3,5% .....	102
<b>Figure 57.</b> Impedance spectra (Nyquist plots) of deposits S1, S2, C1 and C2 in NaCl 3,5% .....	103
<b>Figure 58.</b> Comparison of polarization resistance values obtained from LPR and EIS.....	106
<b>Figure 59.</b> Comparison of corrosion current density values obtained from LPR and EIS.....	108

## List of Tables

Table 1. Some properties of elemental nickel and phosphorus .....	22
Table 2. Hubbell ´s electrolyte composition .....	36
Table 3. Some properties of electroless Ni-P alloy coatings depending of the phosphor content .....	39
Table 4. Corrosion resistance of some electroless Ni-P composite coatings.....	43
Table 5. Equivalent circuit parameters .....	48
Table 6. Compositions of the acidic electroless simple and composite baths prepared at laboratory .....	51
Table 7. Chemical composition of substrate.....	61
Table 8. Measurement conditions for potentiodynamic polarization tests.....	74
Table 9. Measurement conditions for cathodic and anodic polarization tests....	74
Table 10. Measurement conditions for cathodic and anodic polarization tests..	75
Table 11. Measurement conditions for electrochemical impedance tests .....	75
Table 12. Codes of Ni-P and Ni-P-SiC deposits obtained .....	76
Table 13. Chemical analysis of S1 bath .....	78
Table 14. Chemical analysis of S2 bat.....	79
Table 15. Chemical analysis of C1 bath.....	79
Table 16. Chemical analysis of C2 bath.....	79
Table 17. Chemical composition of deposits obtained from EDX.....	87
Table 18. Chemical composition of deposits obtained from GDOS .....	89
Table 19. Thickness measurement by magnetic induction method .....	92
Table 20. Comparison between magnetic induction and SEM methods for thickness determination .....	92
Table 21. Vickers hardness values.....	93

Table 22. Results of test of dummy cell .....	94
Table 23. Evaluation of the change of OCP values after 1 hour of immersion ..	95
Table 24. Parameters resulting from Tafel plots.....	101
Table 25. Electrochemical parameters obtained from LPR.....	102
Table 26. Electrochemical parameters obtained from EIS .....	105



## List of Abbreviations

A	ampere
$\alpha$	phenomenological coefficient caused by depression of the Nyquist plot below real axis
AC	alternate current
ACS	the chemical meets the specifications of the American Chemical Society
AE	auxiliary electrode
approx.	approximately
ASTM	American Society for Testing and Materials
at%	atomic percent
B	Stern-Geary constant
$\beta_a$	slope of the anodic Tafel curve
$\beta_c$	slope of the cathodic Tafel curve
$^{\circ}\text{C}$	Celsius degree
C	capacitor
c	concentration
$\text{cm}^3$	cubic centimeter
CPE	constant phase element
DC	direct current
DIN	Deutsches Institut für Normung
e.g.	for example
$E^{\circ}$	standard electrode potential
EDX	energy-dispersive X-ray spectroscopy
EIS	electrochemical impedance spectroscopy
EN	electroless Nickel
F	force
FRA	frequency response analyzer
g	gram
GDOS	glow discharge optical emission spectroscopy
GPa	gigapascal
h	hour
HV	Vickers hardness

$I_{\text{corr}}$	corrosion current
ISO	International Organization for Standardization
j	$\sqrt{-1}$
kg	kilogram
L	inductor
l	liter
LPR	linear polarization resistance
M	molar concentration (mol/L)
mm <sup>2</sup>	square millimeter
max.	maximal
N	Newton
$\eta$	overvoltage
$\Omega$	ohm
OCP	open circuit potential (or $E_{\text{corr}}$ )
$\theta$	phase angle
p.a.	"pro analysi", specification for chemicals with a guarantee certificate and/or suitable for the stated analytical application
$R_{\text{ct}}$	charge transfer resistance
RE	reference electrode
$R_{\text{p}}$	polarization resistance
$R_{\text{s}}$	solution resistance
%RSD	relative standard deviation
s	second
SCE	saturated calomel electrode
SD	standard deviation
SEM	scanning electron microscope



V	volt/voltage
W	Warburg impedance
$\omega$	frequency
WE	Working electrode
wt%	weight percent
XPS	X-ray photoelectron spectroscopy
XRD	X-ray diffraction
Z	complex impedance
Z'	real component of impedance
Z''	imaginary component of impedance



# 1. INTRODUCTION

## 1.1 Background

Nowadays industrial sectors such as automotive, aerospace, electronics and textile require increasingly the use of materials with suitable properties – chemical, mechanical, and corrosion resistance - for specific applications. One possibility to improve materials performance is to protect them by coatings.

One of the methods to obtain protective coatings is the chemical deposition of Ni-P alloys on different substrates (e.g. metallic) through an autocatalytic reduction process. This method is commonly known as *electroless plating* and involves the reduction of a metallic ion (e.g.  $\text{Ni}^{2+}$ ) from an aqueous solution (electrolytic bath) containing a reducing agent. Thereby, the term *electroless plating*, originally adopted in 1946 by Brenner and Ridell, describes the process of depositing metals and alloys by means of chemical reactions without external electric current application [1].

The Ni-P alloys obtained by *electroless plating* have contributed to a significant advance in the development of protective coatings, because it gives to the base material (substrate) an improvement of properties such as corrosion and abrasion resistance, hardness and surface uniformity. Other special physical properties, e.g. magnetism, solderability and polishability, have been also reported [2].

The structure and properties of electroless Ni-P coatings depend mainly on the phosphorus content, the plating conditions and the subsequent heat treatment among other factors. In previous works [3, 4] the influence of the deposition parameters (bath composition, pH, temperature and time) on the chemical composition, structure and deposition rate have been discussed. Studies showed that the phosphorus content is one of the key factors determining the microstructure of as-deposited Ni-P coatings [2].

In general, electroless Ni-P coatings with different phosphorus contents are classified into three types: low, medium and high phosphorus. The low phosphorus (2 to 4 wt% P) coatings are microcrystalline and possess high as-plated hardness. These coatings are used in applications requiring abrasion and wear resistance. The medium phosphorus coatings (5 to 9 wt% P) are mainly used to meet general purpose requirements for wear and corrosion resistance. The high phosphorus (more than 10 wt% P) coatings are considered amorphous and they have superior resistance against corrosion (e.g. salt-spray and acid resistance in a wide range of applications) [3].

Heat treatment up to about 400°C provides extra hardness to the coating; however, this could reduce the corrosion resistance due to microcracking [1]. The formation of microcracks results from inevitable mismatches in the physical properties of phases present before and after thermal treatment [4]. On the other hand, heat treatment up to 650°C could improve corrosion resistance, since it provides an improved bonding if the substrate is, for example, steel [5].

Although electroless Ni-P coatings give satisfactory performance for several applications, enhancing their performance to meet demanding needs and engineering tasks requires further development. Composite materials can be a good alternative. In order to produce coatings with improved hardness, wear or lubrication; composite coatings have been achieved by incorporating hard/soft particles (e.g. Ni-P-Al<sub>2</sub>O<sub>3</sub>, Ni-P-SiC, Ni-P-B, Ni-P-PTFE, Ni-P-C, Ni-P-Si<sub>3</sub>N<sub>4</sub>, Ni-P-TiO<sub>2</sub>) into the Ni-P matrix [6,7].

Concerning the corrosion properties of Ni-P composite coatings, it is difficult to predict accurately their corrosion resistance because different parameters have influence on the properties of these coatings. In fact, there is still a disagreement among researchers about the corrosion resistance of Ni-P composite coatings because the influence of the dispersed particles in the corrosion properties is still not clear. For example, it has been reported that the corrosion resistance of electroless Ni-P composite coatings is lower than electroless Ni-P alloy coatings due to co-deposited particles present in the electroless nickel matrix could reduce passivity and corrosion resistance [8]. However improved corrosion resistance of Ni-P composites in

comparison with Ni-P alloy coatings has been also reported [9-11]. Thus, the corrosion resistance of these coatings requires further investigation.

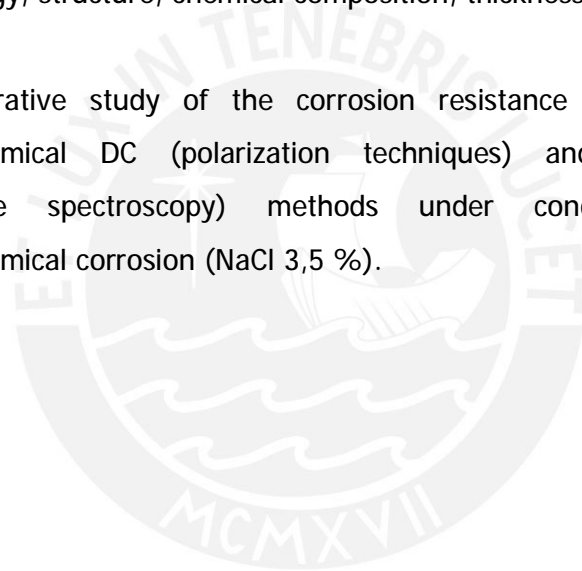
There are different techniques for studying the corrosion resistance of Ni-P coatings; for example: weight loss method, the neutral salt spray test, copper accelerated acetic acid salt spray (CASS) test, as well as electrochemical methods. Among electrochemical methods for corrosion resistance evaluation, the direct current (e.g. linear polarization resistance (LPR) technique and Tafel slopes technique) and alternate current methods (e.g. electrochemical impedance spectroscopy (EIS) and electrochemical noise) can be mentioned. Electrochemical impedance spectroscopy (EIS) is considered to be superior as it provides not only an assessment of the corrosion resistance of different deposits but also enables to determine the mechanistic pathway by which the deposits become corroded.

This research aims to synthesize, to characterize and to evaluate the corrosion resistance in NaCl 3,5% of as-plated Ni-P and Ni-P-SiC coatings with high phosphorus content. The corrosion resistance study involves not only DC electrochemical methods but also an AC electrochemical method (EIS). Then, by using different techniques for evaluation of corrosion resistance, a better understanding about the behavior of Ni-P/Ni-P-SiC coatings can be achieved.

## 1.2 Research purpose

The purpose of this research includes:

- The synthesis of as-plated high phosphorus Ni-P coatings and as-plated high phosphorus composite Ni-P-SiC coatings (with micro-size SiC particles) on carbon steel substrates using the electroless-plating technique.
- The characterization of as-plated high phosphorus Ni-P coatings and as-plated high phosphorus composite Ni-P-SiC coatings. It involves the study of the morphology, structure, chemical composition, thickness and hardness.
- A comparative study of the corrosion resistance of these materials by electrochemical DC (polarization techniques) and AC (electrochemical impedance spectroscopy) methods under conditions that promote electrochemical corrosion (NaCl 3,5 %).



## 2. THEORETICAL BACKGROUND

### 2.1 The nickel-phosphorus alloy system

Nickel and phosphorus can form nickel-phosphorus alloys which are known because of their special mechanical, chemical and physical properties. Some properties of elemental Ni and P are shown in Table 1.

Table 1. Some properties of elemental Nickel and Phosphorus [12]

Property		Nickel	Phosphorus
Character		metal	non metal
Atomic radius	[nm]	0,124	0,128
Crystal structure		cubic body centered	monoclinic
Lattice constant	[nm]	a = 0,352	a = 0,33; b = 0,44; c = 0,11
Melting point	[°C]	1455	44
Density	[g/cm <sup>3</sup> ]	8,9	1,82

Regarding Ni-P alloys, Figure 1 shows the Ni-P phase diagram in which the equilibriums of different phases in dependence of temperature and concentration of nickel and phosphorus are depicted. The phases are under thermodynamic stable conditions.

The equilibrium phase diagram (Figure 1) shows practically no solid solubility of phosphorus in nickel in a temperature range between 20 °C till 1455 °C. That is because the solidus and liquidus curve of Ni coincide with the temperature axes of the phase diagram [1, 12].

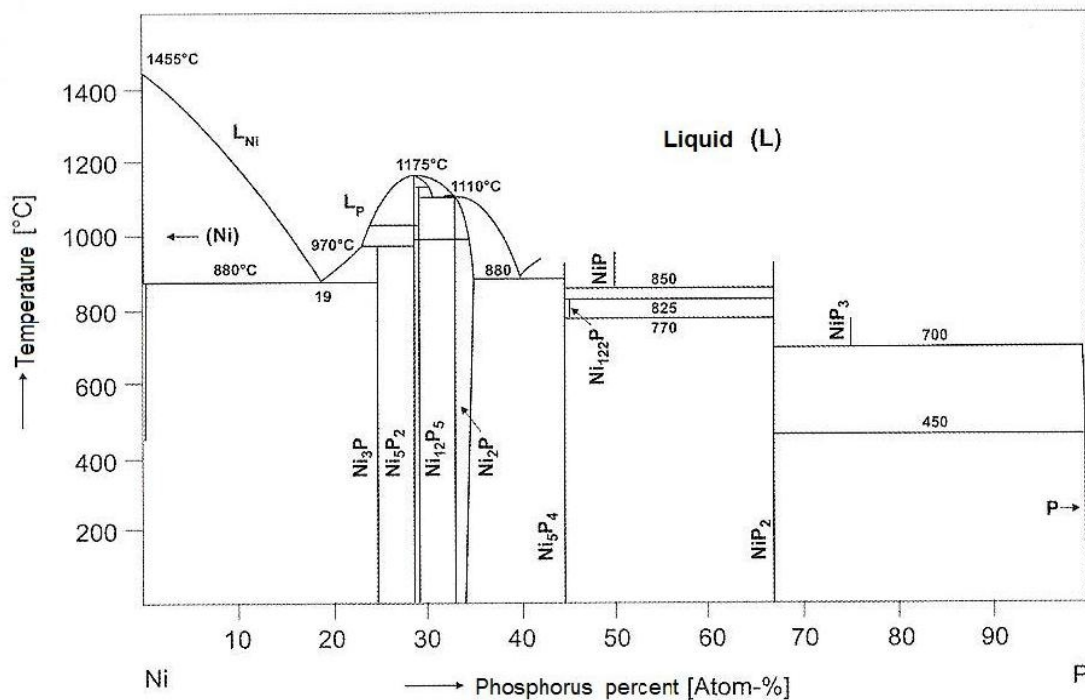


Figure 1. Ni-P alloy equilibrium phase diagram [12]

Another characteristic of the binary alloy system Ni-P is the existence of many intermediate phases called *nickel phosphides* ( $Ni_3P$ ,  $Ni_5P_2$ ,  $Ni_{12}P_5$ ,  $Ni_2P$ ,  $Ni_5P_4$ ,  $Ni_{1,22}P$ ,  $NiP$ ,  $NiP_2$ ,  $NiP_3$ ) [1, 12]. Among this group, the  $Ni_3P$  phase exists at room temperature and forms an eutectic system with Ni. The  $Ni_5P_2$ ,  $Ni_2P_5$  and  $Ni_2P$  intermediate phases are stable at room temperature also. On the other hand,  $Ni_{1,22}P$ ,  $NiP$  and  $NiP_3$  do not exist at room temperature because they are high-temperature modifications.

Phosphor rich alloys (phosphor content  $>40$  at% = 26 wt %) are technically not significant. In addition, there is no available information about any solidus and liquidus curve on this zone [12].

Electroless Ni-P coatings, as plated, are metastable and supersaturated alloys [1, 12]. Therefore, from a thermodynamic point of view, the Ni-P equilibrium phase diagram (Figure 1) can not be used to describe the constitution of these coatings.

Nevertheless, many researches had shown that the Ni-P-phase diagram can be used as a first guideline and a qualitative observation of electroless Ni-P coatings.

A non-equilibrium phase diagram of electroless Ni-P coatings was reported [12] in order to explain accurately the constitution of Ni-P coatings obtained by electroless plating (see Figure 2).

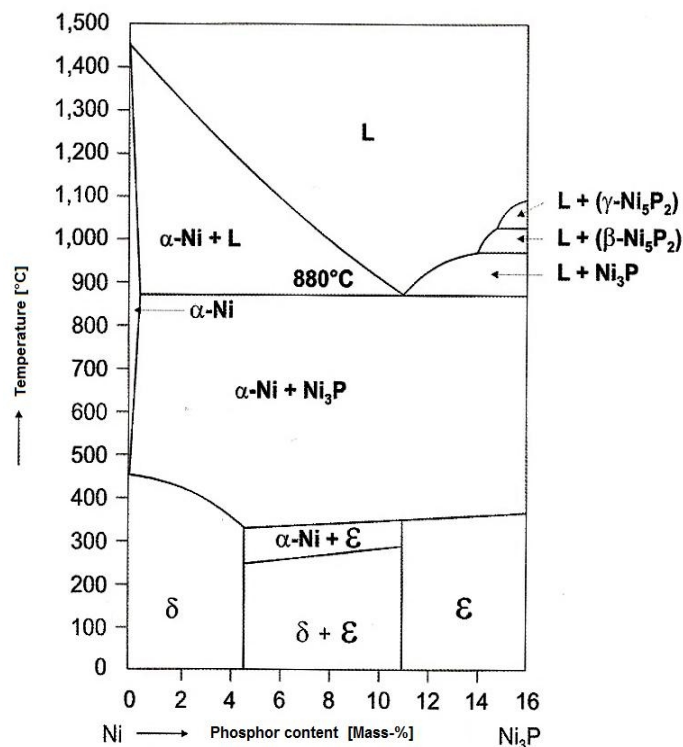


Figure 2. Non- equilibrium electroless Ni-Ni<sub>3</sub>P phase diagram [12]

In this diagram, besides the thermodynamic stable solid phases  $\alpha$ -Ni, Ni<sub>3</sub>P and Ni<sub>5</sub>P<sub>2</sub>, also appear two additional metastable phases named  $\delta$  and  $\epsilon$ .

The  $\delta$ -phase is a mixed crystal made of Ni and P and, unlike  $\alpha$ -Ni, can dissolve up till 4,5 wt% P. The  $\epsilon$ -phase is amorphous and can contain between 11 and 15 wt% P. Between the existing  $\delta$  and  $\epsilon$  phases there is a mixture of both phases ( $\delta + \epsilon$ ) whose existing area reaches from 4,5 to 11 wt% P.



## 2.2 Electroless deposition process

According to Schlesinger and Paunovic [5], the electroless (autocatalytic) deposition process is defined as *"the deposition of a metallic coating by a controlled chemical reduction that is catalyzed by the metal or alloy being deposited"*. Therefore, this method is characterized by the selective reduction of metal ions only at the surface of a catalytic substrate immersed into an aqueous solution of those metal ions. The deposition takes place continuously on the substrate through the catalytic action of the deposit itself [1].

The electroless plating has been used to yield deposits of Ni, Co, Pd, Cu, Au, and Ag as well as some alloys containing these metals plus P or B [5]. Among the variety of metals that can be plated using this method, electroless nickel is one of the most important because of its unique properties such as excellent corrosion and wear resistance. The electroless nickel processes are grouped as Ni-P, Ni-B and pure Ni based respectively on the reducing agents used (e.g. hypophosphite, borohydride or dialkylamine-borane and hydrazine) in the plating bath. Electroless nickel plating process based on hypophosphite as a reducing agent has received commercial success because of its relative low cost and ability to offer good corrosion resistance [6].

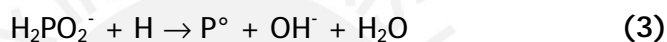
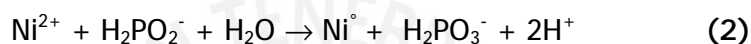
The electroless plating process requires a catalytic surface on which the deposition will proceed. The reduction reaction starts spontaneously only on certain metals (Fe, Co, Ni, Rh, Pd and Pt) in active form. The Pt, Ni, Co, Pd and Rh metals are considered hydrogenation-dehydrogenation catalysts. Metals such as Fe and Al (which are more electropositive than Ni) will first displace nickel from a solution of its ions in order to form a catalytic surface. The equation (1) represents the displacement reaction between Ni and Fe [1]. After this step, the process will be carried out at the catalytic surface.



This process can be divided into elementary consecutive steps mentioned below.

- Diffusion of reactants ( $\text{Ni}^{2+}$ ,  $\text{H}_2\text{PO}_2^-$ ) to the metal surface.
- Adsorption of reactants at the metal/solution interface.
- Electrochemical reaction at the metal/solution interface.
- Desorption of products ( $\text{HPO}_3^-$ ,  $\text{H}_2$ ,  $\text{H}^+$ ) from the metal/solution interface.
- Diffusion of products away from the metal/solution interface.

In general, the whole process (using sodium hypophosphate as a reducing agent) can be conveniently described by three reactions [4]. These are described in equations (2), (3) and (4).



The equations mentioned above describe the net result of a series of simultaneous partial reactions which have been the subject of extensive mechanistic studies and yet are still a topic of discussion.

The main feature of practical importance is that reaction described in (2) (nickel deposition) takes place at a considerably faster rate than reaction described in (3) (deposition of phosphorus) to get nickel rich surface deposits with the formation of orthophosphite ion ( $\text{H}_2\text{PO}_3^-$ ). The overall effect of the three reactions is an increment in the acidity of the bath [4].

The relative rates of reactions (2) and (3) may be controlled either by variation in temperature, in the relative initial concentrations of reducing agent to nickel ion, in the choice of both the nature and concentration of added complexing agents, as well as in the ratio of substrate area to solution volume within the deposition bath [4].

The case of the electroless deposition of Ni-P coatings using sodium hypophosphate as a reducing agent is represented in Figure 3.

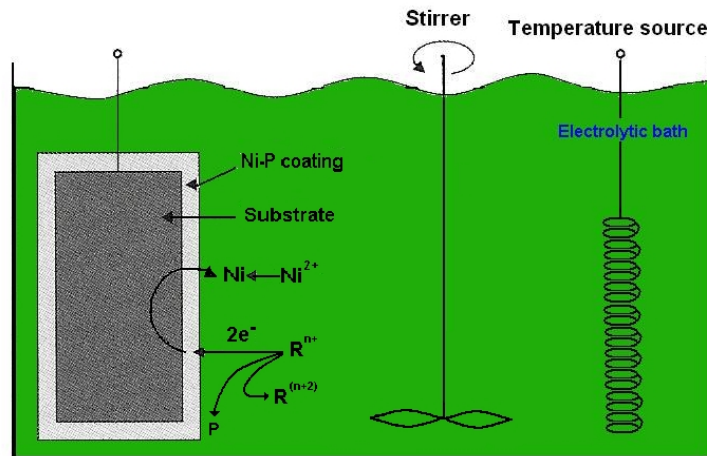


Figure 3. Electroless Ni-P deposition process [12]

## 2.2.1 Mechanism of electroless Ni-P deposition process

Many studies were carried out on the mechanism of the electroless Ni-P plating process. The topic is still in discussion, therefore, different mechanisms have been proposed.

The main reactions responsible for the production of Ni-P coatings can be most accurately described by three mechanisms: The *atomic hydrogen* mechanism, the *hydride* mechanism and the *electrochemical* mechanism [1]. Due to the focus of this research in working Ni-P coatings obtained with acid baths, the mechanisms described below are specific for electroless plating with hypophosphite as a reducing agent under acid conditions.

### 2.2.1.1 The atomic hydrogen mechanism

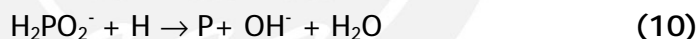
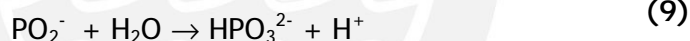
According to Mallory [1], this mechanism was proposed by Brenner and Riddel and modified later by Gutzeit.

The nickel reductant is atomic hydrogen that acts by heterogeneous catalysis at the catalytic nickel surface. Equation (5) describes the production of atomic hydrogen, which is generated by hydrolysis of hypophosphite and then absorbed into the catalytic surface. The reduction of nickel ions by the absorbed atomic hydrogen at the catalytic

surface is shown in equation (6). On the other hand, the evolution of hydrogen gas resulting of the recombination of two atomic hydrogen atoms is represented in equation (7).

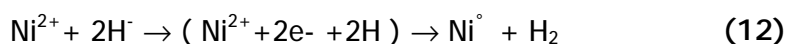
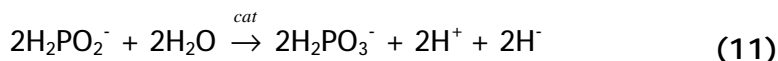
Gutzeit agrees with the Brenner-Riddell atomic hydrogen concept of nickel reduction. However, Gutzeit attributes that the formation of atomic hydrogen results from the dehydrogenation of the hypophosphite ion during formation of metaphosphite ion (equation (8)) followed by the formation of an orthophosphite molecule and an hydrogen ion (equation (9)).

The formation of elemental phosphorus can be explained as the result of a secondary reaction between hypophosphite and atomic hydrogen (equation (10)).



### 2.2.1.2 The hydride transfer mechanism

Mallory [1] reported that this mechanism was proposed by Hersch, who assumed that hypophosphite acts as the donor of hydride ions (H<sup>-</sup>). Thereby, in acid solutions, the primary step in the mechanism involves the hydrolysis of hypophosphite at the catalytic surface (Equation 11).



The reduction of nickel ions by this mechanism proceeds as shown in Equation (12). In addition of that, equation (13) shows that the hydride ion can also react with a hydrogen ion to obtain molecular hydrogen. If equation (10) is included in this part, the co-deposition of phosphorus is also explained.

### 2.2.1.3 The electrochemical mechanism

According to Mallory [1], in this mechanism, there is an anodic reaction (14) by which electrons are released. The reactions (15), (16) and (17) are cathodic and the evolution of hydrogen taking place during the nickel deposition is a result of the secondary reaction (16). This mechanism implies that the nickel concentration should have a significant effect on the rate of deposition; however the converse is true.



### 2.2.2 Electroless Ni-P plating bath

The principal components of an electroless deposition plating bath are: a source of nickel ions, a reducing agent, complexing agents and stabilizers/inhibitors.

The most preferred source of nickel ions is the nickel sulfate solution. Other salts of nickel (as nickel chloride or nickel acetate) are also used, but under certain circumstances the chloride ions cause an adverse effect, e.g. when the substrate is aluminum or when the EN coating will be applied over a ferrous alloy [1].

Sodium hypophosphite is commonly used as a reducing agent in order to obtain Ni-P deposits. Other reducing agents, e.g. sodium borohydride, dimethylamine borane (DMAB) and hydrazine, are also used, but they will yield Ni-B alloy or only Ni deposits [1, 6]. The reducing agents have a common characteristic: to possess two or more

active hydrogens which are involved in the mechanism of the electroless deposition process.

Concerning the complexing agents, organic acids or salts such as propionic, succinic, citric and malic acids among others are mainly used. The main functions of complexing agents are three: to buffer the pH of the plating bath (avoid fast variation of pH), to prevent precipitation of nickel salts (e.g. basic salts or phosphites), and to reduce the concentration of free nickel ion in the solution [1].

The stabilizers are used in small amounts (a few parts per million) and are added to prevent decomposition of the electrolytic bath. The bath decomposition is usually preceded by the increment of volume of hydrogen gas and the appearance of a finely-divided black precipitate throughout the solution. The precipitate consists of nickel particles and nickel phosphide. The most effective stabilizing agents are compounds of elements of Group VI ( e.g. S, Se, Te), ions of heavy metals ( e.g.  $\text{Sn}^{2+}$ ,  $\text{Pb}^{2+}$ ,  $\text{Hg}^+$ ,  $\text{Sb}^{3+}$ ), compounds containing oxygen (e. g.  $\text{AsO}_2$ ,  $\text{IO}_3^-$ ,  $\text{MoO}_4^{2-}$ ) and unsaturated organic acids (e.g. maleic acid) [1].

### 2.2.3 Factors affecting the electroless plating process

There are several parameters affecting the plating process: temperature, pH, nickel and hypophosphite concentration, presence of phosphite anion, the freshness and the loading of the bath, among others. There is evidence also that the amount of complexing agents in a given electrolytic bath can affect the surface morphology, microstructure and deposition rate of the coating [13].

The surface pre-treatment of the substrate is also important because the remotion of foreign contaminants (dust, corrosion products, oxides, etc.) is crucial in order to get high adhesion between substrate and coating. The roughness and mechanical defects of the substrate can affect also the final appearance of the coating.

### 2.2.3.1 Influence of temperature

Catalytic reactions, such as electroless nickel plating, require energy and this is supplied in the form of heat. The effect of the temperature is important because it determines the rate of the deposition. It has been reported that very little plating, if any, occurs at temperatures below 60 °C. The plating rate increases exponentially when the temperature is increased. Commonly the acid hypophosphite plating solutions are operated between 85°C and 90 °C. Above 90 °C, the plating bath becomes unstable with risk of decomposition. Figure 4 shows the effect of temperature on the plating rate.

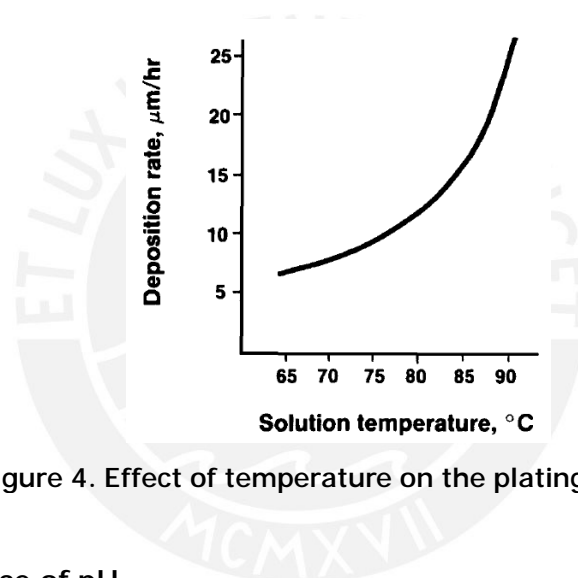


Figure 4. Effect of temperature on the plating rate [1]

### 2.2.3.2 Influence of pH

It has been observed empirically that three moles of  $H^+$  are produced for every mol of  $Ni^{2+}$  deposited. This means that without any type of buffering during deposition, the pH value in a bath will be lower. As a consequence the deposition rate decreases [5]. Figure 5 depicts the influence of the pH on the deposition rate for a determinate plating bath.

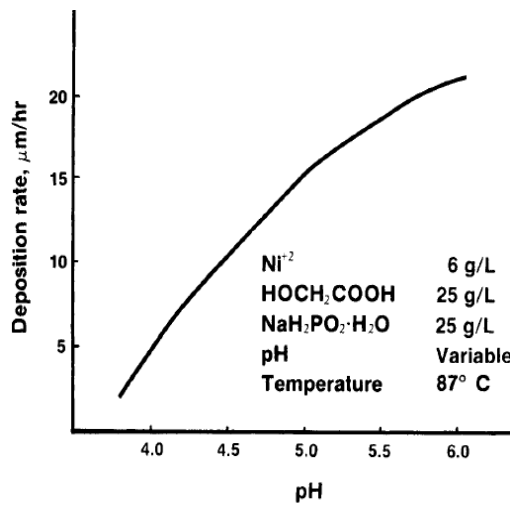


Figure 5. Effect of pH on the rate of deposition [1]

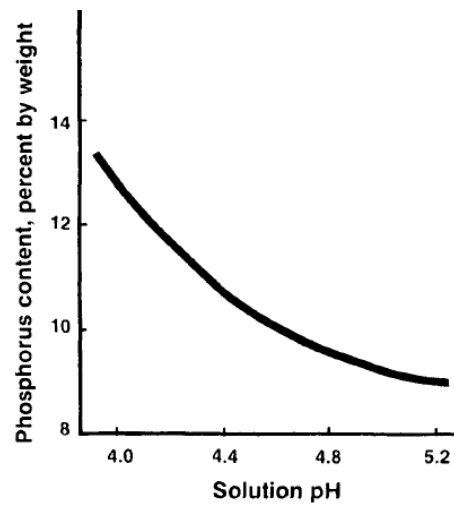


Figure 6. Effect of the pH on phosphorus content [1]

In the practice, variations of pH as a result of the formation of  $\text{H}^+$  is related to the buffer capacity of the complexing agents or other buffers that are present in the plating bath.

Variation of pH in the plating bath also has another effect; it causes a change of the composition of the deposit. Figure 6 shows the effect of the pH on the phosphorus content of a deposit. Variation in the phosphorus content can also result in changes of the properties of the deposits. Thus, depending on the required properties, the pH can be conveniently set. In general, when the phosphorus content of the deposits is above 10 wt%, the Ni-P deposit has low internal intrinsic stress and good corrosion resistance because of the low porosity [1].

### 2.2.3.3 Influence of nickel and hypophosphite ions concentration

It has been observed that the molar ratio of  $\text{Ni}^{2+}/\text{H}_2\text{PO}_2^-$  should be maintained in a range of 0,25 - 0,60 in order to obtain optimal plating conditions.

The nickel concentration of commercial acid type (pH 4 to 6) electroless nickel solutions lies within the range of 0,08 to 0,19 M. Thus, according to the preferred molar ratio of  $\text{Ni}^{2+}/\text{H}_2\text{PO}_2^-$ , the molar concentration range for sodium hypophosphite is between 0,18 to 0,27 M.



The nickel concentration equal or higher than approximately 5 g/L (0,085 M) has little or no effect on the plating rate.

On the other hand, the phosphorus content of Ni-P deposits is influenced by the nickel concentration only when the nickel concentration is less than about 0,1 M. Above 0,1 M nickel concentration, the phosphorus content will be constant, given that the hypophosphite concentration is constant. **Figure 7** depicts the effect of nickel concentration on Ni-P alloy composition [1].

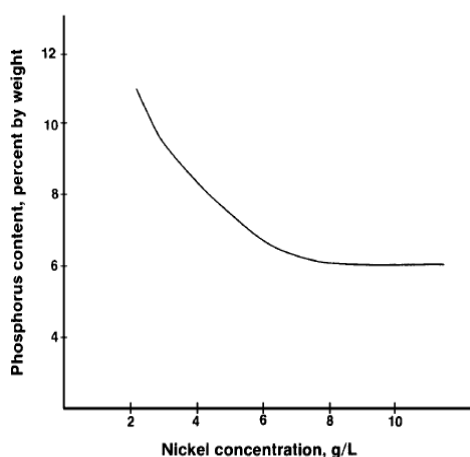


Figure 7. Effect of nickel concentration on Ni-P alloy composition [1]

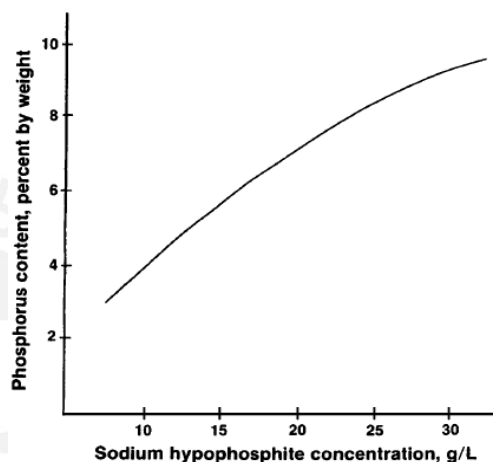


Figure 8. Effect of the hypophosphite concentration on Ni-P alloy composition [1]

Concerning the influence of hypophosphite content, it has been reported that when the concentration of hypophosphite in the bath increases, the phosphorus content in the alloy also increases. This is shown in **Figure 8**.

### 2.3 Electroless Ni-P composite deposition process

The co-deposition of second phase particles in electroless nickel deposits has led to the development of electroless nickel composite coatings.

Several electroless Ni-P composite coatings have been successfully co-deposited using micro- and nano-sized particles [1,7,10-12,14]. Some reported examples are Ni-P-Al<sub>2</sub>O<sub>3</sub>, Ni-P-SiC, Ni-P-B, Ni-P-PTFE, Ni-P-MoS<sub>2</sub>, Ni-P-C, Ni-P-Si<sub>3</sub>N<sub>4</sub>, Ni-P-CeO<sub>2</sub>, Ni-P-TiO<sub>2</sub> and Ni-P-ZrO<sub>2</sub>. The combination of certain type of particles and the Ni-P matrix can

further enhance different properties (e.g. hardness, wear, lubrication) in the composite deposit.

The electroless Ni-P composite plating process uses the conventional autocatalytic reduction process with the difference that deposition baths contain particles in suspension. In general, factors like bath chemistry, particle characterization and operating conditions determine particle concentration in the deposit.

According to Balaraju et al. [6], the main factors determining the particle incorporation are particle size and shape, relative density of the particle, the concentration of particles in the plating bath, the method and degree of agitation and, the orientation of the part being plated.

Concerning the mechanism of particle incorporation into the metallic matrix, there has been several investigations.

Balaraju et al. [6], reported that the electroless composite coating is formed by the impact and settling of particles on the surface of the substrate, and the subsequent envelopment of these particles by the matrix material as it is deposited. No molecular bonding exists between particles and metal matrix.

On the other hand, Kanani [12] reported two models of particle integration in the Ni-P coatings.

In the first model, the integration process of dispersion particles in the Ni-P deposits involves four steps. The first step consists of the release of the particles from the dispersion clot. The second step takes course in the transport (by sedimentation, convection and/or diffusion) of the dispersion particles to the growing metallic deposit. That is followed by the adhesion of the dispersion particles to the metallic surface in a third step. Finally, the fourth step consists of the overgrowing of the dispersion particles by the metal matrix. The amount of stored particles in the film mainly depends on the concentration of particles in the electrolyte, the type of electrolyte, the deposition conditions and the bath movement.

In the second model, the process can be divided into three steps. The first step consists of transport of simple or complex structured ions (by diffusion, convection and migration) and particles (by diffusion, convection and sedimentation) of the dispersed phase from the electrolyte to the substrate surface. The second step involves the reaction of the ions and the particles with the coated surface. These are the chemical and physical processes that cause the dispersed phase to remain at the surface. The influence of any of these processes depends on the properties of the dispersed particles (density, size, shape), the characteristics of the electrolyte and the morphology of the surface (type, shape, roughness). The third step consists of the coating formation and the covering of the dispersed phase by the Ni-P deposit. Once the particles have reached the substrate surface, they are fixed there by adhesion until the embedding by the growing Ni-P deposit. The sedimentation and the stream of the electrolyte are working against the adhesion. At this stage the process depends on the deposition conditions, mainly temperature and intensity of the hydrogen development. Colloid-chemical processes (surface charge, adsorption of ions, adhesion) at the material surface are determining the integration also.

An ideal structure of an electroless Ni-P composite coating is shown in **Figure 9**.

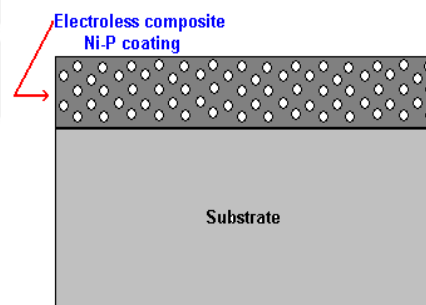


**Figure 9. Ideal structure of a composite Ni-P coating [12]**

The incorporation of SiC particles (micro or nano-size) in the Ni-P matrix has led to the development of Ni-P-SiC composite coatings. They are attractive because of the high wear resistance property. Therefore, these coatings have a wide use in engineering and industry.

The silicon carbide has a tetrahedral structure with alternating Si and C atoms. It possesses a stable structure and it is chemically inert [15]. The structure is not

affected by hydrogen or nitrogen up till 1600°C but in air, SiC begins decomposing above 1000°C. SiC particles have an arbitrary shape, angular and with peaks [12]. The hardness of SiC (measured at different crystallographic faces) is between 21 to 31 GPa, that means in Vickers hardness 21 000 to 37 000 HV. Thus, the co-deposition of SiC-particles increases the hardness and the wear resistance of Ni-P deposits.

The composition of a known Hubbell's base electrolyte for the deposition of Ni-P-SiC coating is shown in Table 2.

**Table 2. Hubbell's electrolyte composition [12]**  
(pH=4,6)

Components	Concentration
NiSO <sub>4</sub> .6H <sub>2</sub> O	0,08 mol/L
NaH <sub>2</sub> PO <sub>2</sub> .H <sub>2</sub> O	0,23 mol/L
Lactic acid	0,30 mol/L
Propionic acid	0,03 mol/L
Pb <sup>2+</sup>	1,00 ppm

The content of SiC in the Ni-P coating increases with the increment of SiC particles dispersed in the solution.

Some reported studies [12] confirmed that Ni-P SiC coatings have different integration rates of SiC particles. In fact, it depends on the streaming conditions in the bath. Areas with strong flow against the deposits and special shaped corners are showing little or nearly no integration of the dispersion. Frontal streamed areas have a uniform coating. To avoid the sedimentation of SiC particles (SiC density = 3,2 g/cm<sup>3</sup>) there must be assured a steady dispersion of the particles in the electrolyte.

The maximal incorporation rate of SiC particles in a Ni-P coating is approximately 5 wt%. It is reached at the range of 15 to 20 g/L of SiC in the electrolyte. An increase of concentration higher above 20g/L does not increase the integration of SiC particles in the Ni-P deposit. This is shown in Figure 10.

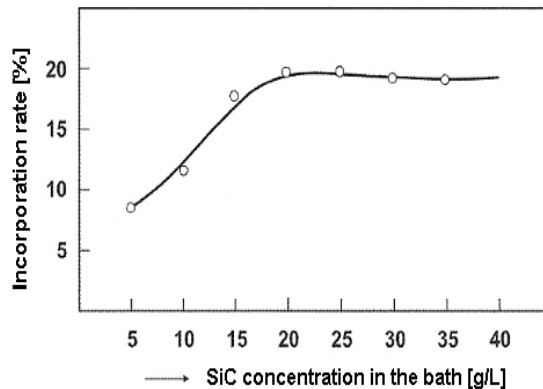


Figure 10. Effect of the SiC concentration in the incorporation rate of a Ni-P-SiC composite coating [12]

#### 2.4 Structure of electroless Ni-P coatings

The structure of as-deposited Ni-P coatings is mainly related to phosphorus content in the alloy.

As-coated electroless Ni-P is a metastable, supersaturated alloy because the conditions existing during plating do not permit the formation of stable phases. X-ray diffraction studies have shown that, as-coated state, low phosphorus (1-4 wt%) coatings are crystalline or microcrystalline, medium phosphorus (7-9 wt%) coatings are either fully amorphous or mixtures of microcrystalline and amorphous phases and high phosphorus coatings (9 wt% and above) are considered to be amorphous [1, 9, 16]. The definition on either amorphous or crystalline structure is based on the possibility to get a characteristic sharp peak in an X-ray diffraction pattern. A sharp peak hereby is defined as a crystalline structure, whereas a non-sharp, hill-like peak defines an amorphous structure. This definition may change with new developments in the field of structure analysis, e.g. new high-resolution transmission electron microscopes.

It is noteworthy that the structure of as-plated electroless Ni-P is in agreement with the electroless Ni- Ni<sub>3</sub>P phase diagram shown in Figure 2; where, depending on the phosphorus content, the metastable phases  $\delta$  (character crystalline) and/or  $\epsilon$  (character amorphous) are present at low temperatures.

In the case of electroless Ni-P composite coatings, it has been reported [6] that the effect of incorporation of TiC, Si<sub>3</sub>N<sub>4</sub>, CeO<sub>2</sub> and TiO<sub>2</sub> particles does not alter the structure of the as plated- electroless Ni-P matrix [6].

For composite coatings with SiC particles, it has been reported that electroless high phosphorus Ni-P-SiC composite coatings with superfine SiC particles (mean sizes of 1000, 110 and 50 nm) have an amorphous structure as plated [18].

## 2.5 Properties of electroless Ni-P coatings

The properties of an electroless Ni-P coating depend on its composition and microstructure. The phosphor content is the principal factor that determines the properties of Ni-P deposits. In general terms, as-plated Ni-P coatings are uniform, wear resistant, hard and corrosion resistant [8]. Table 3 shows the principal properties depending on the phosphor content.

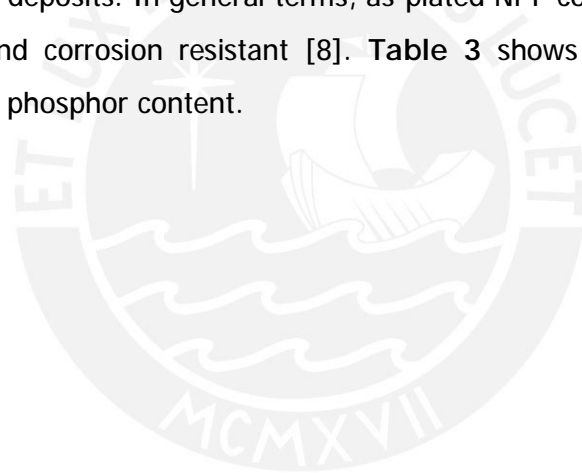


Table 3. Some Properties of electroless Ni-P alloy coatings depending of the phosphor content [12]

Phosphorus content (wt%)	1-4	7-9	10-12
Structure	crystalline		amorphous
<b>Physical properties</b>			
Density (g/cm <sup>3</sup> )	8,5	8,1	7,9
Specific electric resistivity (μΩ.cm)	20-30	50-60	100
Thermal expansion coefficient (μm/m/K)	13	12	11
Magnetic susceptibility (%)	-	4	-
Coercivity (Oe)	~10	1-2	0
<b>Mechanical properties</b>			
Tensile strength (N/mm <sup>2</sup> )	200	800-900	750-900
Elongation at fracture (%)	0,5	0,7	~1,5
Hardness HV	650-700	550-600	500-550
Taber-Abraser-Index	10-12	15-20	20-25
Internal stress (over steel substrate) (N/mm <sup>2</sup> )	-10	±5	+5
<b>Chemical properties</b>			
Salt spray test (h)	24	200	1000
Acid resistance	low	medium	good
<b>Other properties</b>			
Solderability	very good	good	medium

Due to the scope of this research work, hardness and corrosion resistance properties will be described with more detail.

### 2.5.1 Hardness

Hardness is defined as the resistance of a material to permanent deformation by indentation. It is useful in predicting abrasive-wear properties; however, there is no direct relationship with the strength of a material [1].

The hardness values of as-plated Ni-P coatings are in the range of 500 to 600 Kg/mm<sup>2</sup> as measured with a Knoop or Vickers indenter using a 100 g load. Usually hardness of

as-plated Ni-P coatings decreases when phosphorus content in the Ni-P alloys increases [1, 5].

In general, the hardness is affected by heat treatment. There is a general agreement for electroless nickel based coatings which states that a heat treatment at 400°C for 1h, for any content of phosphorus, produces maximum obtainable hardness because of the formation of crystalline Ni and Ni<sub>3</sub>P [6, 7, 17]. In the case of electroless Ni-P composite coatings, the level of incorporation of particles, the phosphorus content of the matrix and heat treatment determine the hardness of the coating. Ceramic (hard) particles increase the electroless Ni-P deposits regardless their phosphorus content (2-13 wt %). However, the influence of the phosphorus is noticed when coatings with phosphorus content higher than 7 wt% are thermally treated and, consequently, large amounts of hard Ni<sub>3</sub>P phase are formed [6].

The influence of heat treatment on the hardness of Ni-P-SiC has been studied in comparison with Ni-P-PTFE and Ni-P electroless coatings [6]. **Figure 11** shows the change in hardness of these electroless Ni-P coatings by heat treatment. The changes in hardness of these coatings have a similar behavior. Increase in hardness up to 400°C is due to precipitation hardening (formation of Ni<sub>3</sub>P phase). The reduction in hardness beyond 400°C is attributed to a decrease in lattice defects and coarsening of Ni<sub>3</sub>P particles.

For Ni-P-SiC coatings, it has been reported [18] that with a heat treatment at high temperature (at 500-600°C for 1h), the final products of the crystallization and reaction of the composite coating were not only Ni and Ni<sub>3</sub>P but also Ni<sub>3</sub>Si and free carbon. The hardness of pure as-plated-Ni-P coatings is 550 HV. With the integration (approx. 5 wt%) of SiC-particles the hardness could be increased to a value between 680 to 700 HV [12].



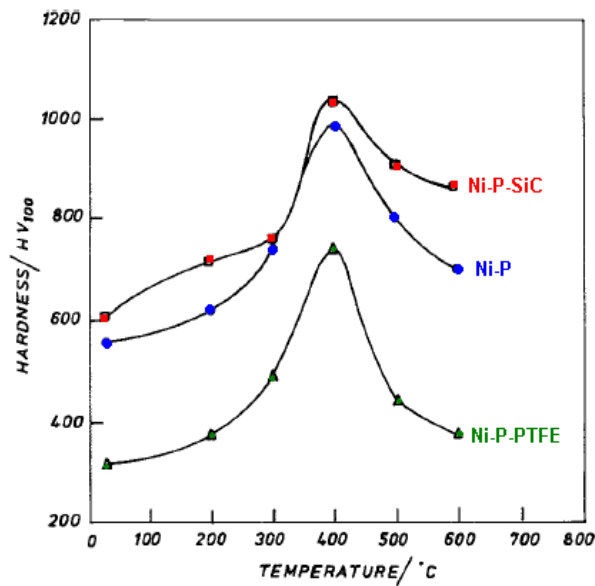


Figure 11. Comparison of change in hardness with heat treatment temperature for electroless Ni-P-SiC, Ni-P and Ni-P-PTFE [6]

### 2.5.2 Corrosion resistance

Electroless Ni-P coatings have good corrosion resistance due to the low porosity of the coatings and the excellent resistance of nickel to many mediums and atmospheric conditions [1].

There are many factors that determine the corrosion resistance of electroless Ni-P coatings:

- Substrate composition, structure and surface finish.
- Pretreatment of the substrate to achieve a clean, uniform surface.
- Thickness of the coating.
- Properties of the coating (composition, porosity, internal stress).
- Plating post-treatment
- Nature of the corrosive medium

According to the literature [19, 20], there has been generally accepted that amorphous Ni-P alloys exhibit superior corrosion resistance (due to the absence of grain boundaries) whereas (re)crystallization neutralizes this effect.

Electroless Ni-P coatings could acquire extra hardness by a process of heat treatment to about 400°C, however the corrosion resistance will be lower. This is maybe due to microcracking [5]. Heat treatment up 650°C improves corrosion resistance since there is improved bonding to the substrate (e.g. steel).

Studies of X-ray photoelectron spectroscopy (XPS) on the surface of Ni-P alloys after electrochemical polarization did not show any nickel oxide on the surface. Thus, it was concluded that passivity observed in electroless Ni-P deposits is different from pure nickel [19].

Elsener et al. [19], mentioned that there have been proposed models for explaining the high corrosion resistance of Ni-P alloys with a high content of phosphorus.

- The formation of a P-rich film at the alloy/solution interface as a consequence of rapid and selective nickel dissolution. The dissolution process is controlled by the diffusion of nickel through this phosphorus rich zone.
- The formation of a protective nickel phosphate film that acts as a diffusion barrier against the dissolution of the alloy.
- Adsorption of hypophosphite ions, forming a barrier layer that prevents the dissolution of nickel atoms at the alloy surface.

Several researches [9, 10, 20] agree with the first model; however the corrosion resistance mechanism is still under debate. In fact, so many parameters influence the properties of an electroless Ni-P coating and it is difficult to predict accurately, a priori, their corrosion resistance.

Regarding electroless Ni-P composite coatings, it has been reported that the corrosion resistance of electroless Ni-P composite coatings is lower than electroless Ni-P alloy coatings [8] because the co-deposited second phase particles present in the electroless nickel matrix could reduce passivity and corrosion resistance. However, Balaraju et al. [6] reported that corrosion performance of electroless Ni-P-SiC coatings was found to be satisfactory in neutral salt spray test. Other studies on the corrosion resistance of electroless Ni-P-Si<sub>3</sub>N<sub>4</sub> coatings in 3,5% sodium chloride solution also revealed a

marginal increase in corrosion resistance compared to an electroless Ni-P coating of similar thickness. Electrochemical impedance studies on Ni-P-Si<sub>3</sub>N<sub>4</sub>, Ni-P-CeO<sub>2</sub> and Ni-P-TiO<sub>2</sub> suggest that these composite coatings provide better corrosion resistances than electroless Ni-P coatings [10].

Table 4 provides some data about corrosion resistance of electroless Ni-P composite coatings.

Table 4. Corrosion resistance of some electroless Ni-P composite coatings [6]

Type of coating**	Method of Evaluation	Result
Ni-P-SiC	Neutral slat spray test; as per ASTM B-117	Same degree of protection offered by electroless Ni-P coating having similar thickness
Ni-P-TiO <sub>2</sub>	CASS * test for 16 h; as per ISO 3770:1976	Same degree of protection offered by electroless Ni-P coating having similar thickness
Ni-P-Si <sub>3</sub> N <sub>4</sub>	Potentiodynamic polarization study in 3,5% NaCl solution	Corrosion current density is 2,5 μAcm <sup>-2</sup>
Ni-P-CeO <sub>2</sub>	Potentiodynamic polarization study in 3,5% NaCl solution	Corrosion current density is 4,0 μAcm <sup>-2</sup>
Ni-PTiO <sub>2</sub>	Potentiodynamic polarization study in 3,5% NaCl solution	Corrosion current density is 6,0 μAcm <sup>-2</sup>
Ni-P-Si <sub>3</sub> N <sub>4</sub>	Electrochemical Impedance study in 3,5% NaCl solution	R <sub>ct</sub> is 90 535 Ωcm <sup>2</sup> C <sub>dl</sub> is 11 μFcm <sup>-2</sup>
Ni-P-CeO <sub>2</sub>	Electrochemical Impedance study in 3,5% NaCl solution	R <sub>ct</sub> is 90 700 Ωcm <sup>2</sup> C <sub>dl</sub> is 11 μ Fcm <sup>-2</sup>
Ni-P-TiO <sub>2</sub>	Electrochemical Impedance study in 3,5% NaCl solution	R <sub>ct</sub> is 58 991 Ωcm <sup>2</sup> C <sub>dl</sub> is 17 μFcm <sup>-2</sup>

\* CASS: Copper Accelerated Acetic Acid Salt Spray.

\*\* All coatings were obtained by electrolessplating.

## 2.6 Electrochemical techniques for corrosion resistance evaluation

When a corrosion process is carried out through an electrochemical mechanism, electrochemical techniques can be applied in order to study the corrosion behavior.

These techniques are divided into stationary and non stationary methods. Direct current (DC) electrochemical test methods belong to stationary methods while alternate current (AC) methods are considered non stationary methods.

### 2.6.1 DC electrochemical test methods

In order to explain these techniques, it is convenient to define the *open circuit potential* (OCP). The OCP of a metal in an aqueous solution is defined as the potential at which the rate of oxidation is exactly equal to the rate of reduction (there is no net current to be measured). The OCP depends on the inherent reactivity of the metal and the oxidizing power of the solution [21].

#### 2.6.1.1 Linear Polarization Resistance (LPR)

The LPR method enables the determination of instantaneous corrosion rates (corrosion currents). The method is based on the Stern-Geary simplified kinetic expression (18) and provides an approximation to the charge transfer controlled reaction kinetics for the case of small polarizations (10 to 20 mV) with respect to the OCP. The polarizing current is assumed to change linearly (not logarithmically) with a change in the potential.

$$R_p = \frac{dV}{dI} = \frac{b_a b_c}{2,3(b_a + b_c)I_{corr}} \quad (18)$$

Then, the Stern-Geary constant can be defined by equation (19).

$$B = \frac{b_a b_c}{2,3(b_a + b_c)} \quad (19)$$

The equation (18) can be rewritten as equation (20) where  $R_p$  ( $\Omega$ ) is the polarization resistance,  $B$  (V) is a proportionality constant that depends on the Tafel slope values  $\beta_a$  (V/dec) and  $\beta_c$  (V/dec) and  $I_{corr}$  (A) is the corrosion current [22].

$$I_{corr} = \frac{B}{R_p} \quad (20)$$

Figure 12 shows a typical linear polarization resistance curve. The most used method to calculate  $R_p$  is to determine the slope of the tangent of this curve at the OCP where the current is zero.

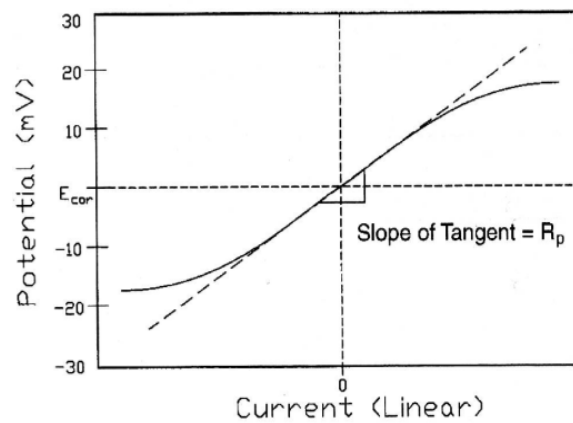


Figure 12. Typical linear polarization resistance curve [21]

### 2.6.1.2 Tafel Plots

This polarization technique is used to measure the corrosion current ( $i_{corr}$ ) in order to calculate the corrosion rate. A Tafel plot can yield  $i_{corr}$  directly or it can yield the Tafel constants ( $\beta_a$  and  $\beta_c$ ). The Tafel constants can then be used with the  $R_p$  value (from the LPR technique) to calculate  $i_{corr}$ .

The anodic or cathodic Tafel plots are described by the Tafel equation [23] (21).

$$h = b(\log I - \log I_{corr}) \quad (21)$$

Where  $h$  (V) is an overvoltage (the difference between the potential of the specimen and the OCP),  $b$  (V/dec) is the Tafel constant,  $I$  (A) is the current at the overvoltage  $h$  and  $I_{corr}$  (A) is the corrosion current.

A Tafel plot is performed on a metal specimen by polarizing anodically the specimen about 250 mV (positive-going potential) and cathodically (negative-going potential) from the open circuit potential (OCP). The resulting current is plotted as shown in Figure 13. Extrapolating the linear portions of the polarization curve found at very distant potentials from the OCP leads to an intersection at the OCP. This intersection point corresponds to the corrosion rate ( $I_{corr}$ ).

The Tafel method is valid for pure charge transfer control. There are several factors that can lead to non-Tafel behavior, for example, diffusion limitations or ohmic resistance that arises from solution resistance, cell geometry and location of the reference electrode [24].

Concerning the analysis issues, a general rule for an accurate Tafel extrapolation says that the extrapolation should start at least 50 to 100 mV away from the OCP [24].

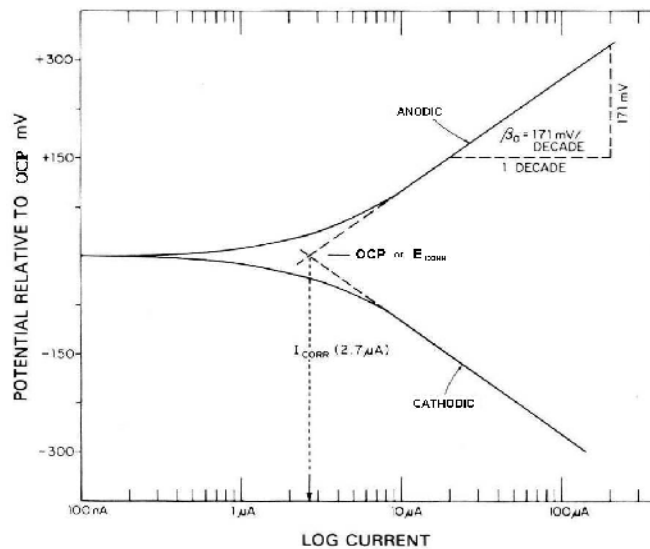


Figure 13. Tafel plot [22]

### 2.6.2 AC electrochemical test method: Electrochemical Impedance Spectroscopy (EIS)

EIS is an important technique for the characterization of electrochemical systems. Thus, an electrochemical process can be modeled by electrical circuit elements such as resistors, capacitors and inductors. The technique helps to understand and to predict accurately corrosion rates and overall corrosion behavior [22].

According to Kelly [24], in this method a small amplitude sinusoidal voltage signal is applied and the resulting current is measured. The equipment processes the current-time and the voltage-time measurements to provide the impedance at different frequencies (impedance spectrum).

When a system is under direct currents (DC) conditions, the DC signal can be viewed as alternating current in the limit of zero frequency. Under these conditions, Ohm's Law can be written as equation (22).

$$R = \frac{V}{I} \quad (22)$$

Where  $V$ , in volts, is the voltage across a resistor  $R$ , in ohms, and,  $I$ , in amperes, is the current.

On the other hand, when the frequency is not zero (AC condition), the Ohm's Law becomes the equation (23). Thereby, the impedance ( $Z$ ) is the term to describe the AC equivalent to DC resistance. Unlike resistance, the impedance of a circuit may depend on the frequency of the applied signal. In this case the resistance is caused by all circuit elements that can impede the current, e.g., resistors, capacitors, and inductors.

$$Z(\omega) = \frac{V(\omega)}{I(\omega)} \quad (23)$$

$$V = V_o \sin(\omega t) \quad (24)$$

$$I = I_o \sin(\omega t + \phi) \quad (25)$$

Where  $\omega$  is the frequency,  $Z(\omega)$  is the impedance (23),  $V(\omega)$  is the time-varying voltage across the circuit (24),  $I(\omega)$  is the time-varying current density through the circuit (25),  $\phi$  is the phase angle and  $t$  is the time.  $Z(\omega)$  is a complex-valued vector quantity with real and imaginary components whose values are frequency dependent (26).

$$Z(\omega) = Z'(\omega) + jZ''(\omega) \quad (26)$$






Where  $Z'(\omega)$  is the real component of impedance,  $Z''(\omega)$  is the imaginary component of impedance and  $j = \sqrt{-1}$  and  $\omega$  is the frequency.

The goal of EIS is to measure the impedance  $Z$  as  $Z'$  and  $Z''$  and then to use basic circuit elements (equivalent circuits) to model the response.

The plot of the real part of impedance against the imaginary part is known as a Nyquist plot, whose advantage is that it gives a quick overview of the data so it is possible to make some qualitative interpretations. An alternative method of plotting is called Bode plot. In this plot, the absolute value of impedance and the phase shifts are plotted as a function of frequency [26].

The equivalent circuit parameters represent and simulate the corroding electrochemical interface. Some of them are depicted in Table 5.

Table 5. Equivalent circuit parameters

Circuit component	Symbol	Impedance
Resistor (R)		$R$
Capacitor (C)		$\frac{1}{j\omega C}$
Inductor (L)		$j\omega L$
Constant Phase Element (CPE)		$\frac{1}{(j\omega C)^a}$
Warburg Impedance infinite diffusion length (W)		$\frac{R}{\sqrt{j\omega}}$



The **resistor (R)** has no imaginary part. The current through a resistor is always in phase with the voltage. Some examples in which a resistor can describe electrochemical phenomena are:  $R_s$  (solution resistance or ohmic resistance) and  $R_{ct}$  (charge transfer resistance).

The **capacitor (C)** describes a double layer capacitance ( $C_{dl}$ ) which exists at the electrode/electrolyte interface. The value of the double layer capacitance depends on many variables including electrode potential, temperature, ionic concentrations, types of ions, electrode roughness, impurity adsorption, etc.

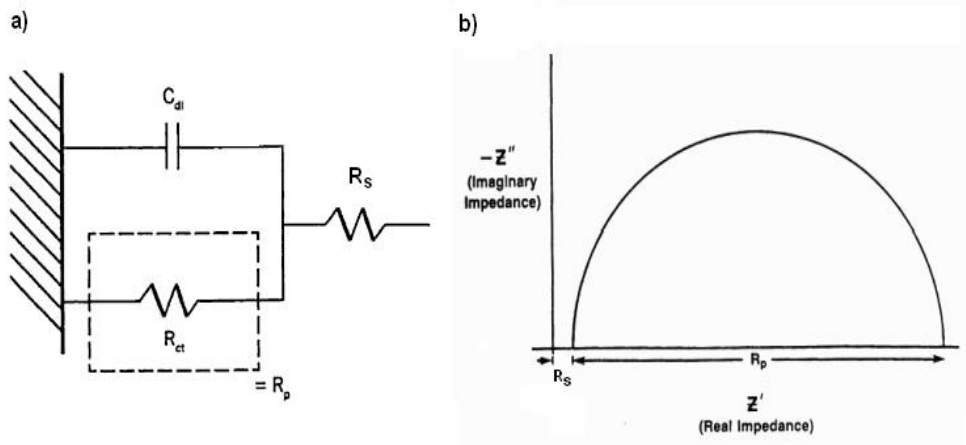
Like a capacitor, an **inductor (L)** has only an imaginary impedance component. In a Nyquist plot, an inductor is represented with a low frequency portion that lies below the real axis. There is no uniform agreement about the causes of an inductive behavior but it can be a result of adsorption processes, inductance of cell cables, etc. [22]

**Constant phase elements (CPEs)** are widely used in data fitting. Capacitors (C) often do not behave ideally; instead, they act like a CPE. For a CPE, the exponent  $\alpha$  is less than one. It has been reported [11] that the physical origin of a CPE may be caused by increase surface roughness or by geometrical effects leading to a non-uniform distribution of the current density on the surface. In a Nyquist plot a CPE can be identified by a depression of a typical capacitive semicircle.

The **Warburg impedance (W)** for infinite diffusion describes the diffusion process. This situation can arise when diffusion through some type of surface film becomes the dominating process. This process may result in the surface being covered with reaction products or adsorbed solution components [22]. The characteristic image in Nyquist plot is the semicircle with the transition into the 45° Warburg line at smaller frequencies [25].

The simplest circuit model is called "Randles circuit" and it is shown in **Figure 14**. The three parameters  $R_{ct}$ ,  $R_s$  and  $C_{dl}$  approximate a corroding electrochemical interface.  $R_s$  is the solution resistance,  $R_{ct}$  is the charge transfer resistance which is, in this case,

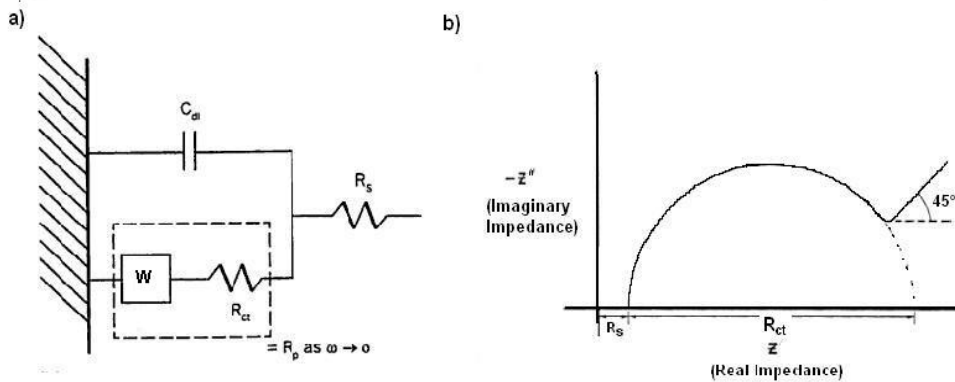
equal to  $R_p$ .  $C_{dl}$  is the double-layer capacitance that appears when an electrochemical interface exists.



a) Electrical equivalent circuit (Randles circuit), b) Nyquist plot of a simple charge transfer corrosion process.

**Figure 14. Model for a simple charge transfer [24]**

Figure 15 shows a model for a simple charge transfer process in presence of diffusion. In this model, unlike the first model, a Warburg component can be observed.



a) Electrical equivalent circuit, b) Nyquist plot of simple charge transfer with diffusion.

**Figure 15. Model for a simple charge transfer process in presence of diffusion [24]**

### 3. EXPERIMENTAL PART

#### 3.1 Synthesis of electroless Ni-P and Ni-P-SiC coatings

##### 3.1.1 Electroless Ni-P bath preparation

Four types of electroless Ni-P baths were prepared: electroless Ni-P baths (electroless simple S1 and S2 baths) and electroless composite baths (C1 and C2). S1 and C1 baths were developed in laboratory whereas S2 and C2 were commercially available baths.

The compositions of the electroless plating baths prepared at the laboratory (S1 and C1) were based on the so-called Hubbell's electrolyte [12] composition. These bath compositions are shown in Table 6.

Table 6. Compositions of the acidic electroless simple and composite baths prepared at the laboratory (pH:4,8, Temperature: 87°C)

Component	Concentration	
	Electroless simple bath (S1)	Electroless composite bath (C1)
NiSO <sub>4</sub> .7H <sub>2</sub> O (Nickel sulfate)	30 g/L	30 g/L
NaH <sub>2</sub> PO <sub>2</sub> .H <sub>2</sub> O (Sodium hypophosphite)	20 g/L	20 g/L
CH <sub>3</sub> CH(OH)COOH (Lactic acid)	25 g/L	25 g/L
CH <sub>3</sub> CH <sub>2</sub> COOH (Propionic Acid)	5 g/L	5 g/L
Pb <sup>2+</sup> as Pb(NO <sub>3</sub> ) <sub>2</sub> (Lead (II) nitrate)	1 mg/L	1 mg/L
SiC (2-5 μm) (Silicon carbide)	-	25g/L

The commercial electroless simple bath S2 consisted of an acid (pH=4,8) type bath with sodium hypophosphite as a reducing agent. The commercial electroless composite bath C2 was prepared by adding SiC micro-particles (25 g/L) to the S2 bath.

### 3.1.1.1 Laboratory materials, equipment and reagents

#### a) Laboratory materials

- 2L beaker
- 25 mL graduated cylinders
- 100 mL glass beakers 100 mL
- Whatman paper N° 42 (particle retention: 2,5 µm)
- 1L volumetric flask 1L
- 1 mL volumetric pipette
- vacuum filtration equipment

#### b) Equipment

- Analytical balance PP 4100S (max. 4100 g, precision: 0, 01 g)
- pH Meter pH M 220
- Electrode pHC 3081 (“single-rod measuring cell”)
- Magnetic stirrer, IKA RCT.

#### c) Reagents

- Nickel sulfate heptahydrate  $\text{NiSO}_4 \cdot 7\text{H}_2\text{O}$ , p.a., Fluka
- Sodium Hypophosphite monohydrate  $\text{NaH}_2\text{PO}_2 \cdot \text{H}_2\text{O}$ , p.a., Fluka
- Lactic Acid  $\text{CH}_3\text{CH}(\text{OH})\text{COOH}$ , p.a., VEB Laborchemie Apolda
- Propionic Acid  $\text{CH}_3\text{CH}_2\text{COOH}$ , p.a., Fluka
- Lead nitrate  $\text{Pb}(\text{NO}_3)_2$ , p.a., Merck
- Sodium hydroxide (NaOH), p.a. CHEMAPOL
- Silicon Carbide (SiC) micro-particles (2-5 µm), flake shape
- Distilled water (max. 3 µS/cm)

### **3.1.1.2 Procedure**

#### **3.1.1.2.1 Preparation of electroless simple bath (S1)**

1L of S1 bath was prepared by weighing and mixing the reagents indicated in Table 6 with approx. 700 mL of distilled water in a 1L beaker. The reagents were dissolved by using a magnetic stirrer.

A 1,6 g/L  $\text{Pb}(\text{NO}_3)_2$  stock solution was prepared and then 1 mL of this solution was added to the bath solution.

Once all the components were dissolved, the pH value was adjusted to 4,8 by adding (drop by drop) NaOH 5N and by reading the variation of pH with a calibrated pH meter. After that, distilled water was added in order to complete a volume of 1L of solution.

Finally, the solution was filtered with vacuum through a Whatman filter paper N° 42 in order to avoid undesirable impurities (e.g. dust) in the electroless bath.

#### **3.1.1.2.2 Preparation of electroless composite bath (C1)**

1L of electroless composite bath C1 was prepared by adding 25 g of SiC micro-particles to 1L of previously prepared electroless simple bath (S1).

#### **3.1.1.2.3 Electroless comercial simple bath (S2)**

1L of electroless comercial simple bath S2 was filtered with vacuum trough a Whatman filter paper N° 42 in order to avoid undesirable particles (e.g. dust).

#### **3.1.1.2.4 Electroless comercial composite bath (C2)**

1L of electroless comercial composite bath C2 was prepared by adding 25 g of the SiC micro particles to 1L of a previous filtered electroless comercial simple bath (S2).

### 3.1.2 Chemical analysis of electroless of Ni-P baths

The electroless Ni-P baths were analyzed before and after the electroless-deposition process in order to control the concentration of some parameters (nickel (II) concentration, hypophosphite concentration and pH value) and to calculate the required quantity of nickel sulfate, sodium hypophosphite for bath replenishment.

After the electroless deposition process the baths were replenished to their initial composition by adding the required volume of NiSO<sub>4</sub> 1M and NaH<sub>2</sub>PO<sub>2</sub> 3M stock solutions. The pH value was also corrected by adding the required volume of NaOH 5N solution. The maximal number of replenishments for a Ni-P electroless baths was three in order to avoid any influence of bath age in the structure and composition deposits.

#### 3.1.2.1 Nickel determination

The nickel concentration can be determined (in a range of pH from 4 to 6) by volumetric titration method with Pb(NO<sub>3</sub>)<sub>2</sub> solution and xylenolorange indicator [36].

##### 3.1.2.1.1 Laboratory materials and reagents

###### a) Laboratory materials

- 10 mL and 25 mL volumetric pipettes
- 300 mL erlenmeyer flask
- 25 mL buret 25 mL
- 25 mL graduated cylinders

###### b) Reagents

- 0,1 M EDTA solution, Titriplex III Merck
- Pb(NO<sub>3</sub>)<sub>2</sub> , ACS, Merck
- Urotropine (hexamethylenetetramine), p.a., Sigma-Aldrich
- Xylenol orange indicator, ACS, Merck
- pH paper indicator (range: 0 to14), Merck
- Distilled water (max. 3 μS/cm)

### 3.1.2.1.2 Analysis

First, the pH value of the bath was verified to be in a range of 4 to 6 with a pH paper indicator.

Then, an aliquot of 10 mL of the bath was taken with a volumetric pipette and then placed in an Erlenmeyer flask. 25 mL of 0,05 M EDTA solution, 20 mL of 20 wt% urotropine solution and a dash (little portion) of solid xylenol orange indicator were added. Distilled water was also added in order to dilute the mixture until 120 mL approximately.

Then, the sample was titrated with 0,05 M  $\text{Pb}(\text{NO}_3)_2$  solution until the color changed from yellow-green to violet-blue. **Figure 16** shows the change of color at the equivalence point in the volumetric titration analysis.

The volume of 0,05 M  $\text{Pb}(\text{NO}_3)_2$  required for carrying out the titration was registered for calculation.

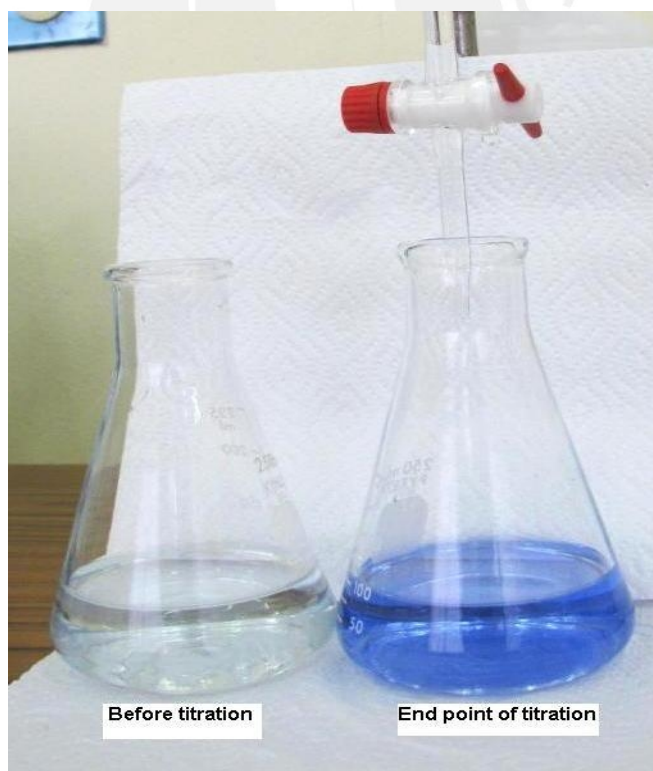


Figure 16. Nickel determination by volumetric titration method

### 3.1.2.1.3 Calculation

The concentration of Nickel (mol/L) was determined according the equation (27).

$$C_{Ni} = \frac{V_{EDTA} \times C_{EDTA} \times f_{EDTA} - V_{Pb} \times C_{Pb} \times f_{Pb}}{V_{sol}} \quad (27)$$

with:

$C_{Ni}$ : Molar concentration (mol/L) of  $Ni_{(ac)}^{2+}$  ions in the bath solution

$V_{EDTA}$ : Volume (mL) of the EDTA solution

$C_{EDTA}$ : Molar concentration (mol/L) of the EDTA solution

$f_{EDTA}$ : Stoichiometric factor of the EDTA solution

$V_{Pb}$ : Volume (mL) of  $Pb(NO_3)_2$  solution

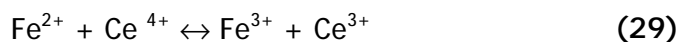
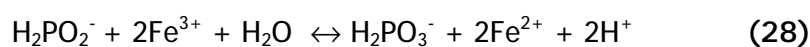
$C_{Pb}$ : Molar concentration of  $Pb(NO_3)_2$

$f_{Pb}$ : Stoichiometric factor of  $Pb(NO_3)_2$

$V_{sol}$ : Volume (mL) of the bath solution

### 3.1.2.2 Hypophosphite Determination

The oxidation of hypophosphite is carried out with Iron (III) ions in hydrochloric acid solution, then the amount of iron (II)-ions formed can be estimated through titration with cerium (IV) - sulfate solution in a sulfuric acid solution with Ferroin indicator [36]. The equations (28) and (29) show chemical reactions involved in the method.



#### 3.1.2.2.1 Laboratory materials, equipment and reagents

##### a) Laboratory materials

- Volumetric pipettes: 5mL, 10 mL, 25 mL
- 300 mL erlenmeyer flask
- 25 mL buret
- Graduated cylinders: 25mL, 50 mL



## b) Equipment

- Hot plate IKA-RCT

## c) Reagents

- $\text{FeCl}_3 \cdot 6\text{H}_2\text{O}$ , ACS, Merck
- HCl acid fuming 37%, p.a., Merck
- $\text{H}_2\text{SO}_4$  95-97%, p.a., Merck
- $\text{Ce}(\text{SO}_4)_2 \cdot 4\text{H}_2\text{O}$ , p.a., Merck
- 0,025 M Ferroin solution, Merck
- Distilled water (max. 3  $\mu\text{S}/\text{cm}$ )

### 3.1.2.2.2 Analysis

A 5 mL aliquot of the bath was taken with a volumetric pipette and then placed in an Erlenmeyer flask. Then 30 mL of 2N HCl solution and 30 mL of 0,1 M  $\text{FeCl}_3$  solution (27g/L  $\text{FeCl}_3 \cdot 6\text{H}_2\text{O}$  in 1N  $\text{H}_2\text{SO}_4$  solution) were added; the solution was diluted until approximately 100 mL with distilled water. The sample was digested in a hot plate for 20 minutes and then cooled to room temperature. After that, 20 mL 10 wt%  $\text{H}_2\text{SO}_4$  solution and two drops of ferroin indicator solution were added.

The sample was titrated with 0,1 N  $\text{Ce}(\text{SO}_4)_2$  solution (40,43 g/L  $\text{Ce}(\text{SO}_4)_2 \cdot 4\text{H}_2\text{O}$  in 0,5 M  $\text{H}_2\text{SO}_4$  solution) until the color changed from orange to yellow-green. **Figure 17** shows the change of color at the equivalence point in the volumetric titration analysis. The volume of 0,1 N  $\text{Ce}(\text{SO}_4)_2$  solution required for carrying out the titration was registered for calculation.



Figure 17. Hypophosphite determination by titration with Cerium (IV)

### 3.1.2.2.3 Calculation

The concentration of hypophosphite (mol/L) was determined according the equation (30).

$$C_{H_2PO_2^-} = \frac{V_{Ce} \times C_{Ce} \times f_{Ce}}{2V_{sol}} \quad (30)$$

with:

$C_{H_2PO_2^-}$  : Molar concentration (mol/L) of  $H_2PO_2^-$  ions in the Ni-electrolyte solution

$V_{Ce}$  : Volume (mL) of  $Ce(SO_4)_2$  solution

$C_{Ce}$  : Molar concentration (mol/L) of the  $Ce(SO_4)_2$  solution

$f_{Ce}$  : Stoichiometric factor of the  $Ce(SO_4)_2$  solution

$V_{sol}$ : Volume (mL) of the electroless Ni-P bath

### 3.1.2.3 pH Determination

The pH values of electroless Ni-P baths were measured using a potentiometer and a glass pH electrode.

### 3.1.2.3.1 Laboratory materials, equipment and reagents

#### a) Laboratory materials

- 25 mL glass beakers
- Magnetic stir bar

#### b) Equipment

- pH Meter Radiometer, pH M 220
- Electrode pHC 3081 (“single-rod measuring cell”)
- Magnetic stirrer IKA-RCT

#### c) Reagents

- Distilled water (max. 3  $\mu\text{S}/\text{cm}$ )
- Calibration buffers: WTW pH 4,01 and pH 7,00

### 3.1.2.3.2 Analysis

It was performed a two points calibration by measuring the pH of commercially available calibration buffers: 4,01 and 7,00. The calibration acceptance criterion was that the slope of calibration must have been within the admissible range: -60 to -50 mV/pH.

Once the calibration was done, an aliquot of sample (approx. 25 mL) was transferred to a glass beaker, and then the solution was slightly stirred. The glass electrode was introduced into the solution and then, after stabilization, the pH value was read and registered.

### 3.1.3 Electroless deposition process of Ni-P and composite Ni-P-SiC coatings

The general process is summarized in the diagram shown in Figure 18.

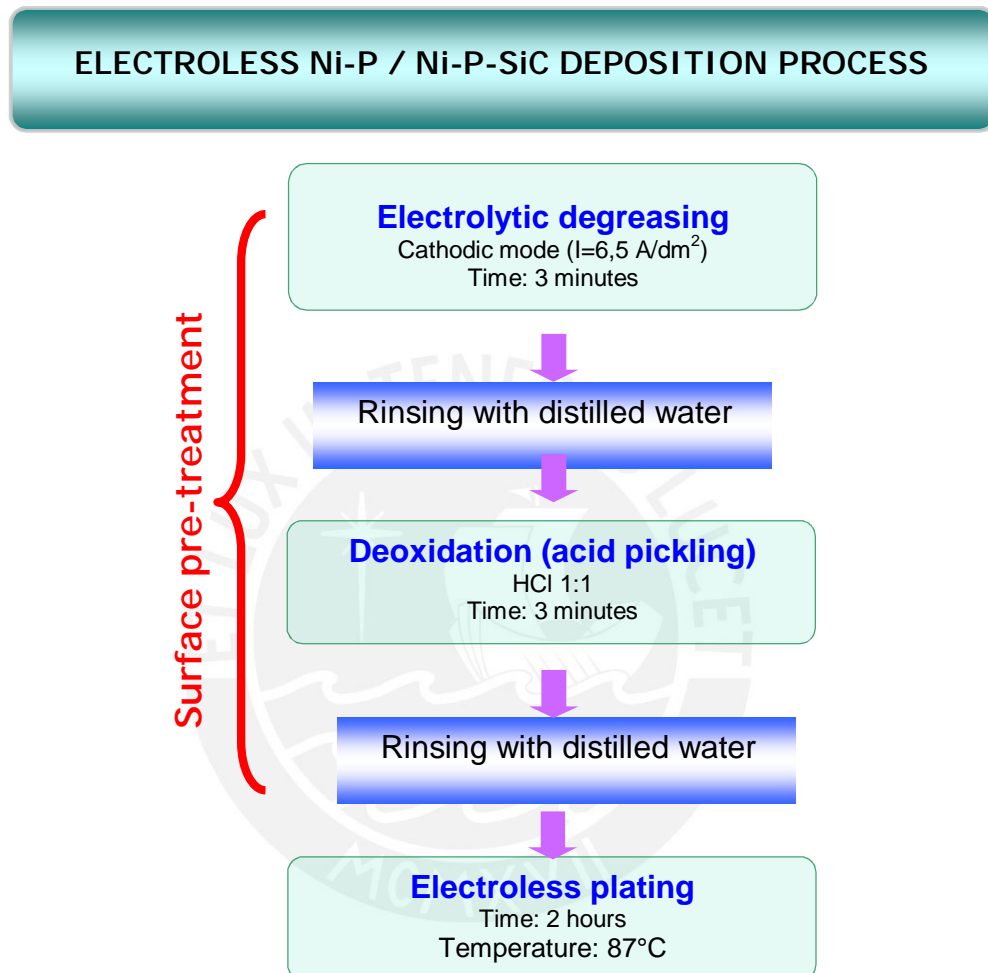


Figure 18. Electroless Ni-P/Ni-P-SiC deposition process

#### 3.1.3.1 Substrate pre-treatment

Low carbon steel panels were used as substrates. The panels were made from standard low-carbon, cold-rolled steel complying with ASTM A1008, A-109, and QQS-698 standard norms [27]. The dimensions of each panel were 9 x 5 x 0,05 cm. The surface finish was smooth ( $R_a$  (average roughness) <20 micro inches). Figure 19 shows a picture of the low carbon steel panel. The chemical composition (\*) of the low carbon steel panel is shown in Table 7.



Figure 19. Low carbon steel panel

Table 7. Chemical composition of substrate [27]

Element	Manganese	Carbon	Phosphorus	Sulfur
Percentage (wt%)	0,60 max	0,15 max	0,03 max	0,035 max

(\*) Fe: Balance

The panels were cut and two sizes of substrates were obtained. For deposition of Ni-P coatings the substrate dimensions were 5 x 4,5 x 0,05 cm; for deposition of Ni-P-SiC composite coatings the substrate dimensions were 2,5 x 4,5 x 0,05 cm.

### 3.1.3.1.1 Laboratory materials, equipment and reagents

#### a) Laboratory materials

- 400 mL glass beakers
- Insulated copper leads and alligator clips
- Stainless steel sheet (anode)
- Holder for substrate
- Chronometer

#### b) Equipment

- Power source Voltcraft DIGI 40 (0-40V/5A)

### c) Reagents

- Commercial alkaline cleaning solution
- HCl acid 37%, p.a., Merck
- Distilled water (max. 3  $\mu\text{S}/\text{cm}$ )

#### 3.1.3.1.2 Procedure

The substrate pre-treatment was done in order to clean the substrate surface and provide a good adhesion between substrate and coating. The most common undesirable contaminants are grease, dust and corrosion products.

The first step was electrolytic degreasing (cathodic mode). The panel was introduced in a beaker containing commercial alkaline cleaning solution at room temperature and then it was connected to a power source. The substrate (cathode) was connected to the negative output and a steel sheet (anode) was connected to the positive output. The time of cleaning was 3 minutes and the applied current density was 6,5 A/dm<sup>2</sup>. The substrate was then rinsed by successive immersion (three times) in distilled water. Figure 20 shows the electrolytic degreasing experimental setup.

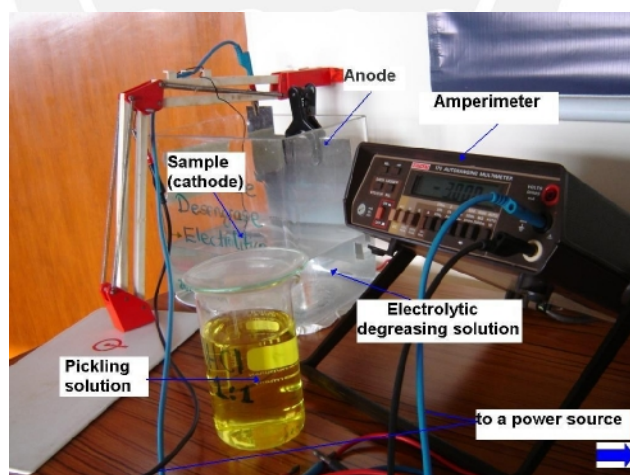


Figure 20. Electrolytic degreasing of the substrate

The second step was the substrate deoxidation (acid pickling). It was made in order to remove any surface oxidation of the substrate. The substrate was immersed in HCl

(1:1 v/v) solution for 3 minutes at room temperature. The substrate was then rinsed by successive immersion (three times) in distilled water.

### 3.1.3.2 Electroless deposition process

#### 3.1.3.2.1 Ni-P coatings

##### 3.1.3.2.1.1 Laboratory materials, equipment and reagents

###### a) Laboratory materials

- 2L glass beaker
- Insulated copper leads
- Holder for the substrate
- Chronometer

###### b) Equipment

- Water bath IKA TE2 (max. 199°C,  $\pm 1^\circ\text{C}$ )
- Hair dryer

###### c) Reagents

- Electroless platings baths S1 and S2 (see section 3.1.1)
- Distilled water

##### 3.1.3.2.1.2 Procedure

The electroless Ni-P plating was carried out immediately after the substrate pre-treatment (see section 3.1.3.1). The substrate was vertically immersed in 1,5 L of electroless Ni-P bath at 87°C. The bath was agitated by natural convection. The bath loading was 0,3 dm<sup>2</sup>/L and the deposition time was 2 hours.

After 2 hours of deposition, the sample was rinsed with distilled water and dried with hot air (using a hair dryer).

The experimental setup is shown in **Figure 21**.

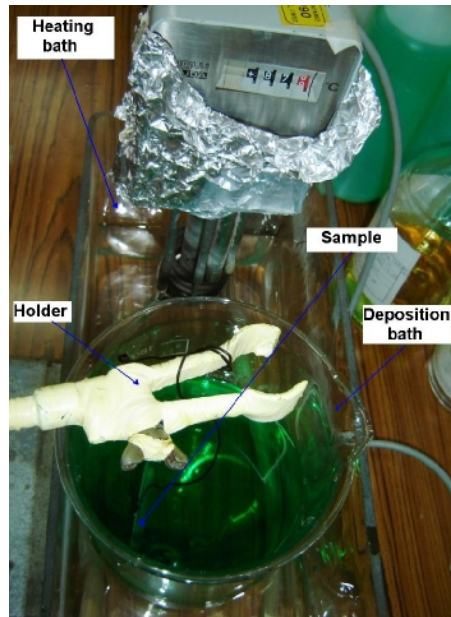


Figure 21. Experimental setup for electroless deposition of Ni-P coatings

### 3.1.3.2.2 Ni-P-SiC composite coatings

#### 3.1.3.2.2.1 Laboratory materials, equipment and reagents

##### a) Laboratory materials

- 2L glass beaker
- Two bladed glass stirring element
- Holder for the substrate.
- Chronometer

##### b) Equipment

- Water bath IKA TE2 (max. 199°C,  $\pm 1^\circ\text{C}$ )
- Mechanical stirrer IKA RW (20.n)
- Hair dryer

##### c) Reagents

- Distilled water
- Electroless platings baths C1 and C2 (see section 3.1.1)



### 3.1.3.2.2 Procedure

The electroless deposition of Ni-P-SiC composite coatings was carried out on the panel of smaller size (see section 3.1.3.1). The bath loading was 0,15 dm<sup>2</sup>/L.

The electroless bath containing dispersed SiC micro- sized particles was mechanically stirred at approx. 500 rpm with a two-bladed glass stirring element. The stirring element was positioned in the center of the bath. In order to maximize the suspension (avoiding sedimentation) of the micro-sized SiC particles, the tip of the stirring element was positioned close to the base of the bath (at approx. 2 cm).

The bath was set to 87°C, then the substrate (previously pre-treated, see section 3.1.3.1) was immersed in the bath. The time of deposition was 2 hours.

The sample was vertically positioned and parallel oriented to the flow direction of the bath. The two faces of the panel were identified: the face in front of the stirring element was labeled as a “front side” and the opposite face was labeled as a “back side”. **Figure 22** depicts a top view schema of the bath setting.

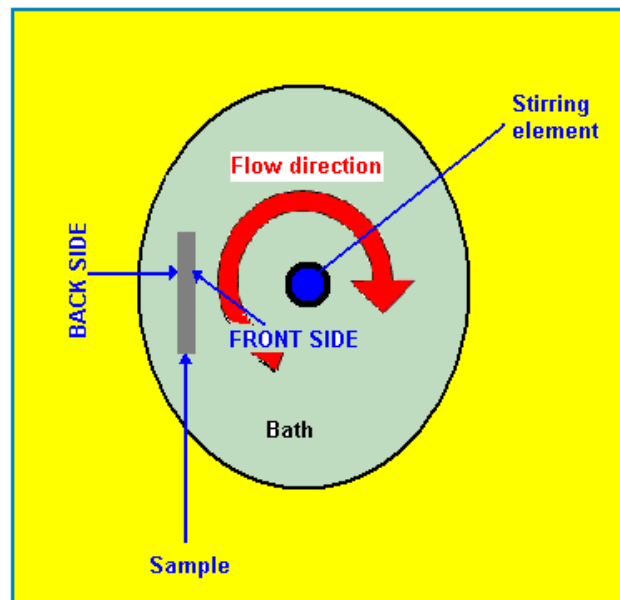


Figure 22. Top view schema of the bath setting

Figure 23 and Figure 24 depict the stirring element and the experimental setup for electroless deposition of Ni-P-SiC composite coatings respectively.



Figure 23. Two-bladed glass stirring element

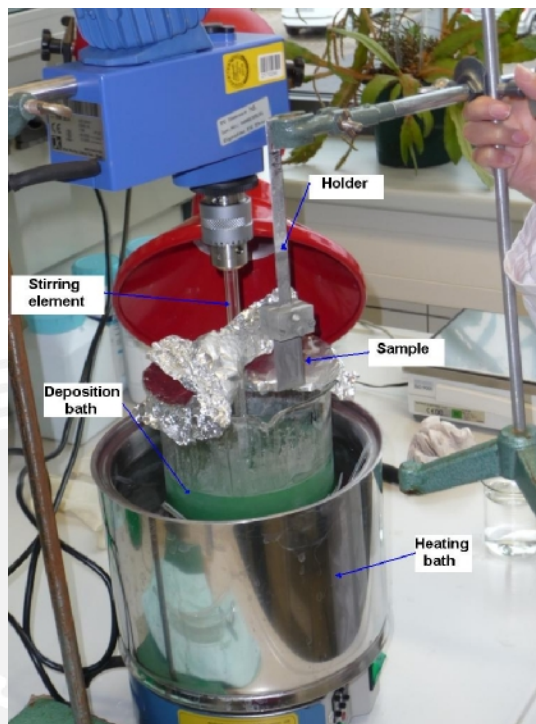


Figure 24. Experimental setup for electroless deposition of Ni-P-SiC composite coatings

After 2 hours of deposition, the sample was rinsed with distilled water and dried with hot air (using a hair dryer).

### 3.2 Characterization of electroless Ni-P and Ni-P-SiC coatings

#### 3.2.1 Surface Morphology

The surface morphology of as-plated Ni-P and Ni-P-SiC coatings was studied by *scanning electron microscopy* (SEM) using a Philips XL 30 scanning electron microscope equipped with a quantitative energy dispersive X-ray spectrometer (FEI Corp.). The samples were examined at top and cross-sectional views.

For studying the cross-section surface, the samples were mounted in resin with the transverse side positioned for examination. The surface was ground with 240, 600 and 1200 SiC papers and then polished with diamond emulsion (3 $\mu$ m and then 1 $\mu$ m).

### 3.2.2 Microstructure

The microstructure of Ni-P and Ni-P-SiC was studied by X-ray diffraction (XRD). An X-ray diffractometer (Bruker AXS D 5000) with Goebel mirror was used. The sizes of the samples were approx. 1cm<sup>2</sup>. Then, the XRD patterns were obtained.

The method of study was *grazing incidence diffraction* [28]. This method is suitable for characterization of surfaces and thin films avoiding the influence of the substrate. For thin films, measurement via grazing incidence diffraction is more suitable, here the x-ray source is fixed at a small angle (1°-3°) whereas the detector is moving. This prevents that X-ray beam from entering too deep into the surface and getting an influence of the substrate in the results. For grazing incidence, it is necessary to have a parallel non divergent beam which is provided by a Goebel mirror [28].

### 3.2.3 Chemical composition

The chemical compositions of Ni-P and Ni-P-SiC deposits were determined by *energy dispersive X-ray analysis* (EDX) and *glow discharge optical emission spectroscopy* (GDOS).

#### 3.2.3.1 Energy dispersive X-ray spectroscopy (EDX)

The incidence of an electron beam on a surface sample can result in the emission of characteristic X-rays. These X-rays are detected and characterized in terms of their wavelength and energy. Thus, simultaneous determination of all chemical elements (from sodium to uranium) in point, line or mapping form on surface samples is possible through EDX analysis [29].

EDX analyses were carried out through a line scan on the top surface of the as-plated Ni-P and Ni-P-SiC deposits. A Philips XL 30 scanning electron microscope equipped with a quantitative energy dispersive X-ray spectrometer (FEI Corp.) was used.

### 3.2.3.2 Glow discharge optical emission spectroscopy (GDOS)

Analysis by GDOS allows the determination of elemental composition as a function of depth (depth-profile analysis). A glow discharge source produces positively charged argon ions to sputter the sample surface, and then the excited sample atoms relax by means of photo emission. The wavelengths of the photons are characteristic for each emitting species. Thereby, the registration of emission intensities over time as surface layers are sputtered away produces the depth-profile of the sample [30].

GDOS analyses were carried out with a GDA 750 Spectrumba instrument equipped with a 2,5 DC source (1000V, 13mA). The diameter of the exposed area was 2,5 mm.

Figure 25 shows a surface area after a GDOS analysis. It can be seen that GDOS is a destructive method of analysis.

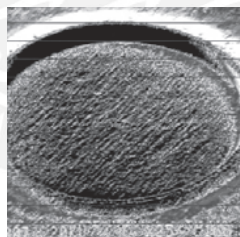


Figure 25. Area of a sample after GDOS analysis [31]

### 3.2.4 Measurement of coating thickness by magnetic induction method

The coatings thickness were determined by magnetic induction method and then confirmed through SEM in the surface cross-section of the samples.

Magnetic induction method is applicable to magnetic substrates plated with autocatalytic nickel deposits containing more than 10 wt% P content (non-magnetic alloys) and that have not been heat-treated [1].

The thickness measurements in the Ni-P and Ni-P-SiC deposits were carried out with a Deltascop MP30 (Fischer ®) thickness tester according with ASTM B 499-96 standard norm [32].

The experimental setup for thickness measurements by magnetic induction method is shown in Figure 26.

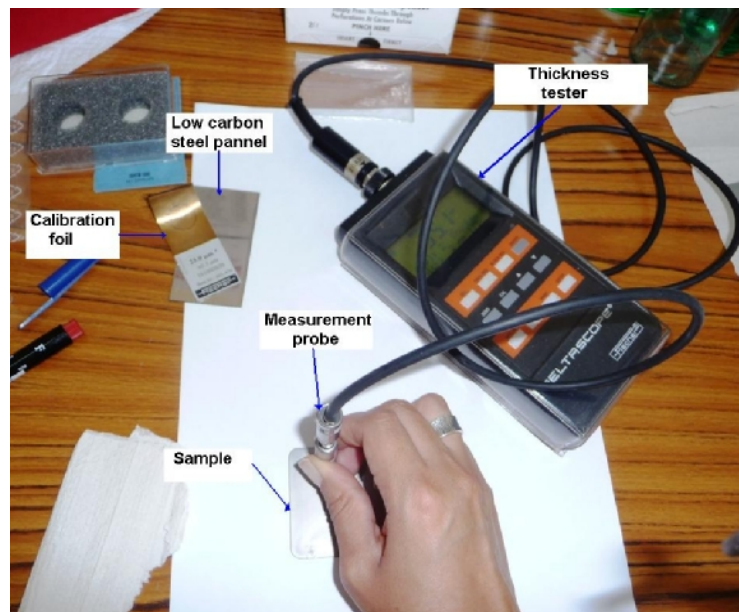


Figure 26. The experimental setup for coating thickness measurement by magnetic induction method

Three readings on each side of the substrate were taken and the thickness values were registered. A calibration procedure was done before each sample measurement; it consisted of the thickness measurement of a calibration foil ( $23\mu\text{m} \pm 0,5 \mu\text{m}$ ) on a low carbon steel panel which was mentioned in section 3.1.3.1.

### 3.2.5 Vickers hardness test

Microhardness measurements were made on the cross-sections of the as-plated deposits of Ni-P and Ni-P-SiC coatings using a Fischerscope H100 micro hardness tester and according to DIN EN ISO 14577. The samples used for cross-section surface SEM analysis (see section 3.2.1) were also used for hardness measurement. Three readings were taken on each sample and the values were then averaged.

The experimental arrangement for Vickers hardness test is illustrated in **Figure 27**. This method uses a square based diamond pyramid indenter and a specific load applied for 10 to 15 seconds.

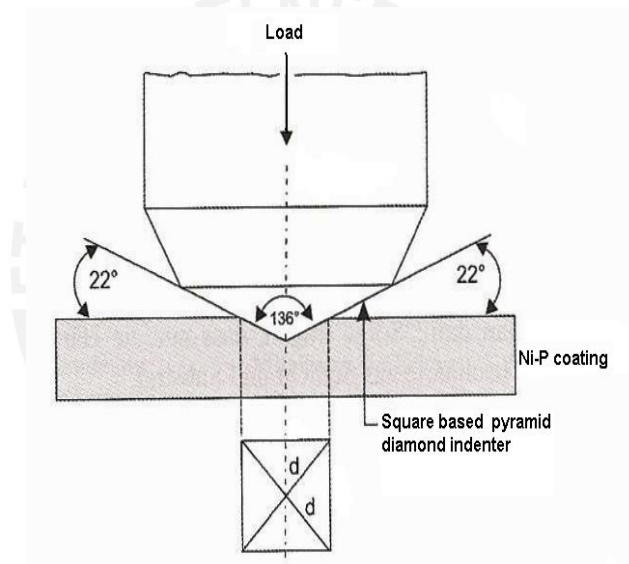


Figure 27. Vickers hardness measurement<sup>12</sup>

The Vickers hardness value is determined by dividing the load by the indented surface area. Thus, the diagonal length of the indentation is measured and used to obtain the hardness according to equation (31).

$$HV = 0,189 \frac{F}{d^2} \quad (31)$$

Where  $F$  is the applied load (N), and  $d$  (mm) is the mean length of indentation diagonals for a standard pyramid angle of 136°.

### 3.2.6 Evaluation of the corrosion resistance in NaCl 3,5 % by electrochemical techniques

#### 3.2.6.1 Electrochemical cell setup

The electrochemical tests were performed by using a conventional three-electrode electrochemical cell setup: the sample (Ni-P or Ni-P-SiC deposit) as the working electrode (WE), a silver/silver chloride electrode (Ag/AgCl 3M KCl; 0,207 V vs. ENH) as the reference electrode (RE) and a platinum wire as the auxiliary electrode (AE). The electrochemical cell consisted of a glass cylinder with a PTFE bottom plate containing a hole in central position. A rubber O-ring seal (diameter 0,5 cm) was located around the hole. The electrochemical cell setup is depicted in Figure 28.

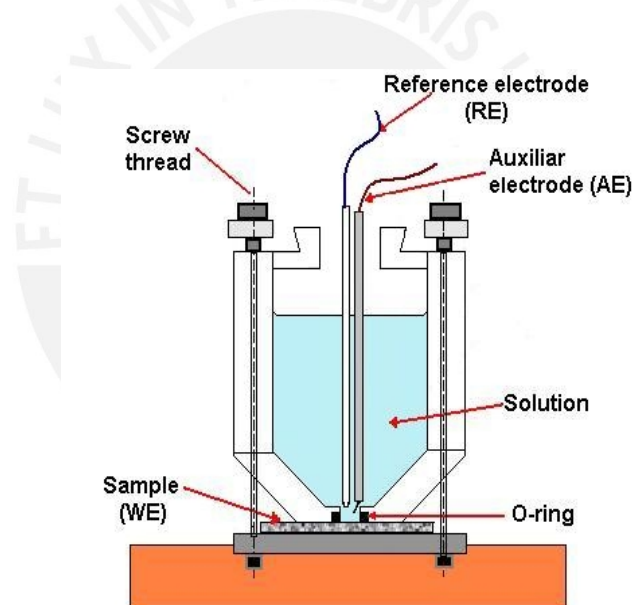


Figure 28. Electrochemical cell setup

#### 3.2.6.2 Test of equipment

All the electrochemical tests were performed using an Autolab PGSTAT 302N potentiostat/galvanostat equipped with a FRA2 impedance module. This equipment was controlled by NOVA software, version 1.4.

The electrical performance of the potentiostat/galvanostat was checked by running an impedance test with a dummy cell (EG&G Princeton Applied Research model 1700–1126 Rev. 0) according to ASTM G106-89 (Reapproved 2010) [37]. The dummy cell consisted of a 10  $\Omega$  resistor placed in series with a circuit element composed of a 100  $\Omega$  resistor in parallel with a 100  $\mu\text{F}$  capacitor. A view of the dummy cell circuit is shown in Figure 29.

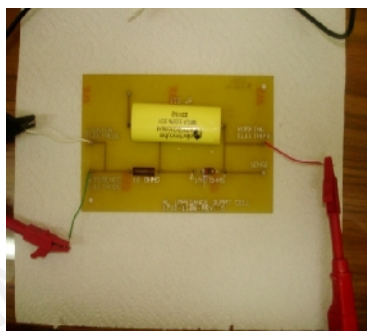


Figure 29. Dummy cell circuit

#### 3.2.6.3 Electrolyte preparation

The electrolytic solution used in this study was prepared by dissolving NaCl (p.a., Merck) in distilled water to give 3,5 wt.%. In order to carry out tests with a constant concentration of oxygen in the salt solution, the electrolyte was air-saturated by bubbling air for 30 minutes. An air membrane pump (WISA Model 120) was used. For each test about 40 mL of solution was used.

#### 3.2.6.4 Sample mounting

Before running an electrochemical test the sample was degreased with acetone, rinsed with distilled water and then dried using a hair drier.

The sample was positioned under the electrochemical cell, and the sample holder and the electrochemical cell were carefully clamped and fixed through two screws, as shown in Figure 30. The exposed area of the sample was 0,2 cm<sup>2</sup>.



The electrolyte solution (NaCl 3,5%) was poured into the electrochemical cell; in case of formation of air bubbles at the sample surface, they were removed with a Pasteur pipette.

The reference electrode (RE) and the auxiliary electrode (AE) were immersed in the electrochemical cell, and both positioned very close (approx. 0,25 cm) to the sample surface., as can be seen in Figure 28. The three electrodes (RE, AE and WE) were connected to the potentiostat/galvanostat through insulated copper leads and alligator clips. The experimental arrangement is shown in Figure 30. All the tests were performed at room temperature (approx. 25 °C).

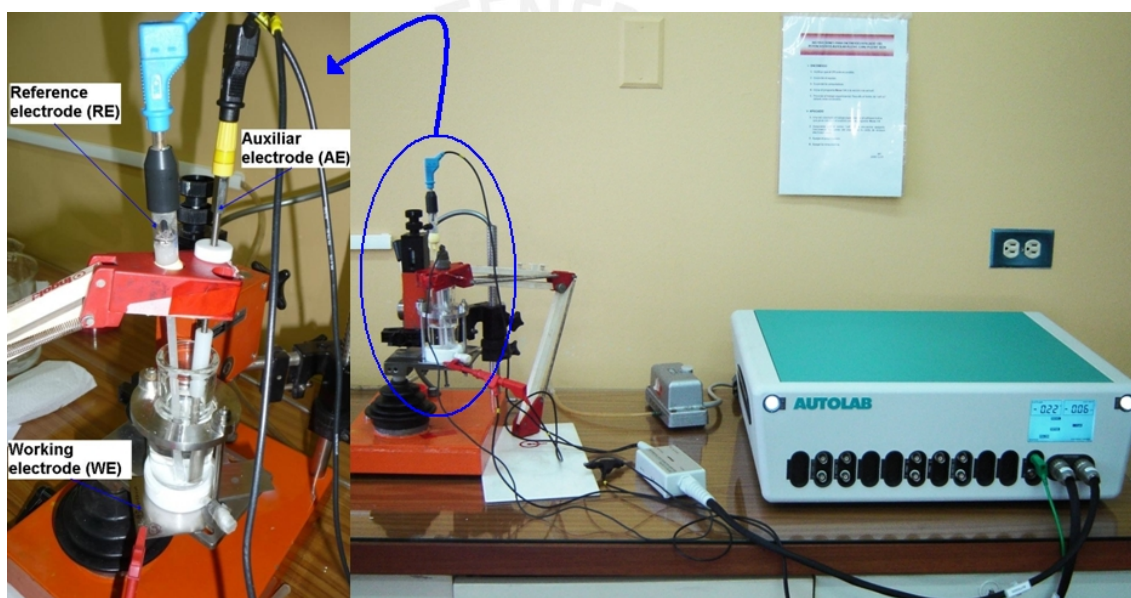


Figure 30. Experimental electrochemical cell connected to the potentiostat/galvanostat equipment

### 3.2.6.5 Open circuit potential (OCP) measurement

The OCP (or *corrosion potential*,  $E_{\text{corr}}$ ) measurement was performed monitoring the voltage of the sample (WE) in the NaCl 3,5% solution versus the reference electrode (RE). A voltage difference less than 5 mV in 10 minutes is a practical criterion to determine a stable OCP value [33].

In order to select the period of time in which the OCP value should be considered to be stable (when the system approach steady state), the OCP value was continuously measured versus the reference electrode (RE) for 2,5 h three times. After evaluation of the results of three measurements, the required time for determining the OCP value was set in 1 hour.

### 3.2.6.6 Potentiodynamic anodic polarization

The potentiodynamic anodic polarization studies were carried out scanning the potential from the previously determined OCP value till 1,0 V versus the OCP value. The measurement conditions are described in Table 8. The scan rate was selected according to ASTM G5-94 (Reapproved 2004) [34].

Table 8. Measurement conditions for potentiodynamic polarization tests

Parameter	Value
Start potential (V)	0,0 vs OCP
Stop potential (V)	1,0 vs OCP
Scan rate (V/s)	$1,6 \times 10^{-4}$
Step potential (V)	$1,0 \times 10^{-3}$
Total number of points	1012

### 3.2.6.7 Cathodic and anodic polarization (Tafel plots)

Tafel plots were obtained by scanning the potential from -0,25V to 0,25V versus the previously determined OCP value (section 3.2.6.6). The electrochemical parameters obtained from this technique are described in section 2.6.1.4. The measurement conditions are described in Table 9.

Table 9. Measurement conditions for Tafel plots

Parameter	Value
Start potential (V)	-0,25 vs OCP
Stop potential (V)	0,25 vs OCP
Scan rate (V/s)	$1,6 \times 10^{-4}$
Step potential (V)	$1,0 \times 10^{-3}$
Total number of points	513

### 3.2.6.8 Linear polarization resistance (LPR)

LPR plots were obtained by scanning the potential from -0,02 V to 0,02 V versus the previously determined OCP value (section 3.2.6.6). The  $R_p$  values were calculated according to section (2.6.1.3). The measurement conditions are described in Table 10.

Table 10. Measurement conditions for LPR tests

Parameter	Value
Start potential (V)	-0,02 vs OCP
Stop potential (V)	0,02 vs OCP
Scan rate (V/s)	$1,6 \times 10^{-4}$
Step potential (V)	$1,22 \times 10^{-3}$
Total number of points	45

### 3.2.6.9 Electrochemical impedance spectroscopy (EIS)

EIS measurements were carried out applying a small-amplitude voltage (10mV) in a sine wave form at the previously determined OCP value (section 3.2.6.6). The scan frequency ranged from 10 kHz to 1 mHz. A Nyquist format (real impedance response versus the negative of the imaginary impedance response) was plotted. The measurement conditions are described in Table 11.

Table 11. Measurement conditions for electrochemical impedance tests

Parameter	Value
Applied AC amplitude (V)	0,01
First applied frequency (Hz)	10000
Last applied frequency (Hz)	0,001
Number of frequencies	50
Wave type	Single sine

## 4. RESULTS AND DISCUSSION

### 4.1 Synthesis of electroless Ni-P and Ni-P-SiC coatings

The Ni-P and Ni-P-SiC coatings obtained from electroless plating process are classified according to the baths employed for their synthesis (see section 3.1.1). The assigned codes of the four deposits are shown in Table 12.

Table 12. Codes of Ni-P and Ni-P-SiC deposits obtained

	Simple baths	Composite baths
Baths prepared at laboratory	S1	C1
Commercial baths	S2	C2

The macroscopic aspect of the obtained Ni-P and Ni-P-SiC deposits is shown in Figure 31. The resulting Ni-P deposits (S1 and S2) were bright and smooth whereas the composite Ni-P-SiC deposits (C1 and C2) were matte and rough.

At first view, the deposits S1 and S2 were uniform on both sides of the samples, whereas composite deposits C1 and C2 showed some defects at the “back” sides (see Figure 22), such as bright zones (apparently without incorporation of SiC particles on the Ni-P matrix). This kind of defect was observed when the synthesis was carried out in substrates with a size of 5cm x 4,5 cm (the same used for obtaining deposits S1 and S2). One example is depicted in Figure 32. It can be seen that the panel has a shiny area (signaled with a white arrow) in which the incorporation of the SiC micro-particles was poor. This failure was observed only on the back side of the samples, which could be ascribed to its position inside the bath. The uniformity and good incorporation of particles at the Ni-P matrix in the frontal sides of substrates could be due to the orientation of these sides in direction of the stirring element, so they had a better contact with the directional flow of the bath.

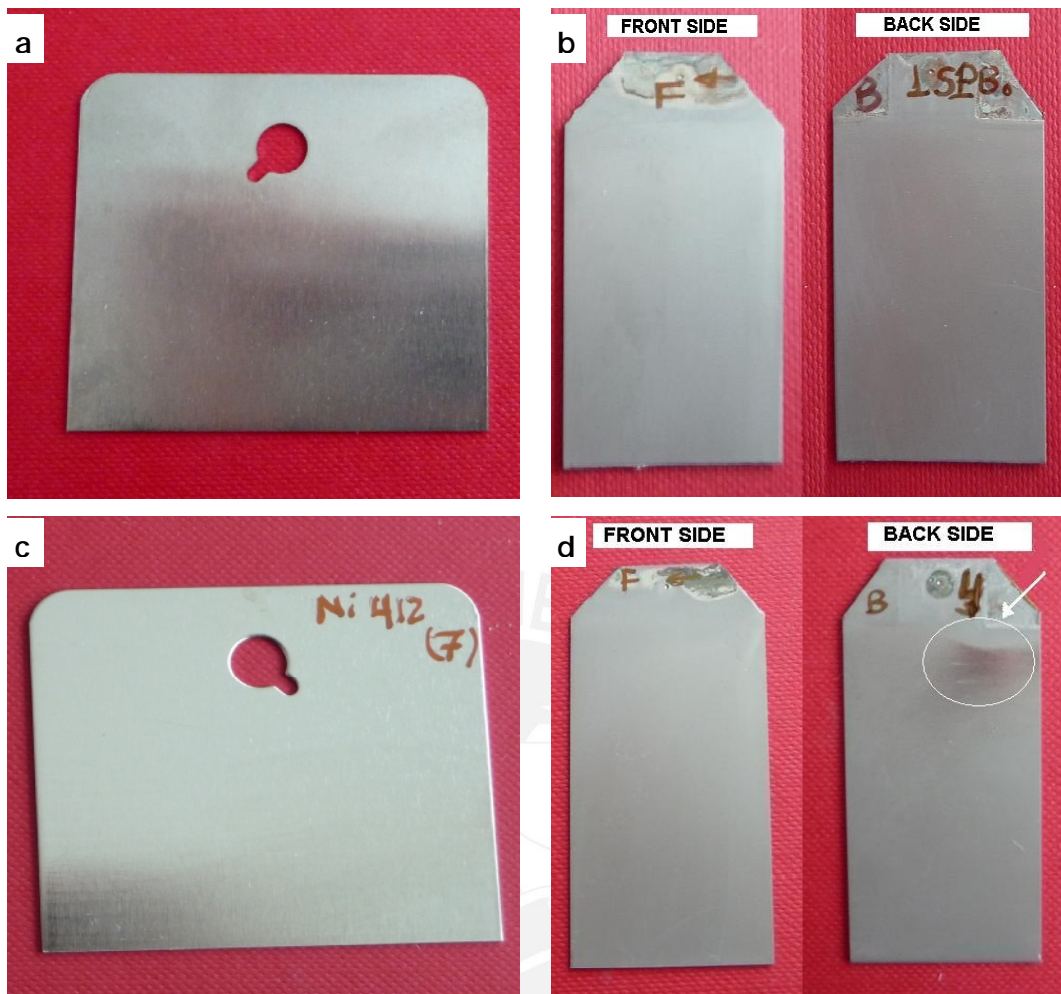


Figure 31. Ni-P and Ni-P-SiC deposits plated on low carbon steel panels obtained according the type of plating bath used: a) S1, b) C1, c) S2, and d) C2



Figure 32. Back side of a substrate after Ni-P-SiC electroless deposition showing a zone with poor SiC incorporation

It was established that working with smaller substrates helped to minimize this problem. For that reason the substrates used for composite deposits were chosen to be smaller (2,5cm x 4,5 cm) than those used for Ni-P deposits (S1 and S2) However, this problem could not be completely avoid. As shown in **Figure 31d**, the back side of the sample still contains a little shiny area (signalled with a white arrow) in which low particles incorporation was evident. To avoid any influence own to the presence of this kind of defects all the different characterization studies and electrochemical tests (with exception of thickness measurement) were performed using only the frontal side of Ni-P-SiC deposits.

#### 4.2 Chemical analysis of electroless Ni-P baths

The results of the chemical analysis of the electroless plating baths are shown in **Tables 13, 14, 15 and 16**. For each type of bath the nickel concentration, hypophosphite concentration and pH value were determined before and after the electroless plating process. The shown values resulted from measurements of three baths with the same composition. Details about the determination of nickel and hypophosphite are described in Appendix 1 and Appendix 2 respectively.

**Table 13. Chemical analysis of S1 bath**

		S1				
Parameter		N° Bath			Average	Variation (%)
		1	2	3		
Nickel Ni <sup>2+</sup> (mol/L)	Before	0,103	0,107	0,105	0,105	-11,4
	After	0,087	0,096	0,097	0,093	
Hypophosphite H <sub>2</sub> PO <sub>2</sub> <sup>-</sup> (mol/L)	Before	0,175	0,188	0,179	0,181	-14,9
	After	0,143	0,169	0,149	0,154	
pH (25°C)	Before	4,80	4,80	4,80	4,80	-10,0
	After	4,12	4,30	4,54	4,32	

Table 14. Chemical analysis of S2 bath

S2						
Parameter		N° S2 Bath			Average	Variation (%)
		1	2	3		
Nickel Ni <sup>2+</sup> (mol/L)	Before	0,101	0,101	0,104	0,102	-5,9
	After	0,096	0,095	0,097	0,096	
Hypophosphite H <sub>2</sub> PO <sub>2</sub> <sup>-</sup> (mol/L)	Before	0,273	0,273	0,273	0,273	-1,1
	After	0,285	0,265	0,261	0,270	
pH (25°C)	Before	4,52	4,62	4,59	4,58	0,2
	After	4,56	4,60	4,62	4,59	

Table 15. Chemical analysis of C1 bath

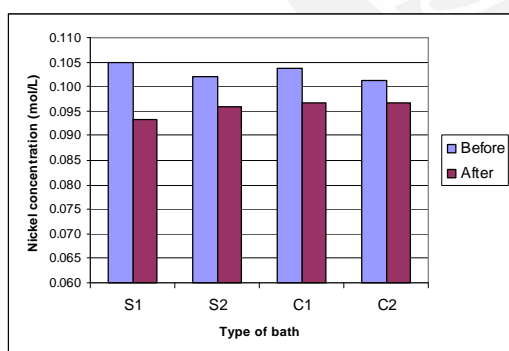
C1						
Parameter		N° C1 Bath			Average	Variation (%)
		1	2	3		
Nickel Ni <sup>2+</sup> (mol/L)	Before	0,104	0,103	0,104	0,104	-6,7
	After	0,094	0,097	0,099	0,097	
Hypophosphite H <sub>2</sub> PO <sub>2</sub> <sup>-</sup> (mol/L)	Before	0,174	0,177	0,179	0,177	-11,3
	After	0,162	0,151	0,157	0,157	
pH (25°C)	Before	4,80	4,80	4,80	4,80	-10,8
	After	4,30	4,26	4,27	4,28	

Table 16. Chemical analysis of C2 bath

C2						
Parameter		N° C2 Bath			Average	Variation (%)
		1	2	3		
Nickel Ni <sup>2+</sup> (mol/L)	Before	0,101	0,1	0,103	0,101	-4,0
	After	0,097	0,095	0,098	0,097	
Hypophosphite H <sub>2</sub> PO <sub>2</sub> <sup>-</sup> (mol/L)	Before	0,274	0,274	0,274	0,274	-0,4
	After	0,272	0,27	0,268	0,270	
pH (25°C)	Before	4,69	4,69	4,66	4,68	1,1
	After	4,73	4,76	4,70	4,73	

The variation of nickel concentration in the different baths can be seen in **Figure 33**. Before the plating process, the four baths had very similar nickel concentration (approx. 0,1 M). After two hours of plating process, the nickel concentration of the baths decreased by 5-11 % compared to their initial concentrations as a result of the nickel consumption in the deposition process.

**Figure 34** depicts the variation of hypophosphite concentration in the different baths. The initial concentrations of commercial baths (S2 and C2) were different from the baths performed in laboratory (S1 and C1). Commercial baths had higher hypophosphite concentration (approx. 0,27 M) than baths performed in laboratory (approx. 0,18 M). After plating process the hypophosphite concentration of the baths decreased by 1-15 % compared to their initial concentrations. From the low percentages of variation of reducing agent, it could be inferred the low consumption of reducing agent; however, changes in volume of the baths (due to evaporation) and consequently operations of water replenishment during the process should be kept in mind. By analyzing the chemical composition of the resulting deposits, a better understanding about consumption of nickel and reducing agent (hypophosphite) can be achieved.



**Figure 33.** Nickel concentration before and after electroless plating process

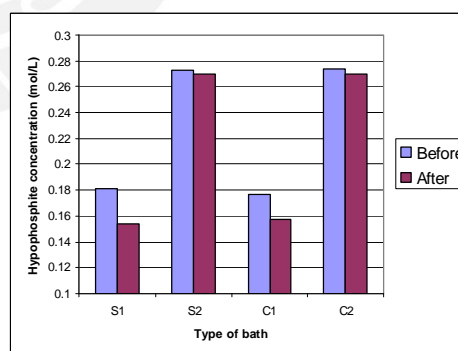


**Figure 34.** Hypophosphite concentration before and after electroless plating process



According to Mallory [1], maintaining the nickel and reducing agent concentration up to 10% to 15% will usually provide consistency in terms of deposition rate. The variations of nickel and hypophosphite concentration of all baths used in this research work were within 15%.

The variation of pH in the baths before and after the deposition process can be seen in **Figure 35**. The initial pH values of the four baths were between 4,8 and 4,6. After deposition process, pH values from baths prepared at the laboratory (S1 and C1) decreased by approx. 11% compared to their initial values. On the other hand, commercial baths maintained their pH values almost without variation. These results suggest that commercial baths had a better buffer on their composition.

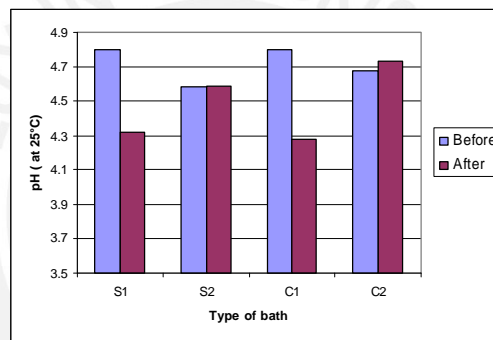


**Figure 35.** pH before and after electroless plating process

The effect of lowering the pH of a deposition bath could have lead in a diminishing of the rate of deposition (see **Figure 5.**) and also in an increment of the phosphor content in the deposit (see **Figure 6.**). From a point of view of structure and properties of deposits with high phosphorus content, a decrease in pH is not considered harmful since the phosphorus content will be increased allowing the deposit to achieve and maintain the amorphous characteristic. Consequently the corrosion resistance will be also conserved [1]. The analysis of microstructure and chemical composition of the different deposits will bring information about the influence of variation of pH of baths S1 and C1.

## 4.3 Characterization of electroless Ni-P and Ni-P-SiC coatings

### 4.3.1 Surface Morphology

Figures 36 a) to d) show SEM micrographs (at scale of 50  $\mu\text{m}$ ) of the surface morphology in top view of electroless Ni-P and Ni-P-SiC samples obtained from baths S1, C1, S2 and C2.

S1 (Figure 36a) and S2 (Figure 36c) are Ni-P deposits. In both cases a regular, continuous and relatively smooth morphology is observed.

In the case of the Ni-P-SiC composite deposits C1 (Figure 36b) and C2 (Figure 36d), a coarse morphology with uniform distribution of SiC particles can be observed. There are neither conglomerated nor depleted zones of particles.

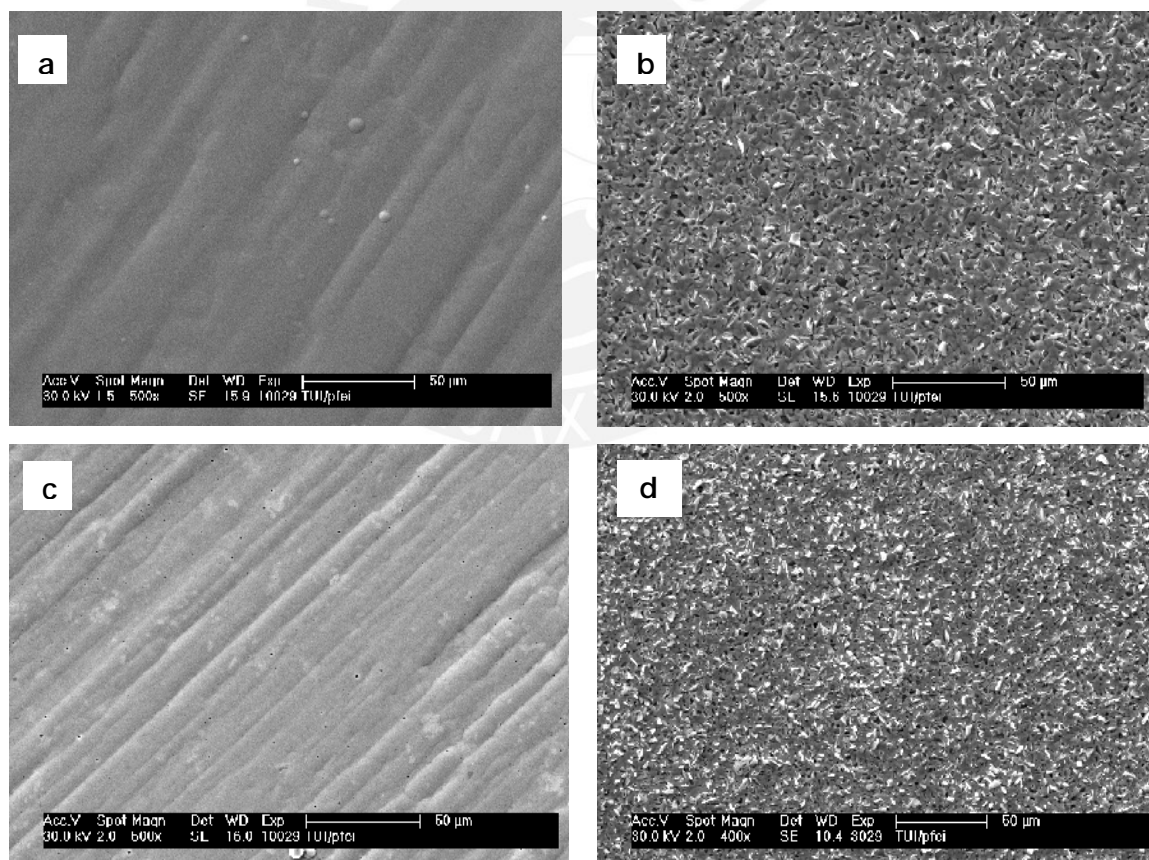


Figure 36. SEM micrographs in top view of Ni-P and Ni-P-SiC coatings obtained according the type of plating bath used: a) S1, b) C1, c) S2 and d) C2

Figures 37 a) to d) show detailed SEM micrographs taken at higher scale (20  $\mu\text{m}$  and 5  $\mu\text{m}$ ).

Deposit S1 (Figure 37a) has some spherical defects at the surface; they could be due to adsorption of tiny  $\text{H}_2$  bubbles that could not be removed from the surface. The presence of these defects could induce formation of pinholes or pits. In deposit S2 (Figure 37c) the presence of micro-pores uniformly distributed along the surface can be observed.

In Ni-P-SiC composite coatings C1 and C2 (Figure 37b and 37d), a uniform distribution of SiC micro-particles can be observed. It is possible to see in detail how the "flake" shaped micro-particles are incorporated in the Ni-P matrix. The micro-particles have geometric shapes with many edges and sharp ends that are uncovered on top of the surface. The particles were incorporated as the layer was forming. In these cases, it is difficult to determine the presence of pores due to the complex morphology of matrix and particles.

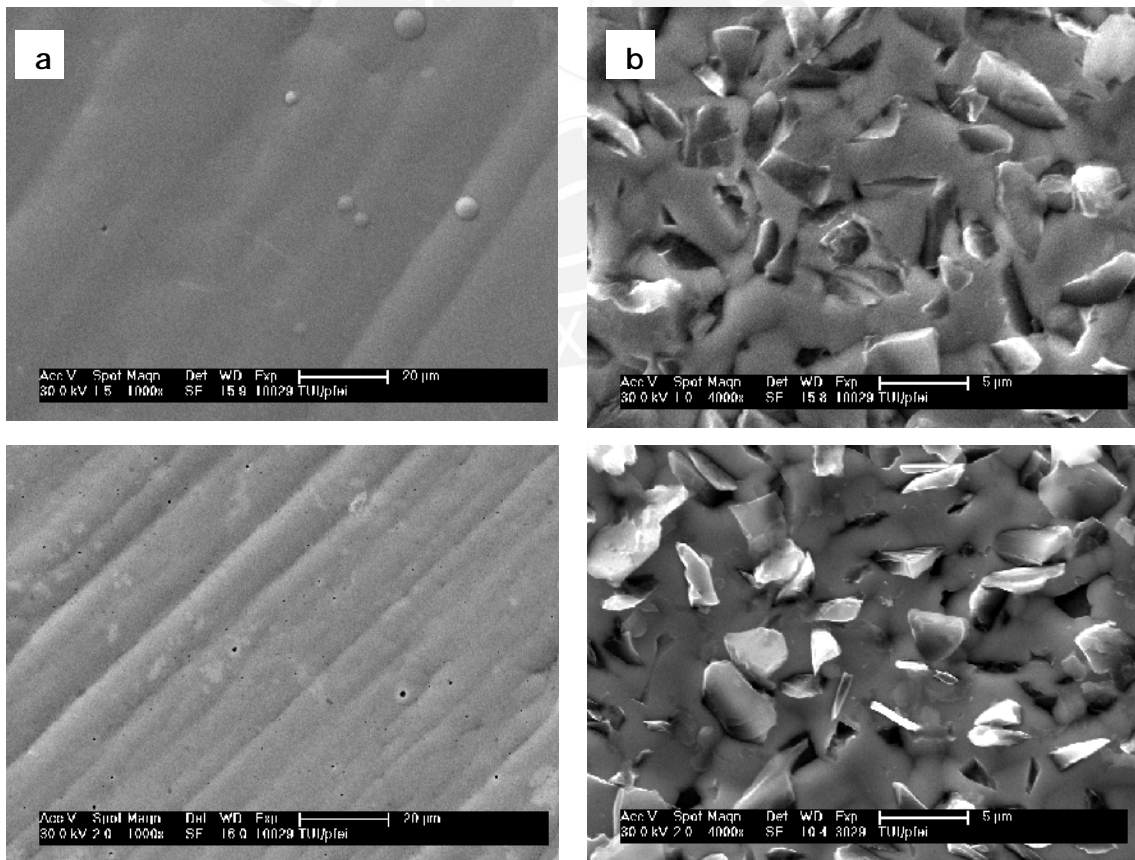


Figure 37. Detailed SEM micrographs in top view of Ni-P and Ni-P-SiC coatings obtained according the type of plating: a) S1, b) C1, c) S2 and d) C2

Figures 38 a) to d) show SEM micrographs taken in cross sectional view (at scales of 10  $\mu\text{m}$  and 20  $\mu\text{m}$ ). All the deposits show a uniform thickness. Deposit S1 (Figure 38a) shows continuity across its thickness and there is no presence of defects or imperfections. In deposit S2 (Figure 38c), the lines orthogonally to the surface imply the presence of pores. According to DIN 50903 [35], these pores seem to be not only open pores but also masked pores. Only on the basis of Figure 38c, it couldn't be determined if the pores reach the substrate.

In composite deposits C1 and C2 (Figure 38b and 38d), it is possible to see a good distribution of SiC micro-particles along the thickness. The images do not show any defects (e.g. pores) in the Ni-P matrix along the thickness.

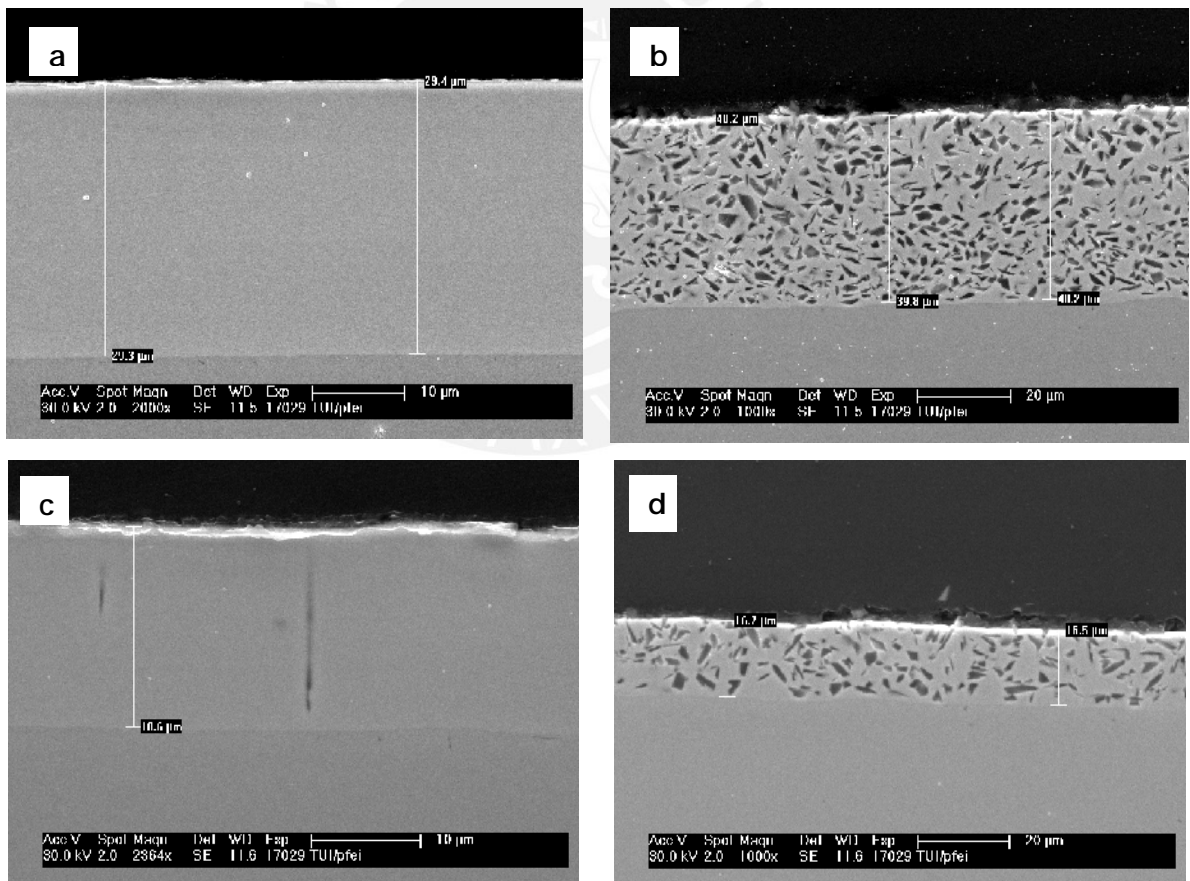


Figure 38. SEM micrographs in cross sectional view of Ni-P and Ni-P-SiC coatings obtained according the type of plating bath: a) S1, b) C1, c) S2 and d) C2.

## 4.3.2 Chemical composition of Ni-P and Ni-P-SiC deposits

### 4.3.2.1 Energy dispersive X-ray spectroscopy (EDX)

The EDX-line scan method was used to investigate the chemical composition along a line on the specimen surface. The electron beam scanned a series of spots (line scan) on the sample surface; then, emitted characteristic X-rays were detected generating a plot of the relative proportions of the elements along that spatial gradient. **Figure 39** is an example describing the line scan on sample C1. The depth of incidence of the electron beam using an accelerating voltage of 30 kV was simulated for nickel (see Appendix 3) and the calculated depth of incidence was approx. 3  $\mu\text{m}$ .

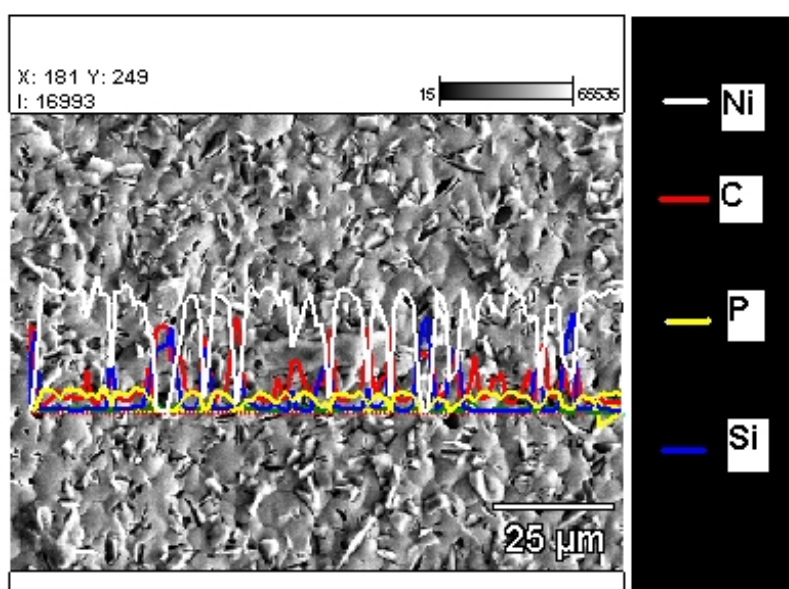


Figure 39. SEM micrograph of composite deposit C1 showing the line scan on the specimen surface.

The results of chemical analysis with this technique are shown in **Figure 40, 41, 42** and **43**. The concentration (wt %) is plotted against the number of points of the line scan.

The concentration of Ni and P can be easily determined in deposits S1 (**Figure 40.**) and S2 (**Figure 41.**). Phosphor content in deposit S2 (average 12,9 wt%) is higher by

approx. 3 wt% than in deposit S1 (average 9,89 wt%). It can be due to the fact that hypophosphite concentration of S2 bath was higher than S1 bath (see Figure 34.).

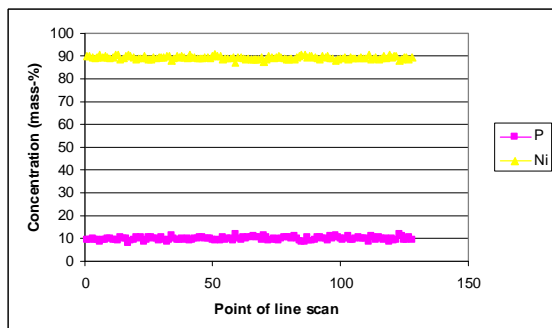


Figure 40. Chemical composition of deposit S1 obtained by EDX line scan

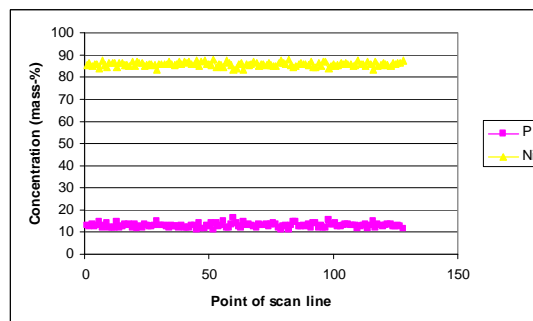


Figure 41. Chemical composition of deposit S2 obtained by EDX line scan

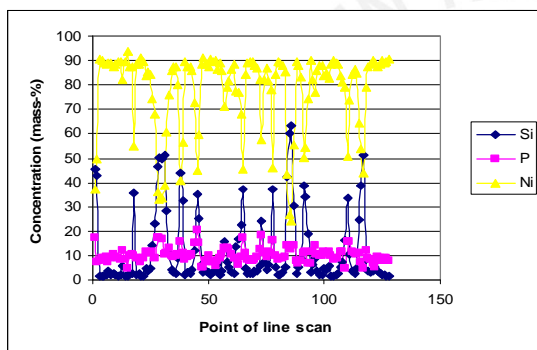


Figure 42. Chemical composition of deposit C1 obtained by EDX line scan

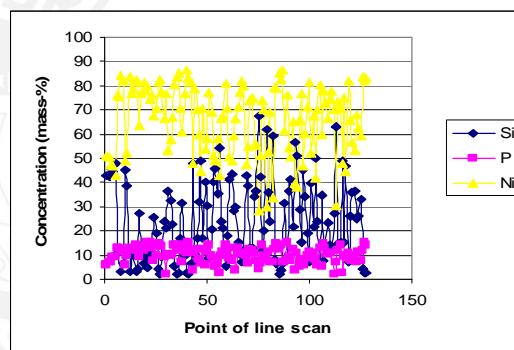


Figure 43. Chemical composition of deposit C2 obtained by EDX line scan

The chemical compositions in Ni-P-SiC composite deposits C1 (Figure 42.) and C2 (Figure 43.) are difficult to determine at first sight because the deposit is heterogeneous. The presence of dispersed SiC micro-particles in the Ni-P matrix produces a composition profile where both rich and depleted zones of SiC (expressed as Si wt %) can be observed.

By observing only the higher concentration values of Ni along the points of line scan (because these points corresponded only to the Ni-P matrix), it is possible to say that Ni-P matrix from deposit C1 has more nickel content (wt %) than Ni-P matrix from deposit C2.

Deposits S1 and C1 (prepared in laboratory) have similar phosphor contents (wt %) considering only the Ni-P matrix. Phosphor contents (wt %) in deposits S2 and C2 (obtained from commercial baths) are also similar.

The average values of chemical compositions obtained by EDX line scan analysis considering only Ni, P and SiC (as Si) are shown in Table 17. The standard deviation (SD) of concentration values from samples C1 and C2 is high due to the fact that the composite deposits contain dispersed SiC micro-particles in the Ni-P matrix. Additionally, the surface roughness (incremented by the addition of SiC micro-particles) must be considered as a cause of deviation of the results. Thus, the average values of chemical composition of deposits C1 and C2 must be considered only as approximate values.

Table 17. Chemical composition of deposits by EDX

Sample	Concentration (wt %)					
	Ni		P		SiC (as Si)	
	Average	SD	Average	SD	Average	SD
S1	89,31	0,68	9,89	0,69	-	-
S2	85,91	0,93	12,90	0,94	-	-
C1	77,92	16,89	10,21	2,98	11,87	15,21
C2	66,18	14,32	10,12	3,22	23,70	16,63

#### 4.3.2.2 Glow discharge optical emission spectroscopy (GDOS)

The results of chemical analysis using GDOS are shown in Figures 44, 45, 46 and 47 (the original plots can be seen in Appendix 4 to Appendix 11). The concentration values (wt %) are plotted against the thickness of deposits.

Comparing Ni-P deposits, S2 (Figure 45.) has higher phosphor content than deposit S1 (Figure 44.) across their thickness. On the other hand, it can be observed that the phosphor content (wt %) in both deposits is not uniform along their thickness. At close distances from top surface, the phosphor content is higher than at deeper measurement points.

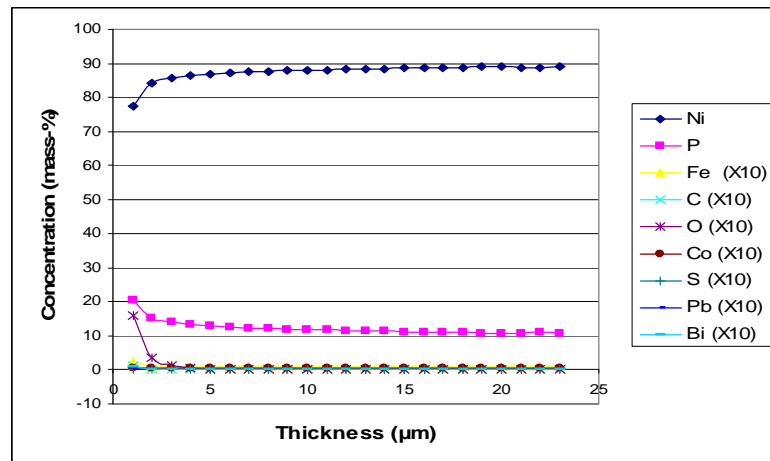


Figure 44. Depth-profile analysis of deposit S1 by GDOS

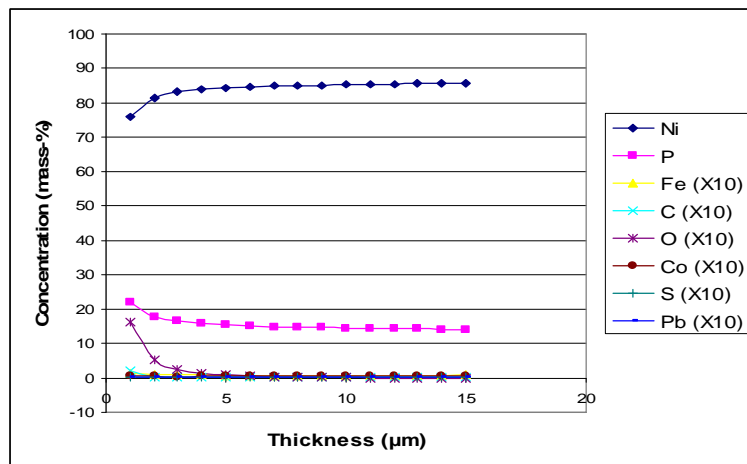


Figure 45. Depth-profile analysis of deposit S2 by GDOS

A similar behavior was found for Ni-P-SiC deposits. C2 (Figure 47) has higher phosphor content than deposit C1 (Figure 46.) along their thickness. Differences of phosphor content along the thickness can be also observed.

Other elements such as Fe, C, Co, S, Pb and Bi were detected in all the deposits in tiny concentrations. These elements were present in the plating baths possibly from the reagents containing some of them as impurities.

Oxygen was also detected in all the deposits on the top surface (approx. 1,5 wt %). Then the presence of oxygen on top surfaces could be explained by the existence of thin layers of oxygen (from air) during GDOS analysis.



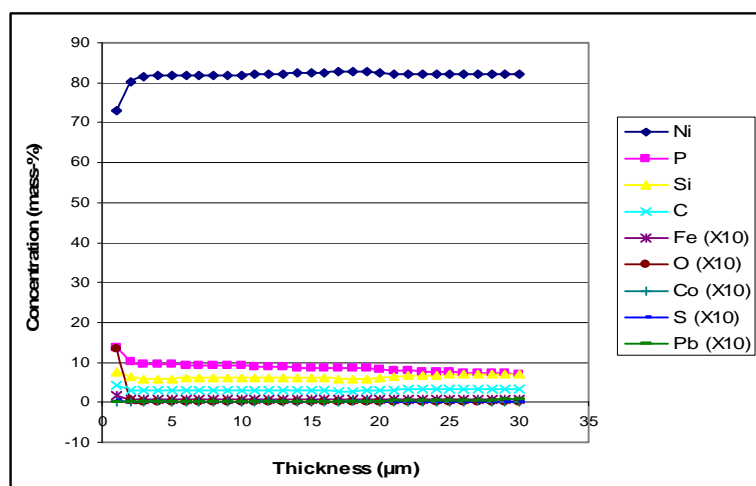


Figure 46. Depth-profile analysis of deposit C1 by GDOS

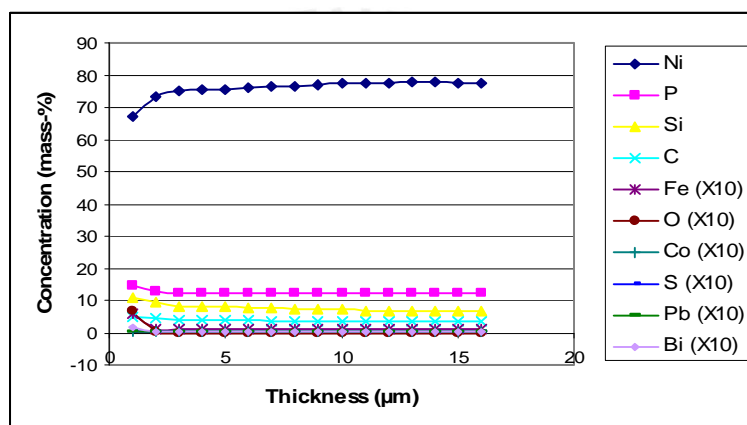


Figure 47. Depth-profile analysis of deposit C2 by GDOS

Table 18. shows the average chemical composition of the coatings obtained by GDOS analysis considering only Ni, P and SiC.

Table 18. Chemical composition of deposits obtained from GDOS

Sample	Concentration (wt %)					
	Ni		P		SiC	
	Average	SD	Average	SD	Average	SD
S1	87,43	2,52	12,25	2,13	-	-
S2	84,13	2,57	15,53	2,09	-	-
C1	81,77	1,72	8,71	1,22	9,35	0,54
C2	76,00	2,57	12,40	0,65	11,35	1,17

Figure 48. shows a comparison of chemical composition results obtained by EDX and GDOS analysis. The degree of agreement between the two methods is relatively good when Ni-P deposits (S1 and S2) are compared.

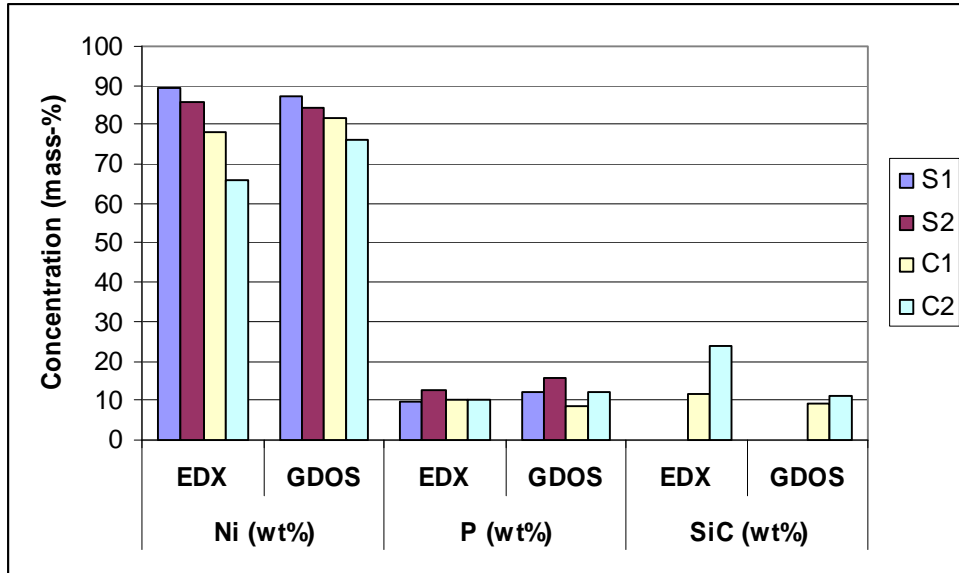


Figure 48. Comparison between EDX and GDOS in chemical analysis of deposits S1, S2, C1 and C2

For Ni-P-SiC (C1 and C2) deposits the difference of results between these two methods is greater due to the presence of SiC micro-particles along the Ni-P matrix. The method that offers more information (depth profile) and more accurate results is GDOS because this method uses a larger volume of sample in comparison with EDX. In other words, the GDOS method uses a more representative quantity of sample.

#### 4.3.3 Microstructure by x-ray diffraction (XRD)

The X-ray diffraction patterns of the as-deposited Ni-P and Ni-P-SiC coatings are shown in Figure 49. All the XRD patterns have a common broad peak at  $\sim 45^\circ$  ( $2\theta$ ) which indicates the amorphous character of the Ni-P matrix of the four deposits [7,13,18, 38].

The higher the phosphorous content in the coating, the higher will be the disorder of the nickel structure and the structure becomes amorphous. Chemical analyses by EDX and GDOS (see section 4.3.2) have shown that all deposits contain more than 10 wt%

P in the Ni-P matrix. Hence, it is evident that these high phosphorus contents have influenced on the distortion of the lattice of nickel and resulted in amorphous structures of Ni-P deposits.

X-ray diffraction patterns of composite deposits C1 and C2 have additionally some well-defined peaks corresponding to the crystal lattices of SiC micro-particles. On the other hand, the occurrence of tiny diffraction peaks of Fe in the XRD profiles can be explained due to the presence of Fe (approx. 0,1 wt% according to GDOS analysis) in the chemical composition of the deposits.

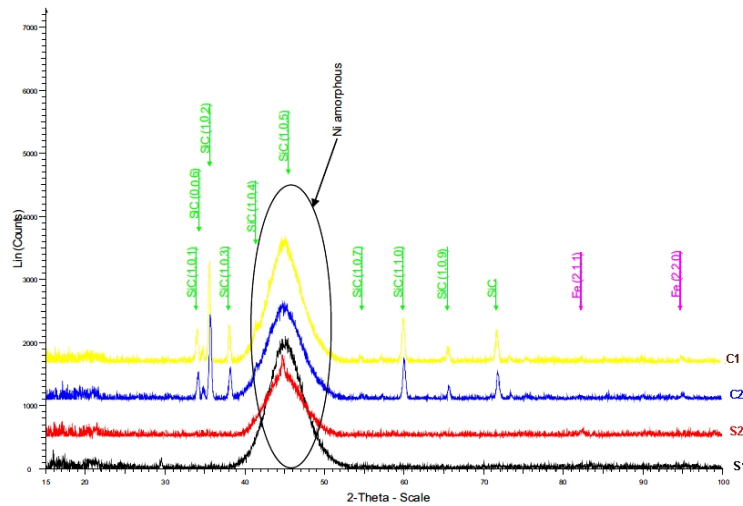


Figure 49. XRD patterns of Ni-P and Ni-P-SiC coatings: C1, C2, S2 and S1

#### 4.3.4 Thickness of deposits by magnetic induction method and SEM

The thickness values of deposits S1, S2, C1 and C2 obtained by magnetic induction method (section 3.2.4) are shown in Table 19. Deposits S1 and C1 (from baths prepared at laboratory) were the ones with high thickness values.

Table 19. Thickness measurement by magnetic induction method

Sample	Thickness (mm)							
	Front side			Back side			Average	SD
	1	2	3	1	2	3		
S1	27	29	29	29	30	29	29	0,98
S2	20	20	19	19	20	21	20	0,75
C1	36	38	39	36	37	38	37	1,21
C2	16	15	16	16	17	16	16	0,63

Table 20. shows a comparison of thickness values between magnetic induction method and SEM. The values obtained from magnetic induction method represent and average value; on the other hand, the values taken from SEM (see Figure 38) represent the thickness in a specific zone. As can be seen, the values are very similar. Then, it is possible to infer that all the deposits had a good uniformity of thickness.

Table 20. Comparison between magnetic induction method and SEM for thickness determination

Sample	Thickness (mm)	
	Magnetic induction method	SEM
S1	29	29,4
S2	20	18,6
C1	37	40,0
C2	16	16,6

By knowing the thickness values and the time of deposition (2 hours), it is possible to calculate the rate of deposition of the deposits. Then the rate of deposition values were: S1: 14,5  $\mu\text{m}/\text{h}$  , S2: 10  $\mu\text{m}/\text{h}$  , C1: 18,5  $\mu\text{m}/\text{h}$  and C2: 8  $\mu\text{m}/\text{h}$ . It can be seen that by comparing the rate of deposition of composite deposits (C1 and C2) with their analogous Ni-P deposits (S1 and S2), the incorporation of particles in the electroless plating bath had influence the rate of deposition. However, no obvious relation was found since between S1 and C1 the deposition rate increased and between S2 and C2 the opposite happened.

#### 4.3.5 Hardness

The results of Vickers hardness measurements (see section 3.2.5) of the as-deposited Ni-P and Ni-P-SiC deposits are listed in Table 21.

Table 21. Vickers hardness values

Sample	Applied load (mN)	Vickers Hardness(HV)				
		1	2	3	Average	SD
S1	500	501	431	474	<b>469</b>	± 35
S2	500	641	632	607	<b>626</b>	± 17
C1	1000	817	823	766	<b>802</b>	± 32
C2	1000	825	811	809	<b>815</b>	± 9

It can be seen that the incorporation of SiC particles has led to increments in hardness values. Comparing deposits S1 (Ni-P deposit) with C1 (Ni-P-SiC), it was found that the hardness values increased from 469 HV to 802 HV. In the case of deposits resulting of commercial baths S2 (Ni-P) and C2 (Ni-P-SiC), the hardness values increased from 626 HV to 815 HV.

The Ni-P-SiC deposits C1 and C2 have similar values of hardness. This is due to both composite coatings have similar degree of SiC particles incorporation. According to GDOS analysis, both deposits have similar SiC average mass content of SiC (9 wt% and 11 wt% respectively).

## 4.4 Evaluation of the corrosion resistance in NaCl 3,5 % by electrochemical techniques

### 4.4.1 Test of equipment

In order to check the overall equipment (potentiostat/galvanostat and frequency response analyzer) performance, a test with a dummy cell was performed (see section 3.2.6.2). The resulting Nyquist plot using a dummy cell circuit used is shown in Figure 50. The corresponding results of the test of the equipment are shown in Table 22.

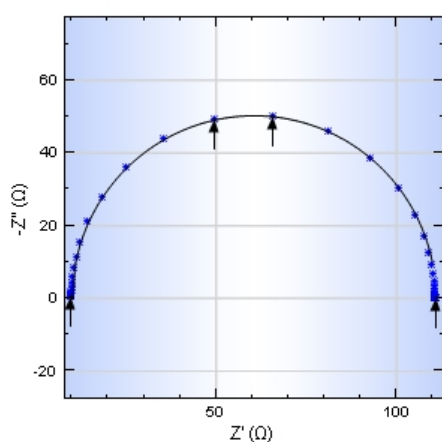


Table 22. Results of test of dummy cell

Components	Expected value	Measured value	Error (%)
Resistor ( $R_s$ )	10 $\Omega$	10,03 $\Omega$	0,3
Resistor( $R_p$ )	100 $\Omega$	100,9 $\Omega$	0,9
Capacitor (C)	100 $\mu\text{F}$	100,3 $\mu\text{F}$	0,3

Figure 50. Nyquist plot of dummy cell circuit

The measured values agreed with the expected values (C: 100  $\mu\text{F} \pm 20\%$ ,  $R_s$ : 10  $\Omega \pm 1\%$ ,  $R_p$ : 100  $\Omega \pm 1\%$ ). The relative error values are also shown.

### 4.4.2 Open circuit potential (OCP) measurement

All the electrochemical tests carried out to evaluate corrosion resistance required a previous determination of the OCP (or, *potential corrosion*,  $E_{\text{corr}}$ ) value. The estimation of the measurement duration until the reached OCP can be considered a stable value (when the system approached to steady state), followed the criterion mentioned in section 3.2.6.5.

Figure 51 depicts the evolution of the OCP over 2,5 hours (9000 s). As can be seen, the initial (t=0) OCP values fluctuate between -0,38 and -0,34 V vs. SCE. As the time goes by, the OCP values tend to go to more positive potential values.

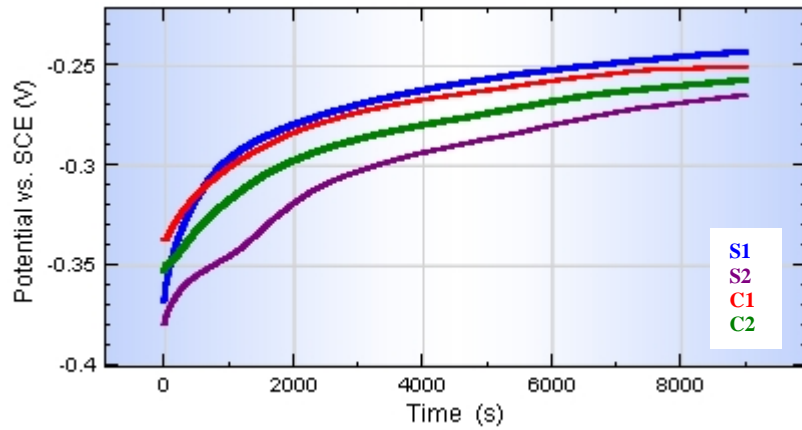


Figure 51. OCP (V) versus Time (s) of deposits S1, S2, C1 and C2 in NaCl 3,5%

Table 23 shows an evaluation of the OCP of the four deposits after 1 hour of immersion in the electrolytic solution (NaCl 3,5%).

Table 23. Evaluation of the change of OCP values after 1 hour of immersion

Sample	Potential vs. SCE (V) at 50 minutes	Potential vs. SCE (V) at 60 minutes	DV (mV) in 10 minutes
S1	-0,270	-0,265	5
S2	-0,303	-0,298	5
C1	-0,275	-0,270	5
C2	-0,287	-0,283	4

The variations of the OCP ( $\Delta V$ ) during the last 10 minutes in all cases were in agreement with the established criterion. Thus, the time for OCP determination was chosen to be 1 hour. To work with larger times could have been experimentally unpractical.

#### 4.4.3 Potentiodynamic anodic polarization

The potentiodynamic anodic polarization plots for the four deposits in NaCl 3,5% are depicted in Figure 52. The reproducibility of these tests is shown in Appendix 12. The current values are shown in logarithmic scale to make easy the visualization of the low current values.

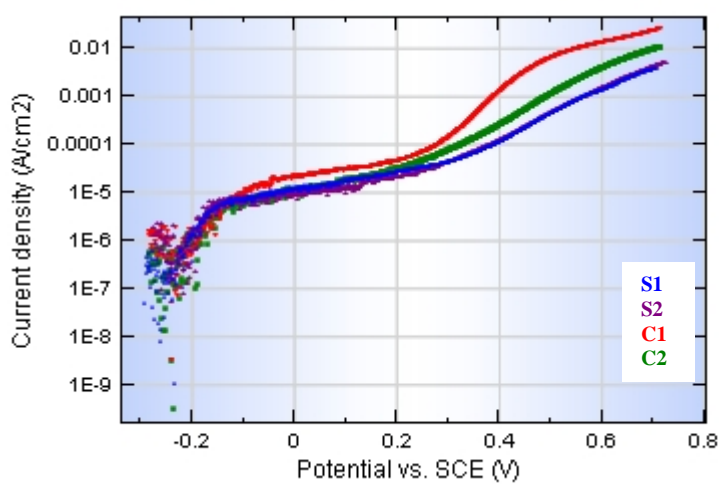


Figure 52. Potentiodynamic anodic polarization plots of deposits S1, S2, C1 and C2 in NaCl 3,5%

In general, the four deposits exhibit a similar anodic behavior. Then, based on the fact that microstructures of Ni-P (or Ni-P matrix in the case of C1 and C2) were amorphous and that the phosphor content of all deposits were high, a direct relationship between the similar anodic behavior of deposits and their similar structural condition was confirmed.

Details about the anodic behavior of deposits can be explained as follows:

- At anodic potentials near to the OCP the current density was very low (values less than 1  $\mu$ A) suggesting the existence of a protective layer at the beginning of the test. According to other investigations [9,10,19,20], for Ni-P deposits with high phosphor content, a preferential dissolution of nickel occurs at OCP,



leading to the enrichment of phosphorus on the surface layer. Then, the origin of such low current values of Ni-P deposits was attributed to the formation of such phosphorus enriched surface layer.

Balaraju, J. et al [10] reported that the barrier-action of the phosphorus enriched surface layer is related to the reaction of such layer with water to form a layer of adsorbed hypophosphite anions. Then, this layer in turn would block the supply of water to the nickel avoiding its dissolution.

In this work, the chemical depth-profile analysis of deposits obtained by GDOS have shown the existence of higher phosphorus content in all deposit's top surfaces in comparison with their deeper zones. It was observed even before deposits were immersed in NaCl 3,5%. This fact could support the findings (presence of the phosphorus enriched surface) reported by other studies [9,10,19,20] since the samples could have been protected by such layer even before the immersion in the corrosive environment (NaCl 3,5%).

- The anodic current density increased slowly until approx. 0,3 V vs. SCE. At potentials above 0,3 V vs. SCE the current density increased quickly, which suggests that the four deposits began to dissolve transpassively since at high polarization conditions, the protective layer (described above) dissolves and then the nickel is oxidized to higher oxidation states ( $\text{Ni}^{2+}$ ,  $\text{Ni}^{3+}$ ) quickly. To make easy the visualization of this fact, **Figure 53** depicts the potentiodynamic anodic polarization plot using a linear scale of current.

Then, it is also possible to see that composite deposits (C1 and C2) had higher dissolution currents in comparison with their analogous simple deposits (S1 and S2). This is possibly due to the presence of SiC micro-particles on the surface would contribute to generate local cells of corrosion due to the high heterogeneity of the surface. Additionally, it can be seen that C1 shows a different transpassive behavior in comparison with C2. In fact, C1 has higher dissolution currents than deposit C2.

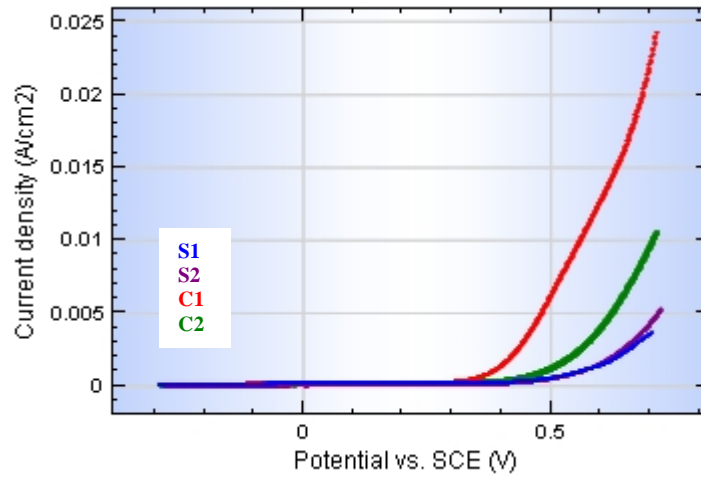


Figure 53. Potentiodynamic anodic polarization plots in linear scale of deposits S1, S2, C1 and C2 in NaCl 3,5%

The Ni-P deposits (S1 and S2) remained bright in appearance after the anodic polarization test. However, evidence of pits was observed in deposit S2 (Figure 54).

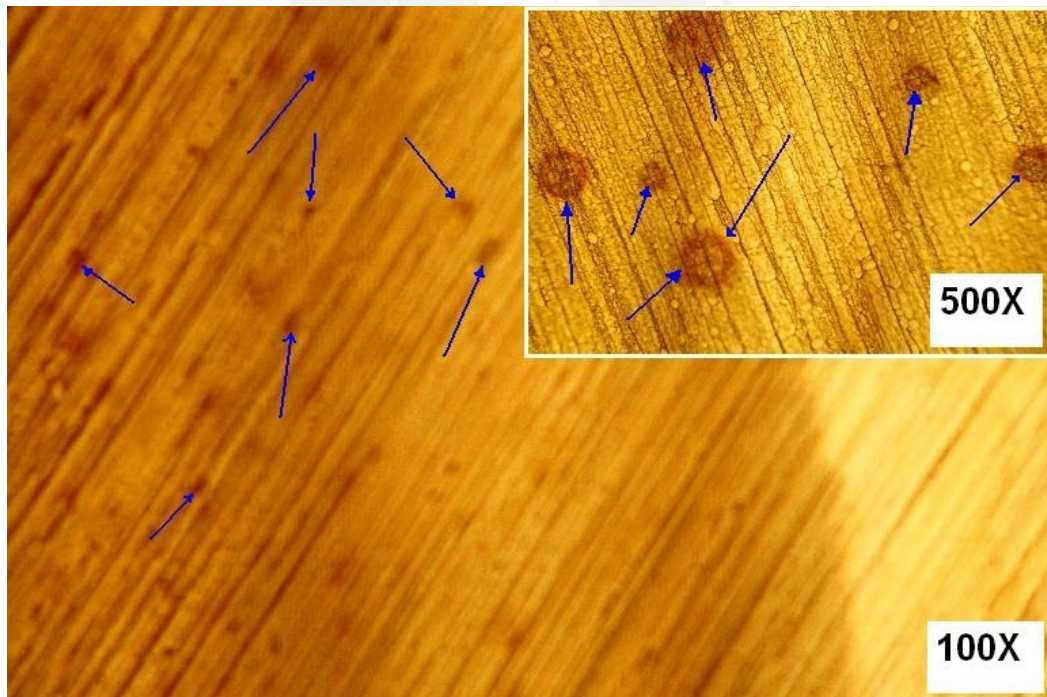


Figure 54. Deposit S2 after a potentiodynamic anodic polarization test

According morphology evaluation (see **Figure 37c** in section 4.3.1), presence of micropores were found in deposit S2. Thus, the occurrence of pits on deposit S2 was expected. No pits were found for deposit S1 and this fact agrees with its good morphology (lack of porosity).

Special attention deserves the fact that the commercial composite deposit C2 did not show presence of pits after anodic polarization in comparison with its analogous Ni-P deposit S2. Then it can be inferred that the presence of dispersed SiC micro-particles prevented the growing of micro-pores (the origin of pits in deposit S2) in deposit C2. SEM images of cross section of composite deposits would support that fact since the deposits C1 and C2 did not show defects (pores) across their thickness.

#### 4.4.4 Cathodic and anodic polarization (Tafel plots)

In this method (see sections 2.6.1.4 and 3.2.6.7), large polarizations were applied to the samples (-250 mV vs. OCP to 250 mV vs. OCP). The Tafel plots resulting of cathodic and anodic polarization are depicted in **Figure 55**. The current values are shown in logarithmic scale.

All deposits showed a Tafel behavior because at large polarizations lineal responses of current (in logarithmic scale) were obtained. This suggests that at those potentials the corrosion process is controlled by charge transfer. Studies of EIS (which is discussed later in section 4.4.6) confirmed that charge transfer is the mechanistic pathway controlling the corrosion process of all deposits. Since the potential values did not reach the 0,3 V vs. SCE value the possible action of local cells mentioned before (section 4.4.3) did not take place.

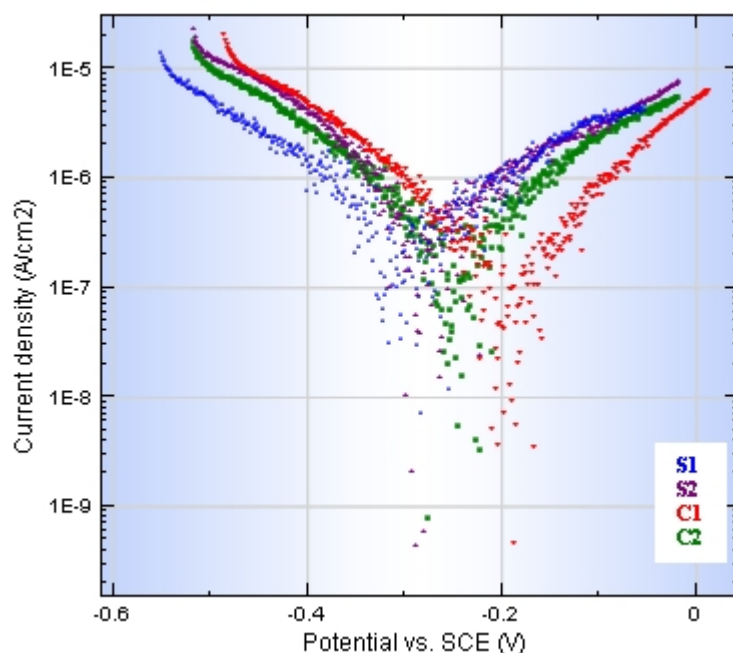


Figure 55. Tafel plots of deposits S1, S2, C1 and C2 in NaCl 3,5%

It is advisable to extend the linear portion of the cathodic and anodic at least 1 decade in order to get an accurate determination of Tafel slopes [40]. On the other hand, a general rule for an accurate Tafel extrapolation suggests that the extrapolation should start at least 50 to 100 mV away from the OCP [24].

For all plots, it can be seen that the linear portion of cathodic and anodic branches covered a little less than 1 decade of current density; however the lineal current response is far enough from OCP value and a manual fitting was possible.

Table 24 shows the parameters obtained from Tafel plots. Each result corresponds to the average of three measurements. The parameters were obtained according to the description in section 2.6.1.4.

The runned tests for evaluation of reproducibility, the diagrams used for the determination of Tafel slopes, and the resulting electrochemical parameters for all deposits are shown in Appendix 13.

Table 24. Parameters resulting from Tafel plots

Sample	OCP vs. SCE	$b_a$	$b_c$	$i_{corr}$	B
	(V)	V/dec	V/dec	$mA/cm^2$	(V)
S1	-0,273	0,050	0,045	0,730	0,051
S2	-0,272	0,040	0,043	0,713	0,045
C1	-0,249	0,027	0,033	0,173	0,032
C2	-0,257	0,038	0,041	0,483	0,043

The composite Ni-P-SiC deposits (C1 and C2) showed lower corrosion current density ( $i_{corr}$ ) than the simple deposits; among them, deposit C1 was the one with the lowest corrosion current density. Ni-P deposits (S1 and S2) experienced very similar current density values.

#### 4.4.5 Linear polarization resistance (LPR) determination

The obtained LPR plots (see also section 2.6.1.3) are depicted in Figure 56.

A rule of thumb is that  $1\mu A/cm^2$  is approximately equivalent to a penetration rate of 0,013 mm/y (millimeters penetration per year) for a wide range of structural materials, including ferrous-, nickel- and copper-based alloys [33]. On the other hand, a metal with a penetration rate lower than 0,15mm/y falls into a category of materials with good corrosion resistance [40]. Thus, current density values of  $1\mu A/cm^2$  can be considered as low values.

According to Figure 56, the current density values can be considered as very low values. In fact, from the results of  $i_{corr}$  obtained with Tafel plots, it was expected that current values near the OCP would be in the order of millionths of an ampere.

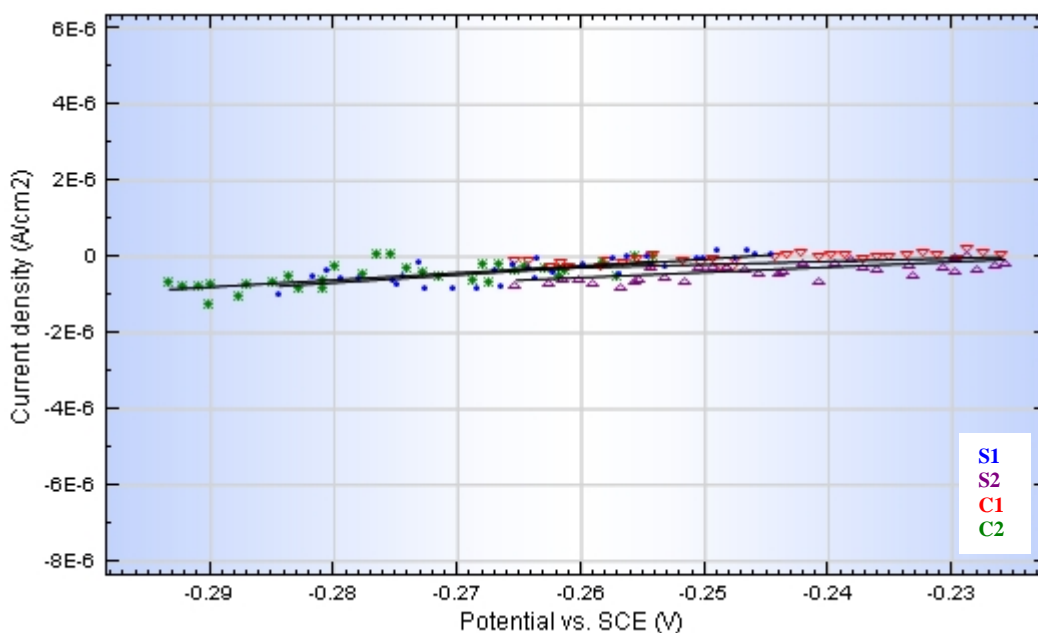


Figure 56. Linear polarization resistance plots of deposits S1, S2, C1 and C2 in NaCl 3,5%

Table 25 shows the average values of the electrochemical parameters obtained from LPR experiments. Each result corresponds to the average of three measurements. The runned tests for evaluation of reproducibility and the calculated  $R_p$  values for all deposits are shown in Appendix 14.

Table 25. Electrochemical parameters obtained from LPR

Sample	OCP vs. SCE	$R_p$ (average)	B (*)	$i_{corr}$
	(V)	( $\Omega \cdot \text{cm}^2$ )	(V)	$\text{mA}/\text{cm}^2$
S1	-0.264	49693	0,051	1,033
S2	-0.258	55501	0,045	0,803
C1	-0.246	103611	0,032	0,312
C2	-0.267	77954	0,043	0,550

(\*) B values were calculated from Tafel slopes method.

(\*\*)  $i_{corr}$  values were calculated with the Stern-Geary simplified kinetic expression (section 2.6.1.3, Equation 20).

$R_p$  and B values were used for this calculation.

According Table 25, the composite Ni-P-SiC deposits (C1 and C2) were the ones with higher polarization resistance ( $R_p$ ). Among them, deposit C1 was the one with the highest  $R_p$  value. Ni-P deposits (S1 and S2) have lower  $R_p$  values. According to the

Stern-Geary simplified kinetic expression (section 2.6.1.3, Equation 20), high  $R_p$  values imply low  $I_{corr}$  values

At this point, it is important to mention that the relative standard deviations (%RSD) values of  $R_p$  values (see Appendix 14) are high (between 21 and 33). This is because the used data for this method is based on the measurement of low values of current (order lower than millionths of an ampere).

#### 4.4.6 Electrochemical impedance spectroscopy (EIS)

The obtained impedance spectra (Nyquist plot, see section 3.2.6.9) of the four deposits are shown in **Figure 57**. Each point of the spectra represents experimentally obtained data whereas the lines represent the respective fits.

All deposits have, as a common feature, the presence of one big capacitive loop. That represented one time-constant on the impedance spectra and, in consequence, one reaction on the electrode/electrolyte interface responsible for the corrosion behavior of each sample. Thus, the charge transfer resistance ( $R_{ct}$ ) is considered to be the electrochemical parameter that indicates the corrosion resistance of deposits. In other words  $R_{ct}$  becomes  $R_p$ .

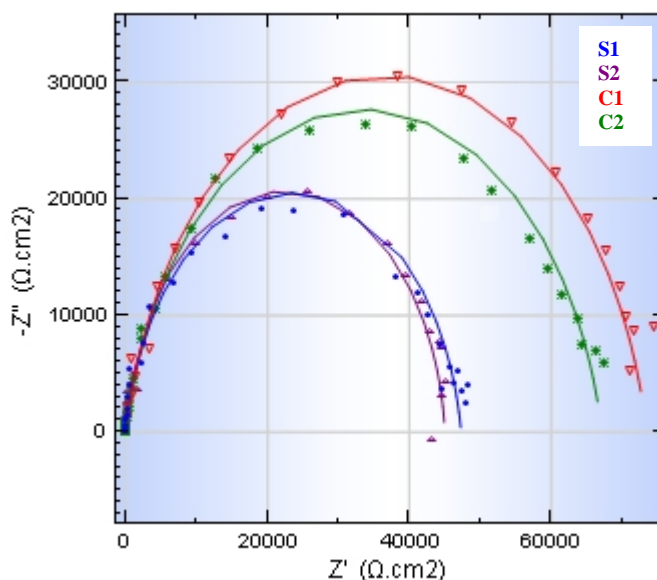
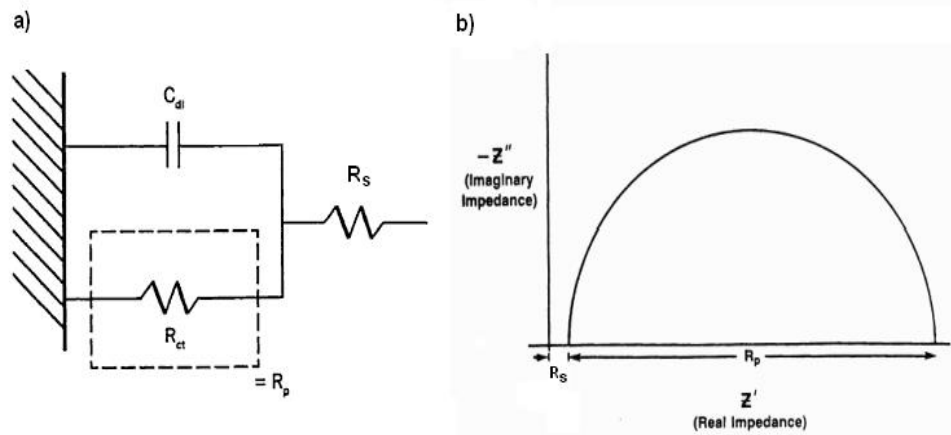


**Figure 57. Impedance spectra (Nyquist plots) of deposits S1, S2, C1 and C2 in NaCl 3,5%**

The diameter of the capacitive loops informs about corrosion resistance of each sample as it represents the charge transfer resistance ( $R_{ct}$ ) values of deposits. Bigger capacitive loop diameters represent better corrosion resistance properties.

In order to calculate the electrochemical parameters that can be obtained from impedance spectra, an equivalent circuit was used to fit the data. An equivalent circuit simulates the electrochemical behavior of the Ni-P or Ni-P-SiC surface-solution interface. The impedance spectra fitted into the so-called Randles circuit (described in section 2.6.2). The equivalent contains elements corresponding to the solution resistance ( $R_s$ ), the charge transference resistance ( $R_{ct}$ ) and the double-layer capacitance ( $C_{dl}$ ). This is shown in **Figure 14** (see also section 2.6.2).



a) Electrical equivalent circuit (Randles circuit), b) Nyquist plot of a simple charge transfer corrosion process.

**Figure 14. Model for a simple charge transfer [24]**

To model the double-layer capacitance ( $C_{dl}$ ), a constant phase element (CPE) was used instead of a single capacitance. Usually, the use of a CPE is recommended in order to compensate the heterogeneity of the system [11, 40]. In this case, an example of heterogeneity is the presence of rough surface in deposits C1 and C2 due the presence of dispersed SiC micro-particles. The CPE is defined by two parameters,  $Y_0$  (admittance) and  $\alpha$  (an empirical exponent related to the surface roughness). If  $\alpha$  is equal to 1, the CPE is identical to a capacitor. Values of the double layer capacitance ( $C_{dl}$ ) were calculated from the CPE parameters using equation (31) [20].  $\omega_{max}$  is the frequency of the maximum of  $Z''$  (imaginary component of impedance).

$$C_{dl} = Y_0 (\omega_{max})^{\alpha-1} \quad (31)$$



The fitted results are shown in Table 26. Each result corresponds to the average of three measurements. The runned tests for evaluation of reproducibility and the electrochemical parameters for all deposits are shown in Appendix 15.

Table 26. Electrochemical parameters obtained from EIS

Sample	OCP vs. SCE	$R_s$	$R_{ct}$	$Y_0$	$a$	$W_{max}$	$C_{dl}$	$i_{corr}^{(*)}$
	(V)	( $\Omega \cdot cm^2$ )	( $\Omega \cdot cm^2$ )	(mMho)		(Hz)	( $mF/cm^2$ )	$\mu A/cm^2$
S1	-0,258	11,72	47 687	3,13	0,90	0,24	17,96	1,077
S2	-0,278	11,39	46 729	3,90	0,95	0,16	21,38	0,953
C1	-0,271	12,79	71 001	3,80	0,89	0,13	24,01	0,456
C2	-0,246	12,45	66 047	4,29	0,89	0,09	28,18	0,649

(\*)  $i_{corr}$  values were calculated with the Stern-Geary simplified kinetic expression (Equation 20).  $R_{ct}$  (which is equal to  $R_p$ ) and B values (which were calculated from Tafel slopes) were used for this calculation.

The above electrochemical results showed  $R_{ct}$  values of Ni-P-SiC composite deposits C1 and C2 to be higher than the ones obtained for Ni-P deposits. The corrosion resistance values of deposits can be ordered as follows:  $C1 > C2 > S1 \approx S2$ . Deposit C1 exhibits the higher  $R_{ct}$  ( $R_p$ ) value

It is possible to calculate corrosion current density ( $i_{corr}$ ) using the  $R_{ct}$  values and according to the Stern-Geary simplified kinetic expression (see section 2.6.1.3, Equation 20). The use of the Stern-Geary constant (B) (obtained from Tafel plots experiments, see section 4.4.4) was required. One more time, the better corrosion behavior of composite deposits C1 and C2 in comparison with deposits S1 and S2 can be demonstrated since the lower current density values were observed for composite deposits C1 and C2 (0,45 and 0,65  $\mu A/cm^2$  respectively) in comparison to deposits S1 and S2 values (approx. 1  $\mu A/cm^2$ ).

The obtained values of  $R_s$  are approx. 12  $\Omega \cdot cm^2$ . These low values were expected since a relative concentrated salt solution (NaCl 3,5%) was used.  $R_s$  values, in comparison with the high  $R_{ct}$  values, were minimal.

The  $\alpha$  values of all deposits are lower than 1, this means that there were some heterogeneity in the system possibly due to the surface roughness of deposits. Composite deposits C1 and C2 showed lower values of  $\alpha$  in comparison of the Ni-P deposits S1 and S2. This is because the surface roughness of composite deposits was higher than deposits S1 and S2 because of the presence of SiC micro-particles. As a consequence, the  $C_{dl}$  values of composite deposits C1 and C2 were higher than S1 and S2.

#### 4.4.7 Comparison of results among the different electrochemical techniques

Figures 58 and 59 help to evaluate the different electrochemical techniques for corrosion evaluation employed in this study.

Figure 58 shows that the polarization resistance values ( $R_p$ ) of composite coatings C1 and C2 are higher than those obtained for S1 and S2 coatings according to results from LPR and EIS methods.

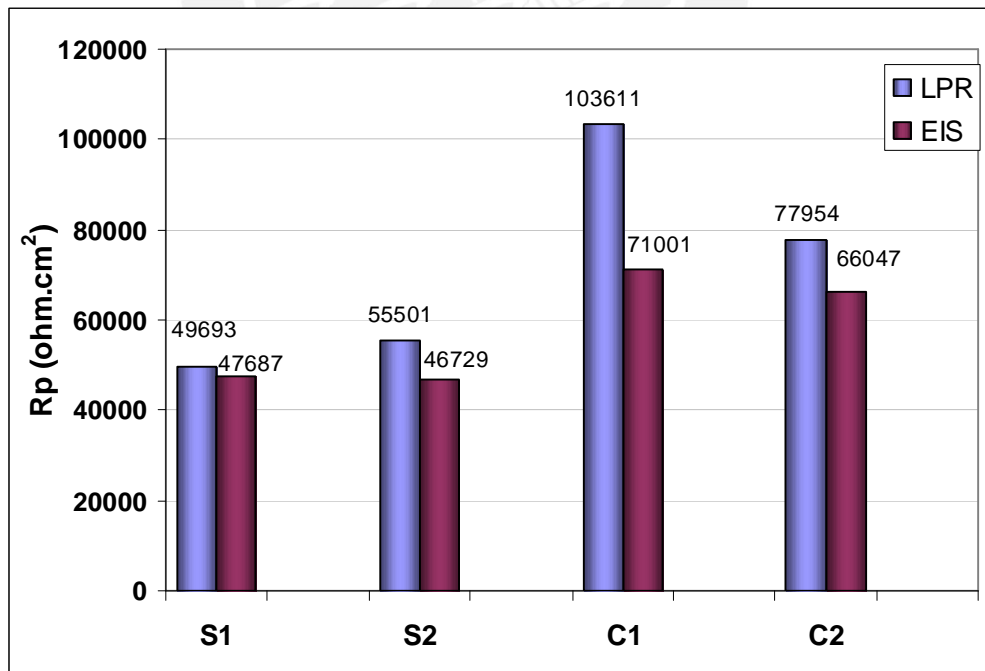


Figure 58. Comparison of polarization resistance values obtained from LPR and EIS

This fact can be ascribed to the decrease (due to the presence of SiC micro-particles) in the effective metallic area available for corrosion. The characterization of Ni-P deposits (S1 and S2) and Ni-P matrices from composite deposits (C1 and C2) have demonstrated that their morphology and microstructure are very similar. Thus, knowing that SiC particles are chemically inert in salt solution medium, the origin of the higher resistance values in composite deposits is attributed to the lower available surface metallic area at the interface metal/solution.

Concerning to the methods (LPR and EIS) employed to obtain the polarization resistance ( $R_p$ ) values. With the LPR (DC technique) only one value of resistance ( $R_p$ ) is obtained whereas using EIS (AC technique) it is possible to separate the charge transfer resistance from other resistances (e.g. solution resistance) since the responses occur at different frequencies. On the other hand, in this study the  $R_p$  values obtained by EIS were the ones with better reproducibility (lower %RSD values) in comparison with LPR technique. Thus, EIS would be the more suitable technique.

The plot shown in **Figure 59** also displays the better corrosion behavior of composite deposits C1 and C2 (compared to deposits S1 and S2) according to results from EIS, LPR and Tafel plots. The lower corrosion current density values corresponded to composite deposits C1 and C2.

The reason of these findings can also be ascribed to the decrease in the effective metallic area available for corrosion in composite coatings (as explained above).

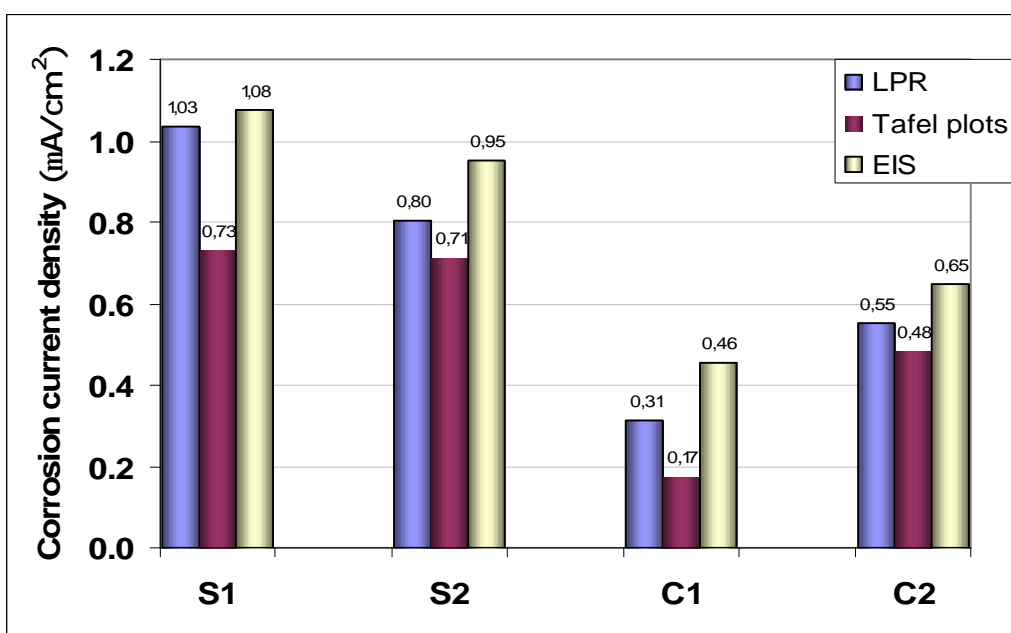


Figure 59. Comparison of corrosion current density values obtained from LPR and EIS

Among the three different techniques used to obtain corrosion current values (LPR, Tafel plots and EIS), the less suitable would be LPR since  $R_p$  values (used to calculate  $i_{corr}$ ) are the ones with higher %RSD values.

It is difficult to see which one is the more suitable technique between the Tafel plots method and EIS since to obtain  $i_{corr}$  values from EIS data, to use the data (Stern-Geary constant B) from Tafel plots is required. On the other hand, Tafel plots technique involves perturbation of the potential relatively far from the OCP (steady-state corrosion potential). Despite the differences of the techniques explained above, the tendencies of current density values for all deposits were in agreement.

The obtained values of the electrochemical parameters ( $R_p$  and  $i_{corr}$ ) corresponding to Ni-P and Ni-P-SiC were similar to the ones reported by Balaraju et al. [10]. Balaraju et al. studied the corrosion resistance of Ni-P-Si<sub>3</sub>N<sub>4</sub>, Ni-P-CeO<sub>2</sub> and Ni-P-TiO<sub>2</sub> deposits in NaCl 3,5% and the reported  $R_p$  values were in a range of 90 700 and 59 000  $\Omega \cdot \text{cm}^2$ , and  $i_{corr}$  values were between 0,66 and 0,33  $\mu\text{A}/\text{cm}^2$ . On the other hand, Song et al. [11] studied electroplated Ni-P-ZrO<sub>2</sub> deposits in NaCl 3,5% and reported  $R_p$  values of approx. 24 931  $\Omega \cdot \text{cm}^2$ .

## 5. CONCLUSIONS AND RECOMMENDATIONS

### 5.1 Conclusions

- 5.1.1 From bath formulations prepared in laboratory, it has been possible to obtain high phosphorus Ni-P deposits (S1) and Ni-P-SiC (C1) with similar (physical, chemical, corrosion resistance) properties to the ones obtained from commercial formulations (S2 and C2, respectively). This would provide a basis for the development of new bath formulations to be tested and evaluated in the laboratory.
- 5.1.2 The two electroless plating bath formulations used for the synthesis of Ni-P and Ni-P-SiC deposits led to different deposition rates. Deposits S1 and C1 were thicker than S2 and C2 after 2 hours of deposition. This fact, in addition to the studies of structure, morphology, hardness and corrosion resistance, seems to show that the use of the bath formulation prepared at laboratory is more suitable than the commercial formulation.
- 5.1.3 It was verified the general knowledge that there are several experimental factors that can influence the mechanism of incorporation of micro-particles for composite coatings obtained by "electroless" plating. In this particular study, it was found that to use mechanical stirring as the method to suspend and to disperse micro-particles in the plating bath could lead to obtain defects in deposits (low SiC incorporation into the Ni-P matrix) since a homogeneous agitation around the whole geometry of the substrate could not be reached. However, such problem could be minimized by working with small substrates.
- 5.1.4 Comparative studies about morphology and examination of occurrence of pits (after anodic polarization tests) between deposits synthesized with commercial baths (S2 and the composite C2) seem to show that the presence of dispersed SiC micro-particles prevented the growing of micro-pores during the synthesis of C2. Further investigation about the relation between concentration of

incorporated SiC micro-particles and occurrence of pores would confirm this observation.

- 5.1.5 The electrochemical methods (LPR, EIS, Tafel plots) used to study the corrosion resistance of Ni-P coatings and Ni-P-SiC composite coating agreed to show the better corrosion resistance of Ni-P-SiC composite coatings over the Ni-P coatings. This fact can be ascribed to the decrease in the effective metallic area available for corrosion.
- 5.1.6 Concerning to the mechanism by which the Ni-P and Ni-P-SiC become corroded, EIS experiments demonstrated that the corrosion process involved a charge transfer mechanism due to the occurrence of a single semicircle (loop) in the Nyquist plots of all deposits. Tafel plots also corroborated the charge transfer mechanism since of all deposits showed a Tafel behavior (lineal responses at large polarizations).
- 5.1.7 Through the incorporation of SiC particles into the Ni-P matrix, it was possible to increase the hardness values of Ni-P deposits. The hardness values of the composite deposits C1 was 802 HV (71% more than S1) whereas for C2 was 815 HV (30% more than S2). Then, electroless Ni-P composite deposits can be a better option in comparison with other materials (e.g. hard chromium coatings) in applications that require wear and corrosion resistance.
- 5.1.8 Since both corrosion resistance and hardness of composite Ni-P-SiC coatings (C1 and C2) were better in comparison to the Ni-P coatings (S1 and S2), the composite coatings will offer an improved performance in industrial applications that demand materials with properties such as corrosion and wear resistance.

## 5.2 Recommendations

5.2.1 Regarding to the synthesis of Ni-P-SiC composite coatings, the evaluation of other methods (e.g. substrate rotation, circulation by pumping) different than mechanical stirring is recommended.

5.2.2 To improve the buffering capacity of the bath formulation developed in laboratory is recommended (e.g. by studying the influence of concentration of organic acids in the buffering capacity and other properties).

5.2.3 Studies about how the addition of SiC micro-particles in the plating bath could influence on the rate of deposition are also recommended since the rate of deposition obtained for Ni-P-SiC composite coatings were different in comparison with their analogous Ni-P simple deposits.

5.2.4 Studies about corrosion resistance of deposits after heat treatment are also recommended.

5.2.5 Regarding to corrosion resistance studies, it would be required long-term studies under real conditions to verify the results of corrosion studies by electrochemical techniques.

5.2.6 To continue the development of Ni-P composite materials with micro-and nano-particles of ceramic materials that may have a favorable effect on wear and corrosion resistance is recommended.

## References

1. Mallory, G.O. (1990). *Electroless Plating: Fundamentals and Applications* (Reprint Ed.). USA: Noyes Publications/ William Andrew Publishing.
2. Yu, H.S.; Luo, S.F. and Wang, Y.R. (2001). A comparative study on the crystallization behavior of electroless Ni-P and Ni-Cu-P deposits. *Surface and Coatings Technology*, **148**, 143-148.
3. ASTM B 733 (2004) Standard Specification for Autocatalytic (Electroless) Nickel-Phosphorus Coatings on Metal.
4. Burnell-Gray, J.S. and Datta, P.K. (1996). *Surface Engineering Casebook: Solutions to corrosion and wear related failures* (1st Ed.) England: Woodhead Publishing.
5. Schlesinger, M. and Paunovic M. (2000). *Modern Electroplating* (4th Ed.). USA: John Wiley & Sons, Inc.
6. Balaraju, J.N.; Sankara, T.S.N. and Seshadri, S.K. (2003). Electroless Ni-P composite coatings. *Journal of Applied Electrochemistry*, **33**, 807-816.
7. Agarwala, R.C.; Agarwala, V. and Sharma, R. (2006). *Electroless Ni-P Based Nanocoating Technology-A review. Synthesis and reactivity in Inorganic, Metal-Organic and Nano-Metal Chemistry*, **36**, 493-515.
8. Davis, R.J. (2000) *Nickel, cobalt and their alloys* (1<sup>st</sup> Ed.). USA: ASM International.
9. Bigdeli, F. and Allahkaram, S.R. (2008). The Corrosion Behaviour of Electroless Ni-P-SiC Nano-Composite Coating. *International Journal of Modern Physics B*, **22**, 3031-3036.



10. Balaraju, J.N.; Sankara Narayanan, T.S.N.; Seshadri, S.K. (2001) Evaluation of the corrosion resistance of electroless Ni-P and Ni-P composite coatings by electrochemical impedance spectroscopy. *Journal of Solid State Electrochemistry*, 5, 334-338.
11. Song, Y.W.; Shan, D.Y. and Han, E.H. (2007). Comparative study on corrosion protection properties of electroless Ni-P-ZrO<sub>2</sub> and Ni-P coatings on AZ91D magnesium alloy. *Materials and Corrosion*, 58,506-510.
12. Kanani, N. (2007) *Chemische Vernicklung: Nickel-Phosphor-Schichten Herstellung-Eigenschaften -Anwendungen*. Germany: Leuze.
13. Cheng, Y. H.; Zou, Y.; Cheng, L. and Liu, W. (2008) Effect of complexing agents on properties of electroless Ni-P deposits. *Materials Science & Technology*, 24, 4, 457-460.
14. Zhao, Q. y Liu, Y. (2005). Comparisons of corrosion rates of Ni-P based composite coatings in HCl and NaCl solutions. *Corrosion Science*, 47, 2807-2815.
15. Harper, C.A. (2001). *Handbook of Ceramics, Glasses, and Diamonds*. USA: McGraw-Hill.
16. Keong, K.G.; Sha, W. and Malinov S. (2002). Crystallisation kinetics and phase transformation behaviour of electroless nickel-phosphorus deposits with high phosphorus content. *Journal of Alloys and Compounds*, 334, 192-199.
17. Agarwala, R.C. and Agarwala, V. (2003) Electroless alloy/composite coatings: A review. *Sadhana*, 28, 3-4, 475-493.
18. Jiaqiang , G.; Lei, L.; Yating,W.; Bin,S. and Wenbin, H.(2006). Electroless Ni-P-SiC composite coatings with superfine particles. *Surface & Coatings Technology*, 200, 5836–5842.

19. Elsener, B.; Crobu, M.; Scorciapino, M.A. and Rossi, A. (2008). Electroless deposited Ni-P alloys: corrosion resistance mechanism. *Journal of Applied Electrochemistry*, **38**, 1053-1060.
20. Królikowski, A.; Karbownicka, B. and Jaklewicz, O. (2006). Anodic dissolution of amorphous Ni-P alloys. *Electrochimica Acta*, **51**, 6120-6127.
21. Thompson, N.G. and Payer, J.H.(1998) *DC Electrochemical Test Methods* (1st Ed.). USA: NACE International.
22. Baboian, R. (1986) *Electrochemical Techniques for Corrosion Engineering*. USA: NACE International.
23. Pourbaix, M. (1987) *Lecciones de Corrosión Electroquímica* (3rd Ed.).Belgium:CEBELCOR.
24. Kelly, R.G. (2003) *Electrochemical techniques in corrosion science and engineering*. USA: CRC Press.
25. Plieth, W. (2008). *Electrochemistry for Materials Science* (1st Ed.). Germany: Elsevier.
26. Cottis, R. and Turgoose, S. (1999) *Electrochemical Impedance and Noise* (1<sup>st</sup> Ed.). USA: NACE International.
27. Available on: [http://www.q-lab.com/EN\\_WebLit/PanelSheetsABC-EX.pdf](http://www.q-lab.com/EN_WebLit/PanelSheetsABC-EX.pdf)
28. Spieß, L.; Teichert, G.; Schwarzer, R.; Behnken, H. and Genzel, C.(2009 ) *Moderne Röntgenbeugung* (2d Ed.) Germany: Vieweg+Teubner.
29. Kanani, N. (2004) *Electroplating: basic principles, processes and practice*. USA:Elsevier.

30. Czichos, H.; Saito, T. and Smith, L.(2006) *Springer handbook of materials measurements methods*. Germany:Springer.
31. Available on: [http://spectro.cz/download/spectrums\\_gda\\_750-550.pdf](http://spectro.cz/download/spectrums_gda_750-550.pdf)
32. ASTM B 499 (2002) *Standard Test Method for Measurement of Coating Thicknesses by the Magnetic Method: Nonmagnetic Coatings on Magnetic Basis Metals*.
33. Kelly R.; Scully J.; Shoesmith D.; Buchheit, R. (2003) *Electrochemical Techniques in Corrosion Science and Engineering*. USA: Marcel Dekker.
34. ASTM G5 94(2004) *Standard Reference Test Method for Making Potentiostatic and Potentiodynamic Anodic Polarization Measurements*.
35. DIN 50903 (1967) *Metallic coatings; Pores, Inclusions, Blisters and Cracks, Definitions*.
36. Jenilek, T.W. (1999) *Prozessbegleitende Analytik in der Galvanotechnik*. Germany: Leuze Verlag.
37. ASTM G106-89 (Reapproved 2004) *Standard Practice for Verification of Algorithm and Equipment for Electrochemical Impedance Measurements*.
38. Balaraju, J. N.; and Rajam, K.S. (2007). Electroless Deposition and Characterization of High Phosphorus Ni-P-Si<sub>3</sub>N<sub>4</sub> Composite Coatings. *Int. J. Electrochem. Sci.*, 2, 747 – 761.
39. Frankel, G.S. (2008) *Electrochemical Techniques in Corrosion: Status, Limitations, and Needs*. *Journal of ASTM International*, 5, No. 2.
40. Uhlig, H. and Winston, R. (1984) *Corrosion and Corrosion Control*. Canada: John Wiley and Sons.

## Determination of Nickel

S1 bath									
N°		$V_{EDTA}$	$C_{EDTA}$	$f_{EDTA}$	$C_{Pb}$	$f_{Pb}$	$V_{sol}$	$V_{Pb}$	$C_{Ni}$
Bath		(mL)	(mol/L)		(mol/L)		(mL)	(mL)	Ni <sup>2+</sup> (mol/L)
1	initial	25	0,05	1,0	0,05	0,96	10	4,5	0,103
	final	25	0,05	1,0	0,05	0,96	10	7,9	0,087
2	initial	25	0,05	1,0	0,05	0,99	10	3,6	0,107
	final	25	0,05	1,0	0,05	0,99	10	5,9	0,096
3	initial	25	0,05	1,0	0,05	0,99	10	4,1	0,105
	final	25	0,05	1,0	0,05	0,99	10	5,7	0,097
S2 bath									
N°		$V_{EDTA}$	$C_{EDTA}$	$f_{EDTA}$	$C_{Pb}$	$f_{Pb}$	$V_{sol}$	$V_{Pb}$	$C_{Ni}$
Bath		(mL)	(mol/L)		(mol/L)		(mL)	(mL)	Ni <sup>2+</sup> (mol/L)
1	initial	25	0,05	1,0	0,05	0,96	10	5,0	0,101
	final	25	0,05	1,0	0,05	0,96	10	6,0	0,096
2	initial	25	0,05	1,0	0,05	0,96	10	5,0	0,101
	final	25	0,05	1,0	0,05	0,96	10	6,3	0,095
3	initial	25	0,05	1,0	0,05	0,96	10	4,4	0,104
	final	25	0,05	1,0	0,05	0,96	10	5,8	0,097
C1 bath									
N°		$V_{EDTA}$	$C_{EDTA}$	$f_{EDTA}$	$C_{Pb}$	$f_{Pb}$	$V_{sol}$	$V_{Pb}$	$C_{Ni}$
Bath		(mL)	(mol/L)		(mol/L)		(mL)	(mL)	Ni <sup>2+</sup> (mol/L)
1	initial	25	0,05	1,0	0,05	1,0	10	4,3	0,104
	final	25	0,05	1,0	0,05	1,0	10	6,3	0,094
2	initial	25	0,05	1,0	0,05	1,0	10	4,5	0,103
	final	25	0,05	1,0	0,05	1,0	10	5,6	0,097
3	initial	25	0,05	1,0	0,05	1,0	10	4,2	0,104
	final	25	0,05	1,0	0,05	1,0	10	5,3	0,099
C2 bath									
N°		$V_{EDTA}$	$C_{EDTA}$	$f_{EDTA}$	$C_{Pb}$	$f_{Pb}$	$V_{sol}$	$V_{Pb}$	$C_{Ni}$
Bath		(mL)	(mol/L)		(mol/L)		(mL)	(mL)	Ni <sup>2+</sup> (mol/L)
1	initial	25	0,05	1,0	0,05	0,96	10	4,9	0,101
	final	25	0,05	1,0	0,05	0,96	10	5,8	0,097
2	initial	25	0,05	1,0	0,05	0,96	10	5,2	0,100
	final	25	0,05	1,0	0,05	0,96	10	6,3	0,095
3	initial	25	0,05	1,0	0,05	0,96	10	4,5	0,103
	final	25	0,05	1,0	0,05	0,96	10	5,7	0,098

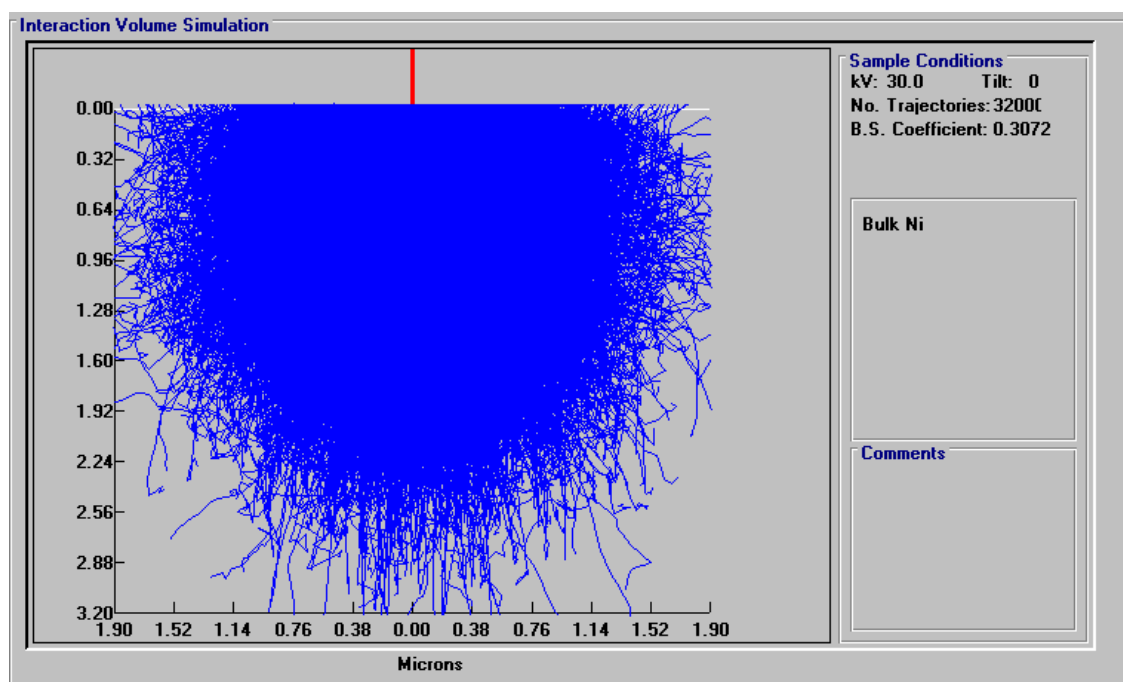
## Determination of Hypophosphite

S1 bath						
N° Bath		V <sub>Ce</sub>	C <sub>Ce</sub>	f <sub>Ce</sub>	V <sub>sol</sub>	C <sub>H2PO2-</sub>
		(mL)	(mol/L)		(mL)	H <sub>2</sub> PO <sub>2</sub> <sup>-</sup> (mol/L)
1	initial	17,5	0,1	1,0	5,0	0,175
	final	14,3	0,1	1,0	5,0	0,143
2	initial	18,8	0,1	1,0	5,0	0,188
	final	16,9	0,1	1,0	5,0	0,169
3	initial	17,9	0,1	1,0	5,0	0,179
	final	14,9	0,1	1,0	5,0	0,149
S2 bath						
N° Bath		V <sub>Ce</sub>	C <sub>Ce</sub>	f <sub>Ce</sub>	V <sub>sol</sub>	C <sub>H2PO2-</sub>
		(mL)	(mol/L)		(mL)	H <sub>2</sub> PO <sub>2</sub> <sup>-</sup> (mol/L)
1	initial	27,3	0,1	1,0	5,0	0,273
	final	28,5	0,1	1,0	5,0	0,285
2	initial	27,3	0,1	1,0	5,0	0,273
	final	26,5	0,1	1,0	5,0	0,265
3	initial	27,3	0,1	1,0	5,0	0,273
	final	26,1	0,1	1,0	5,0	0,261
C1 bath						
N° Bath		V <sub>Ce</sub>	C <sub>Ce</sub>	f <sub>Ce</sub>	V <sub>sol</sub>	C <sub>H2PO2-</sub>
		(mL)	(mol/L)		(mL)	H <sub>2</sub> PO <sub>2</sub> <sup>-</sup> (mol/L)
1	initial	17,4	0,1	1,0	5,0	0,174
	final	16,2	0,1	1,0	5,0	0,162
2	initial	17,7	0,1	1,0	5,0	0,177
	final	15,1	0,1	1,0	5,0	0,151
3	initial	17,9	0,1	1,0	5,0	0,179
	final	15,7	0,1	1,0	5,0	0,157
C2 bath						
N° Bath		V <sub>Ce</sub>	C <sub>Ce</sub>	f <sub>Ce</sub>	V <sub>sol</sub>	C <sub>H2PO2-</sub>
		(mL)	(mol/L)		(mL)	H <sub>2</sub> PO <sub>2</sub> <sup>-</sup> (mol/L)
1	initial	27,4	0,1	1,0	5,0	0,274
	final	27,2	0,1	1,0	5,0	0,272
2	initial	27,4	0,1	1,0	5,0	0,274
	final	27,0	0,1	1,0	5,0	0,270
3	initial	27,4	0,1	1,0	5,0	0,274
	final	26,8	0,1	1,0	5,0	0,268

## EDX-line scan: Depth of incidence simulation

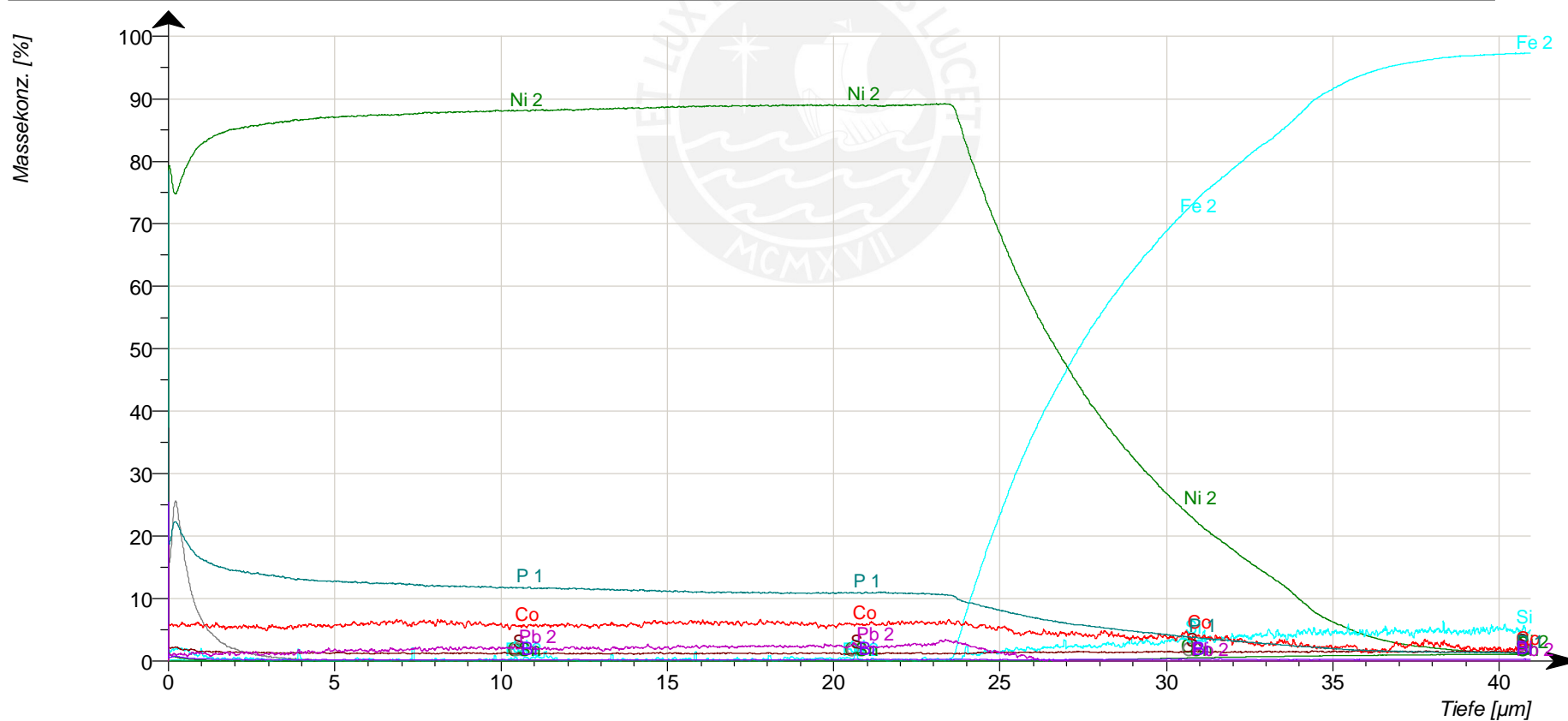
Accelerating voltage: 30 kV

Material: Nickel



GDOS ANALYSIS - Sample S1

Probenbezeichnung: S3-4	GDS-Bedingungen: 1000V, 13mA / 2,5	Datum/Zeit: 13.02.2009 12:56:13
RAW=D:\IImenau\Ergebnisse\MFPA\13_02_09_schmidt\S3_4.raw : MTH=NickelP_neu_DC_2,5mm		
Fe 2 C - (x 10) O - (x 10) Ni 2 Si - (x 100) S - (x 100) Co - (x 100) P 1 Sn - (x 10000) Pb 2 - (x 100)		



## APPENDIX 5

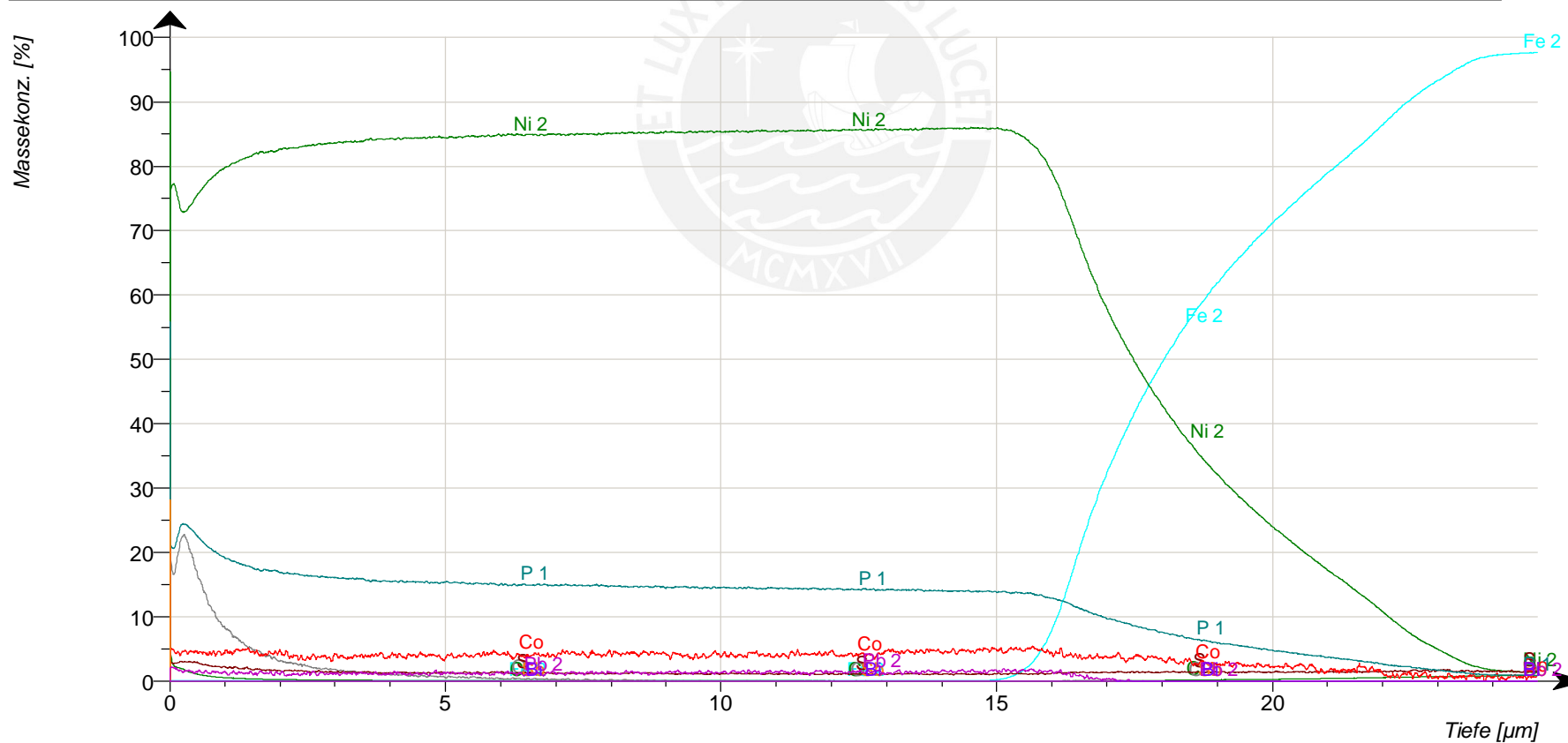
## GDOS ANALYSIS - Sample S1

Thickness [ $\mu\text{m}$ ]	Concentration (mass-%)								
	Ni	P	Fe X10	C X10	O X10	Co X10	S X10	Pb X10	Bi X10
1	77.25	20.55	2.26	1.14	16.18	0.55	0.24	0.10	0.91
2	84.23	15.17	0.96	0.09	3.59	0.55	0.14	0.11	0.28
3	85.57	14.09	0.91	0.04	1.17	0.53	0.13	0.12	0.22
4	86.34	13.41	0.89	0.03	0.45	0.54	0.13	0.12	0.21
5	86.89	12.88	0.85	0.03	0.17	0.56	0.13	0.15	0.21
6	87.20	12.59	0.84	0.02	0.03	0.58	0.12	0.16	0.21
7	87.41	12.38	0.82	0.02	0.00	0.62	0.12	0.17	0.20
8	87.65	12.14	0.84	0.02	0.00	0.61	0.12	0.18	0.19
9	87.84	11.95	0.81	0.02	0.00	0.61	0.12	0.20	0.18
10	87.98	11.80	0.80	0.02	0.00	0.59	0.12	0.20	0.20
11	88.09	11.70	0.79	0.02	0.00	0.56	0.12	0.20	0.19
12	88.19	11.60	0.79	0.02	0.00	0.57	0.12	0.19	0.18
13	88.28	11.52	0.78	0.02	0.00	0.56	0.12	0.20	0.20
14	88.43	11.37	0.79	0.02	0.00	0.58	0.12	0.19	0.19
15	88.54	11.25	0.78	0.02	0.00	0.60	0.12	0.21	0.18
16	88.69	11.10	0.78	0.02	0.00	0.62	0.12	0.22	0.17
17	88.79	10.99	0.78	0.02	0.00	0.61	0.12	0.23	0.18
18	88.85	10.94	0.76	0.02	0.00	0.61	0.12	0.24	0.19
19	88.90	10.89	0.77	0.02	0.00	0.61	0.12	0.23	0.18
20	88.92	10.86	0.77	0.02	0.00	0.58	0.12	0.24	0.21
21	88.88	10.90	0.78	0.02	0.00	0.58	0.12	0.24	0.20
22	88.88	10.91	0.77	0.02	0.00	0.60	0.12	0.23	0.23
23	88.99	10.79	0.77	0.02	0.00	0.61	0.12	0.26	0.22



GDOS ANALYSIS - Sample S2

Probenbezeichnung: 54-4	GDS-Bedingungen: 1000V,13mA / 2,5	Datum/Zeit: 17.02.2009 12:24:23
RAW=D:\lmenau\Ergebnisse\MFPA\13_02_09_schmidt\54-5.raw : MTH=NickelP_neu_DC_2,5mm		
<ul style="list-style-type: none"> <li>Fe 2</li> <li>C - (x 10)</li> <li>O - (x 10)</li> <li>Ni 2</li> <li>S - (x 100)</li> <li>Co - (x 100)</li> <li>P 1</li> <li>Sb - (x 100)</li> <li>Pb 2 - (x 100)</li> <li>Bi - (x 10000)</li> </ul>		

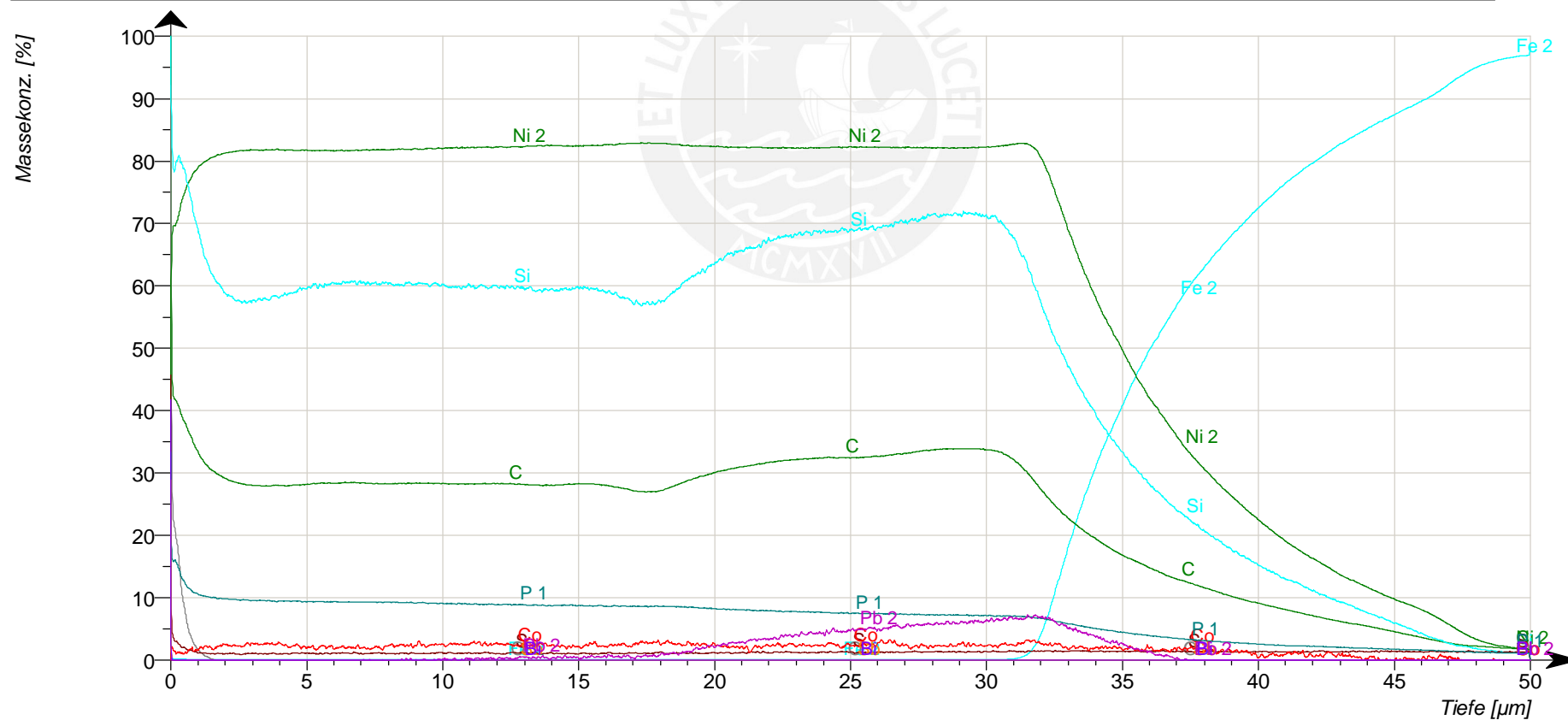


## GDOS ANALYSIS - Sample S2

Thickness [ $\mu\text{m}$ ]	Concentration (mass-%)							
	Ni	P	Fe X10	C X10	O X10	Co X10	S X10	Pb X10
1	75.82	22.17	1.14	2.02	16.08	0.43	0.29	0.14
2	81.49	17.79	0.87	0.36	5.25	0.45	0.18	0.12
3	83.15	16.45	0.79	0.2	2.38	0.38	0.15	0.11
4	83.98	15.74	0.75	0.14	1.32	0.39	0.13	0.12
5	84.40	15.37	0.72	0.11	0.83	0.39	0.13	0.12
6	84.63	15.17	0.72	0.09	0.54	0.41	0.13	0.12
7	84.89	14.93	0.7	0.08	0.35	0.4	0.13	0.12
8	84.97	14.87	0.72	0.06	0.2	0.42	0.12	0.12
9	85.17	14.68	0.69	0.06	0.11	0.43	0.12	0.13
10	85.31	14.55	0.67	0.05	0.02	0.4	0.11	0.13
11	85.40	14.46	0.67	0.05	0.01	0.41	0.11	0.14
12	85.49	14.38	0.67	0.04	0	0.42	0.11	0.14
13	85.62	14.25	0.64	0.04	0	0.41	0.11	0.14
14	85.72	14.15	0.63	0.04	0	0.46	0.11	0.14
15	85.86	13.98	0.84	0.04	0	0.47	0.11	0.15

GDOS ANALYSIS - Sample C1

Probenbezeichnung: SPB-1	GDS-Bedingungen: 1000V,13mA / 2,5	Datum/Zeit: 13.02.2009 13:57:24
RAW=D:\Ilmenau\Ergebnisse\MFPA\13_02_09_schmidt\SPB_1.raw : MTH=NickelP_neu_DC_2,5mm		
Fe 2	Bi - (x 100)	
C - (x 10)		
O - (x 10)		
Ni 2		
Si - (x 10)		
S - (x 100)		
Co - (x 100)		
P 1		
Sb - (x 10)		
Pb 2 - (x 100)		



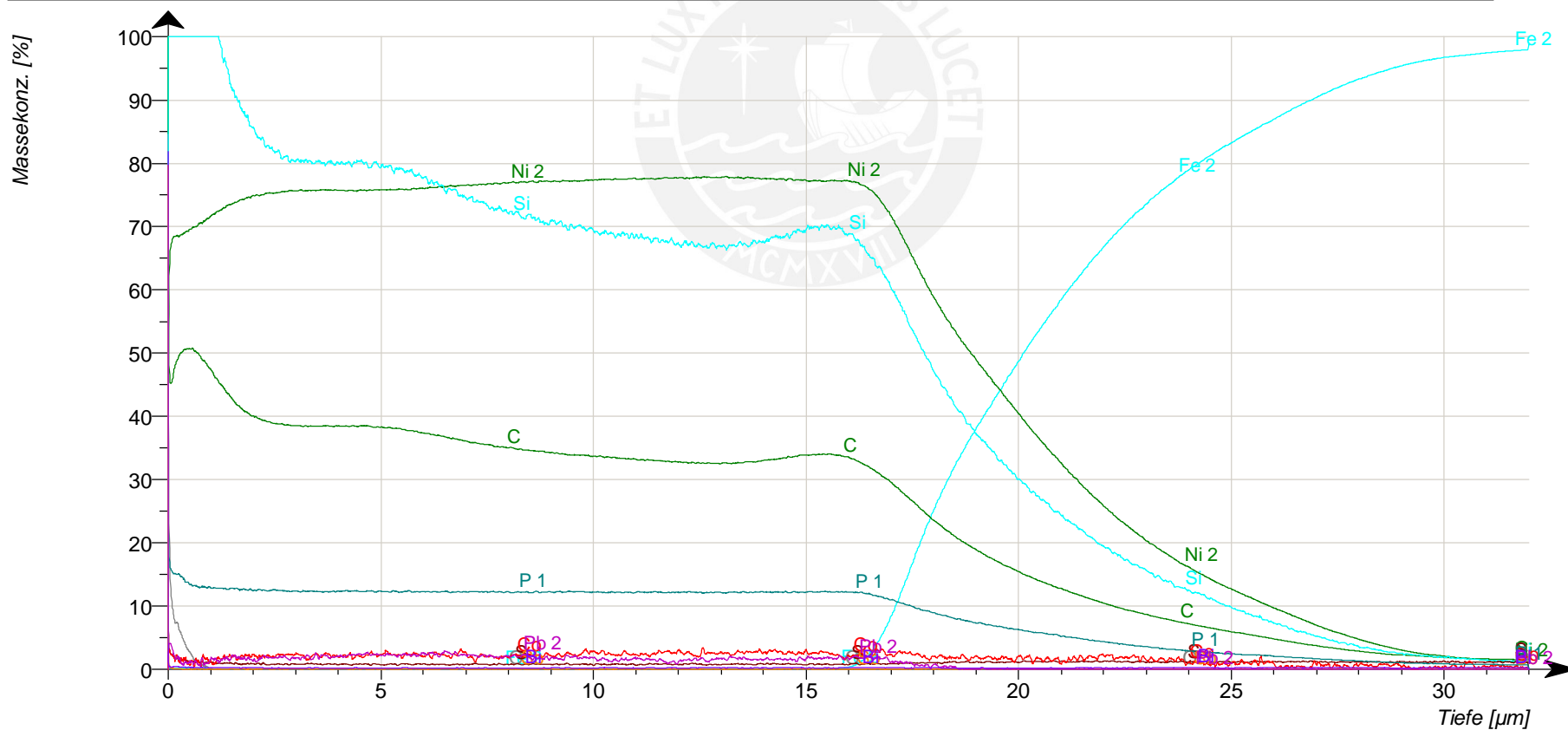
## APPENDIX 9

## GDOS ANALYSIS - Sample C1

Thickness [ $\mu\text{m}$ ]	Concentration (mass-%)								
	Ni	P	Si	C	Fe X10	O X10	Co X10	S X10	Pb X10
1	72.98	13.53	7.81	4.10	1.61	13.36	0.13	0.29	0.00
2	80.37	10.12	6.28	3.08	0.75	0.43	0.21	0.10	0.00
3	81.58	9.70	5.78	2.84	0.64	0.00	0.24	0.10	0.00
4	81.77	9.54	5.79	2.80	0.63	0.00	0.26	0.10	0.00
5	81.73	9.47	5.90	2.80	0.64	0.00	0.23	0.10	0.00
6	81.67	9.39	6.01	2.83	0.66	0.00	0.21	0.10	0.00
7	81.68	9.34	6.05	2.84	0.65	0.00	0.20	0.11	0.00
8	81.78	9.26	6.04	2.83	0.67	0.00	0.19	0.11	0.00
9	81.86	9.19	6.03	2.83	0.66	0.00	0.23	0.11	0.00
10	81.95	9.09	6.03	2.83	0.65	0.00	0.25	0.11	0.00
11	82.10	8.99	5.99	2.83	0.66	0.00	0.25	0.11	0.01
12	82.18	8.90	5.99	2.83	0.66	0.00	0.27	0.11	0.02
13	82.24	8.85	5.98	2.82	0.65	0.00	0.25	0.11	0.03
14	82.40	8.75	5.94	2.81	0.67	0.00	0.24	0.11	0.04
15	82.41	8.73	5.95	2.82	0.66	0.00	0.22	0.10	0.04
16	82.46	8.67	5.95	2.82	0.66	0.00	0.24	0.10	0.05
17	82.68	8.61	5.84	2.77	0.67	0.00	0.24	0.11	0.06
18	82.88	8.58	5.72	2.71	0.66	0.00	0.28	0.11	0.06
19	82.65	8.55	5.90	2.79	0.67	0.00	0.27	0.11	0.11
20	82.37	8.35	6.23	2.94	0.67	0.00	0.25	0.11	0.18
21	82.23	8.12	6.48	3.06	0.67	0.00	0.22	0.11	0.26
22	82.15	7.95	6.64	3.13	0.67	0.00	0.20	0.12	0.32
23	82.08	7.81	6.78	3.19	0.69	0.00	0.24	0.12	0.37
24	82.08	7.70	6.85	3.23	0.69	0.00	0.24	0.12	0.42
25	82.17	7.56	6.88	3.24	0.69	0.00	0.24	0.13	0.46
26	82.21	7.47	6.92	3.25	0.70	0.00	0.24	0.12	0.49
27	82.16	7.41	6.98	3.29	0.69	0.00	0.28	0.12	0.52
28	82.13	7.30	7.07	3.34	0.71	0.00	0.22	0.13	0.56
29	82.08	7.24	7.14	3.38	0.71	0.00	0.23	0.13	0.59
30	82.13	7.17	7.15	3.38	0.70	0.00	0.24	0.13	0.62

GDOS ANALYSIS - Sample C2

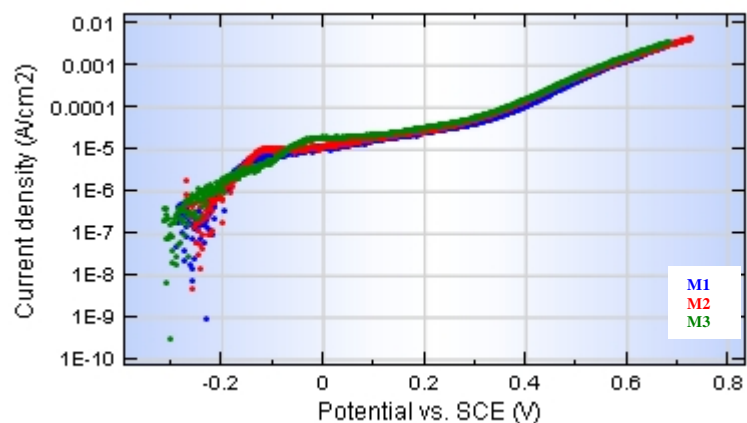
Probenbezeichnung: SP-3	GDS-Bedingungen: 1000V, 13mA / 2,5	Datum/Zeit: 13.02.2009 11:38:49
RAW=D:\lmenau\Ergebnisse\MFPA\13_02_09_schmidt\SP_3.raw : MTH=NickelP_neu_DC_2,5mm		
Fe 2 C - (x 10) O - (x 10) Ni 2 Si - (x 10) S - (x 100) Co - (x 100) P 1 Sb - (x 10) Pb 2 - (x 100)		



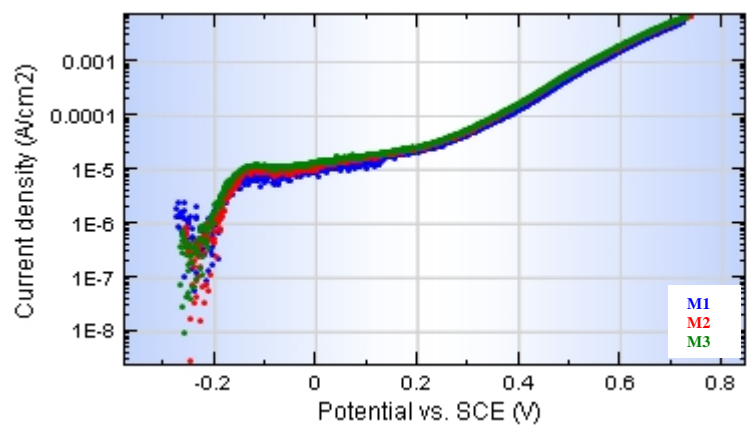
## GDOS ANALYSIS - Sample C2

Thickness [ $\mu\text{m}$ ]	Concentration (mass-%)									
	Ni	P	Si	C	Fe X10	O X10	Co X10	S X10	Pb X10	Bi X10
1	67.40	14.79	11.12	5.10	5.98	6.73	0.14	0.17	0.13	1.66
2	73.42	12.70	9.38	4.32	1.15	0.01	0.18	0.09	0.16	0.23
3	75.25	12.42	8.25	3.91	1.03	0	0.21	0.08	0.17	0.21
4	75.70	12.26	8.02	3.85	0.99	0	0.21	0.08	0.19	0.2
5	75.68	12.30	8.00	3.84	0.99	0	0.21	0.08	0.23	0.19
6	75.90	12.24	7.89	3.79	1.01	0	0.23	0.08	0.22	0.19
7	76.32	12.21	7.62	3.67	0.97	0	0.23	0.07	0.24	0.2
8	76.73	12.21	7.35	3.55	0.96	0	0.19	0.08	0.2	0.2
9	77.08	12.15	7.14	3.47	0.95	0	0.21	0.08	0.19	0.18
10	77.23	12.20	7.01	3.40	0.97	0	0.24	0.08	0.18	0.2
11	77.49	12.13	6.88	3.34	0.94	0	0.25	0.08	0.15	0.21
12	77.60	12.15	6.79	3.30	0.94	0	0.25	0.08	0.14	0.21
13	77.74	12.13	6.71	3.26	0.96	0	0.25	0.08	0.15	0.22
14	77.71	12.13	6.72	3.27	0.95	0	0.27	0.08	0.16	0.21
15	77.47	12.16	6.86	3.34	0.95	0	0.27	0.08	0.15	0.22
16	77.24	12.20	6.98	3.39	1.27	0	0.24	0.08	0.17	0.21

Potentiodynamic anodic polarization of Ni-P and Ni-P-SiC deposits



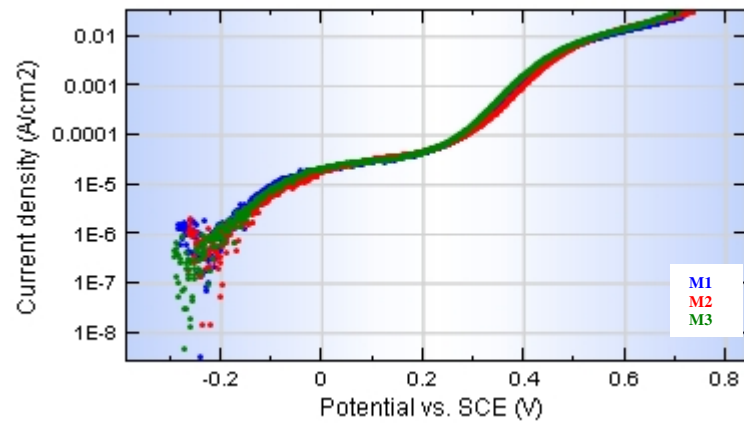
Deposit S1



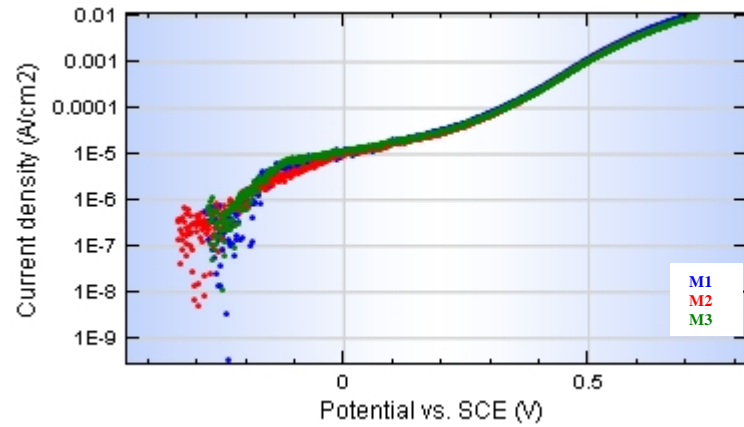
Deposit S2

M1: Measurement 1  
 M2: Measurement 2  
 M3: Measurement 3

Potentiodynamic anodic polarization of Ni-P and Ni-P-SiC deposits



Deposit C1



Deposit C2

M1: Measurement 1  
M2: Measurement 2  
M3: Measurement 3



Images of deposits after potentiodynamic anodic polarization

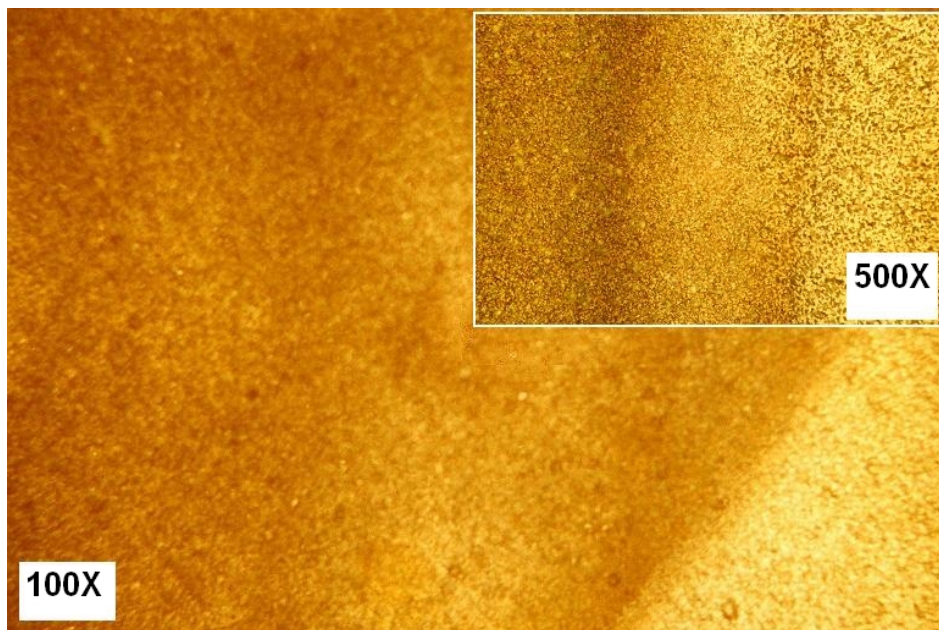


Deposit S1 after potentiodynamic anodic polarization

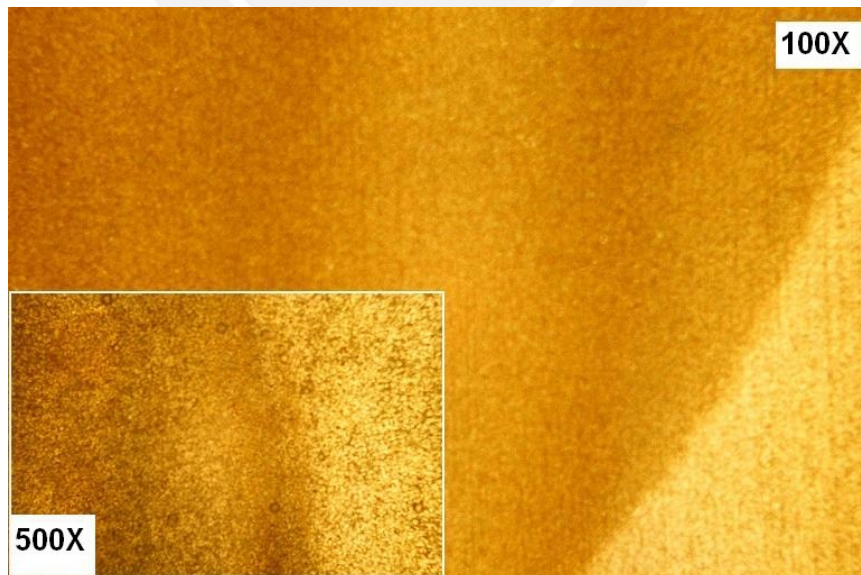


Deposit S2 after potentiodynamic anodic polarization  
(Pittings are signalled with arrows)

Images of deposits after potentiodynamic anodic polarization

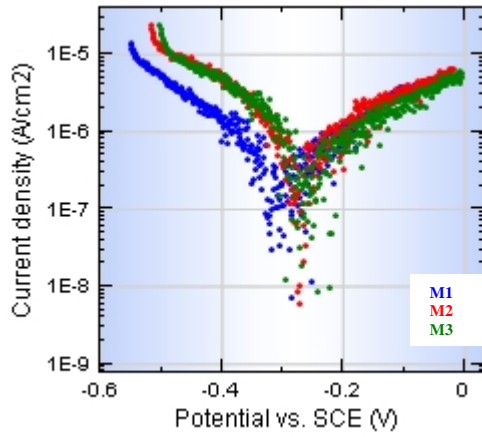


Deposit C1 after potentiodynamic anodic polarization

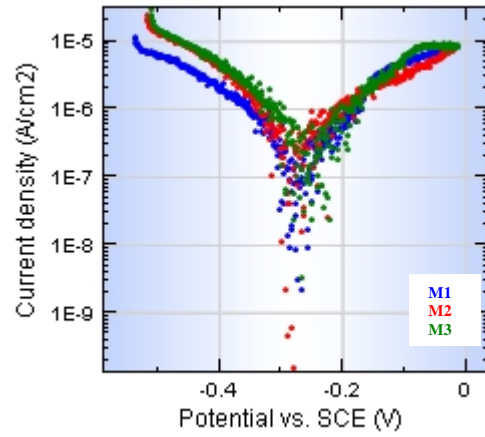


Deposit C2 after potentiodynamic anodic polarization

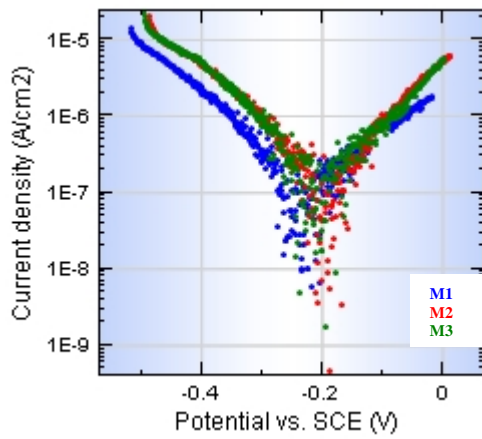
Cathodic and anodic polarization (Tafel plots) of Ni-P and Ni-P-SiC deposits



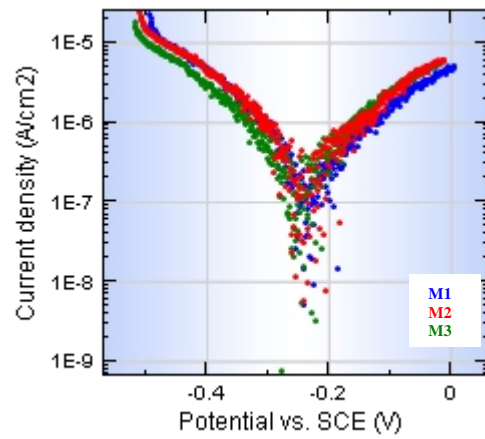
Deposit S1



Deposit S2



Deposit C1

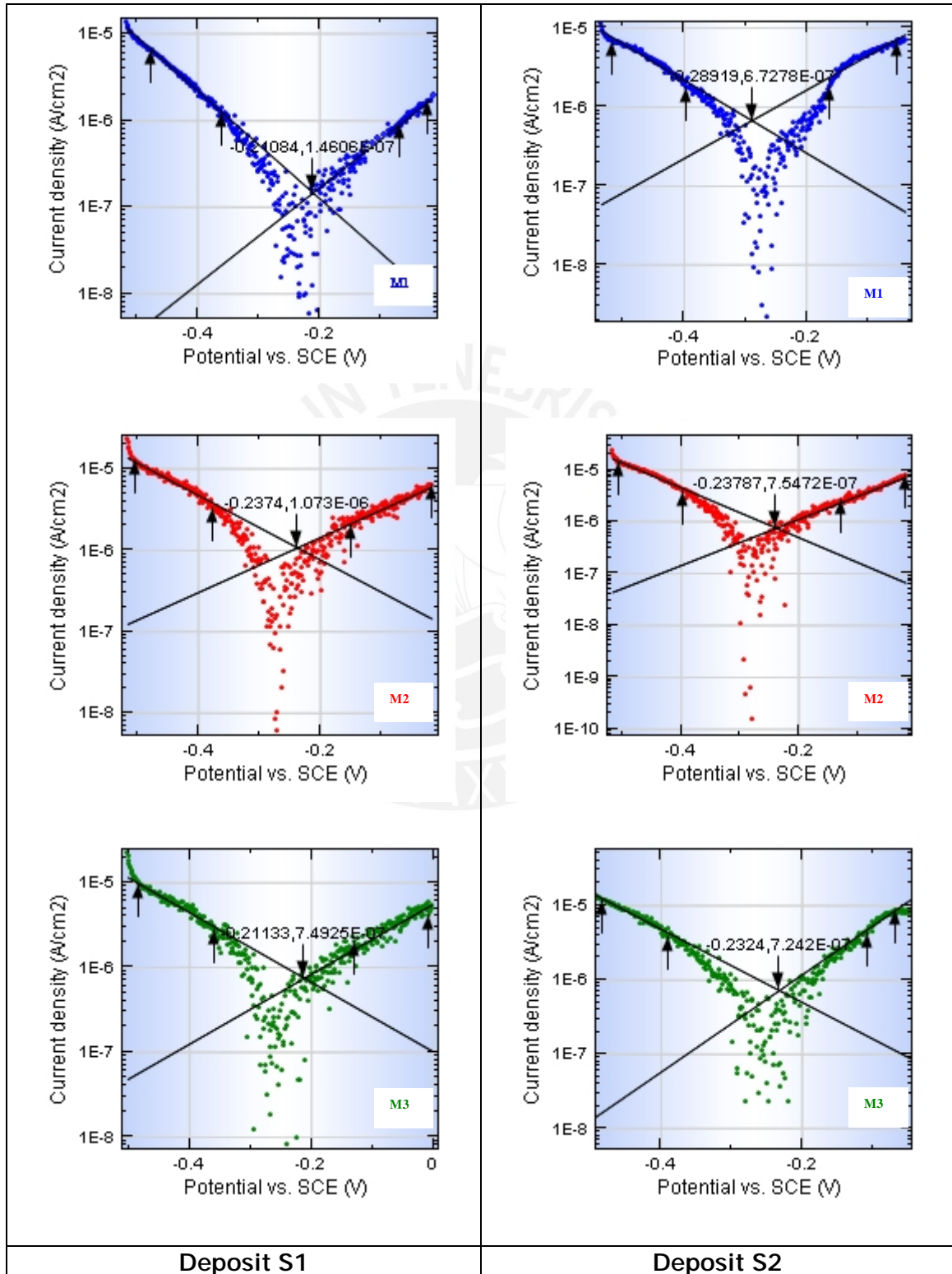


Deposit C2

M1: Measurement 1  
M2: Measurement 2  
M3: Measurement 3

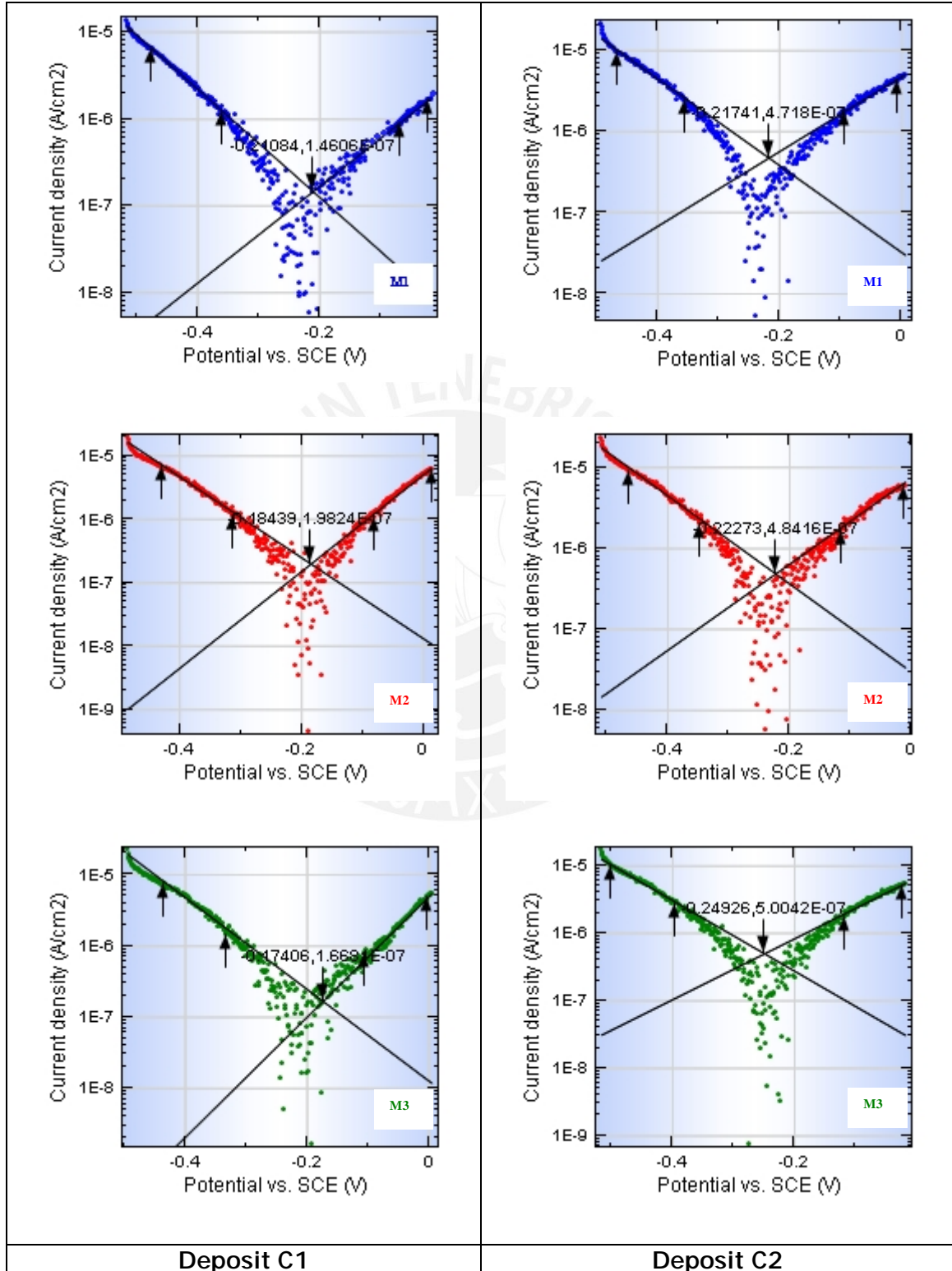


Tafel slopes determination for Ni-P and Ni-P-SiC deposits



M1: Measurement 1  
M2: Measurement 2  
M3: Measurement 3

Tafel slopes determination for Ni-P and Ni-P-SiC deposits



M1: Measurement 1  
M2: Measurement 2  
M3: Measurement 3

Electrochemical parameters from Tafel plots for Ni-P and Ni-P-SiC deposits

Deposit S1

Measurement	OCP vs. SCE (V)	$b_a$ V/dec	$b_c$ V/dec	$i_{corr}$ mA/cm <sup>2</sup>	$E_{corr}$ (V)	B (V)
1	-0,300	0,2079	0,1804	0,370	-0,294	0,0420
2	-0,266	0,2956	0,252	1,070	-0,237	0,0591
3	-0,252	0,2438	0,2427	0,750	-0,211	0,0529
<b>Average</b>	<b>-0,273</b>	<b>0,2491</b>	<b>0,2250</b>	<b>0,730</b>	<b>-0,247</b>	<b>0,0513</b>
<b>%RSD</b>	9	18	17	48	17	17

Deposit S2

Measurement	OCP vs. SCE (V)	$b_a$ V/dec	$b_c$ V/dec	$i_{corr}$ mA/cm <sup>2</sup>	$E_{corr}$ (V)	B (V)
1	-0,287	0,231	0,217	0,670	-0,289	0,049
2	-0,267	0,209	0,225	0,750	-0,238	0,047
3	-0,262	0,153	0,203	0,720	-0,232	0,038
<b>Average</b>	<b>-0,272</b>	<b>0,198</b>	<b>0,215</b>	<b>0,713</b>	<b>-0,253</b>	<b>0,045</b>
<b>%RSD</b>	5	20	5	6	12	13

Deposit C1

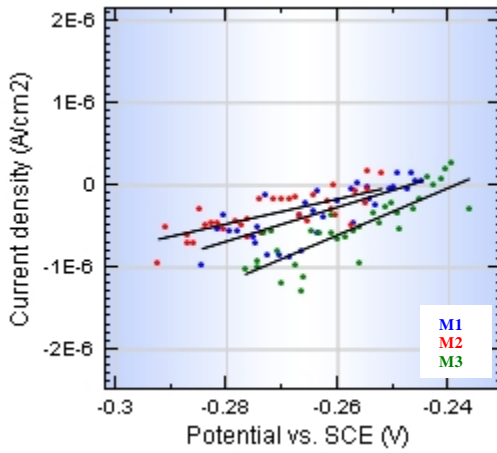
Measurement	OCP vs. SCE (V)	$b_a$ V/dec	$b_c$ V/dec	$i_{corr}$ mA/cm <sup>2</sup>	$E_{corr}$ (V)	B (V)
1	-0,267	0,160	0,180	0,150	-0,211	0,037
2	-0,236	0,131	0,157	0,200	-0,218	0,031
3	-0,245	0,118	0,155	0,170	-0,174	0,029
<b>Average</b>	<b>-0,249</b>	<b>0,137</b>	<b>0,164</b>	<b>0,173</b>	<b>-0,201</b>	<b>0,032</b>
<b>%RSD</b>	6	16	8	15	12	12

Deposit C2

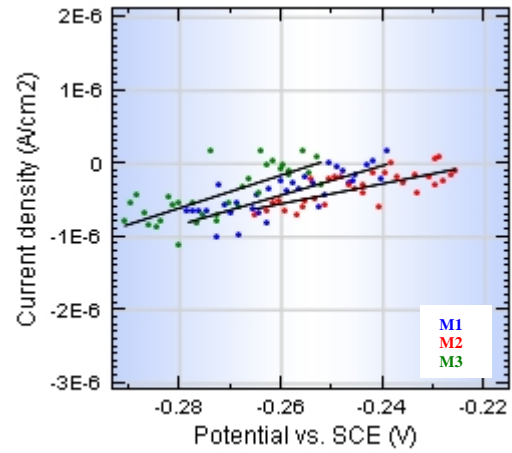
Measurement	OCP vs. SCE (V)	$b_a$ V/dec	$b_c$ V/dec	$i_{corr}$ mA/cm <sup>2</sup>	$E_{corr}$ (V)	B (V)
1	-0,243	0,187	0,217	0,470	-0,217	0,044
2	-0,260	0,188	0,184	0,480	-0,223	0,040
3	-0,268	0,191	0,222	0,500	-0,249	0,045
<b>Average</b>	<b>-0,257</b>	<b>0,189</b>	<b>0,207</b>	<b>0,483</b>	<b>-0,230</b>	<b>0,043</b>
<b>%RSD</b>	5	1	10	3	7	5

$$B = \frac{b_a b_c}{2,3(b_a + b_c)}$$

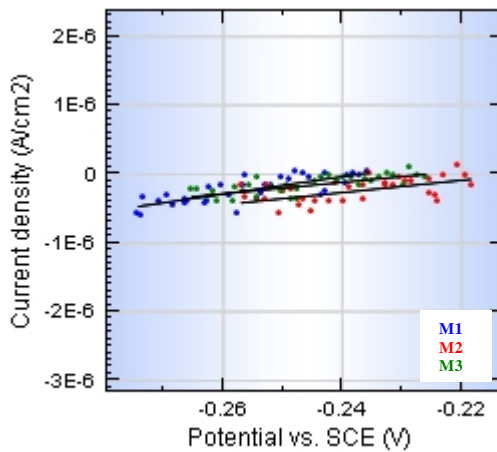
Linear polarization resistance plots of Ni-P and Ni-P-SiC deposits



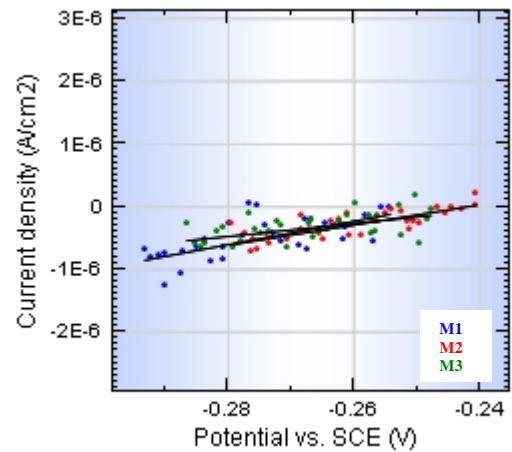
Deposit S1



Deposit S2



Deposit C1



Deposit C2

M1: Measurement 1  
 M2: Measurement 2  
 M3: Measurement 3

APPENDIX 14 (2/2)

Parameters from linear polarization resistance test for Ni-P and Ni-P-SiC deposits

Deposit S1

Measurement	OCP vs. SCE	Slope	Correlation	Rp
	(V)	1/Rp	coefficient R <sup>2</sup>	(W.cm <sup>2</sup> )
1	-0,263	2,07E-05	0,74	48 216
2	-0,271	1,52E-05	0,75	66 007
3	-0,257	2,87E-05	0,82	34 857
<b>Average</b>	-0,264	-	-	49 693
<b>%RSD</b>	3	-	-	31

Deposit S2

Measurement	OCP vs. SCE	Slope	Correlation	Rp
	(V)	1/Rp	coefficient R <sup>2</sup>	(W.cm <sup>2</sup> )
1	-0,259	2,03E-05	0,79	49 322
2	-0,244	1,38E-05	0,72	72 664
3	-0,271	2,25E-05	0,72	44 516
<b>Average</b>	-0,258	-	-	55 501
<b>%RSD</b>	5	-	-	27

Deposit C1

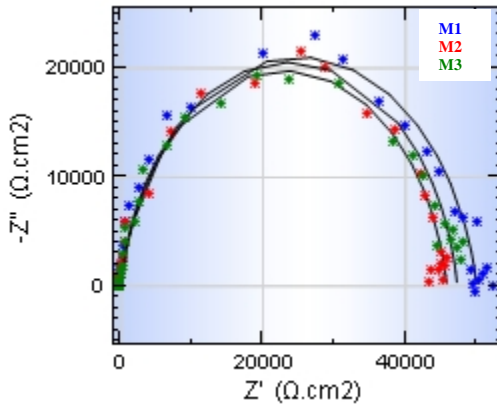
Measurement	OCP vs. SCE	Slope	Correlation	Rp
	(V)	1/Rp	coefficient R <sup>2</sup>	(W.cm <sup>2</sup> )
1	-0,255	1,27E-05	0,78	78 895
2	-0,237	8,88E-06	0,60	112 658
3	-0,246	8,38E-06	0,74	119 281
<b>Average</b>	-0,246	-	-	103 611
<b>%RSD</b>	4	-	-	21

Deposit C2

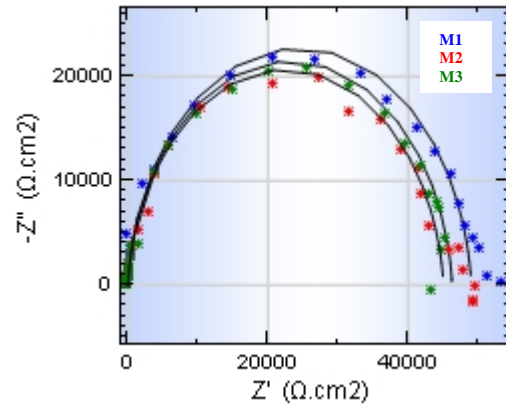
Measurement	OCP vs. SCE	Slope	Correlation	Rp
	(V)	1/Rp	coefficient R <sup>2</sup>	(W.cm <sup>2</sup> )
1	-0,274	3,53E-06	0,66	56 678
2	-0,260	2,85E-06	0,77	70 277
3	-0,267	1,87E-06	0,52	106 906
<b>Average</b>	-0,267	-	-	77 954
<b>%RSD</b>	3	-	-	33



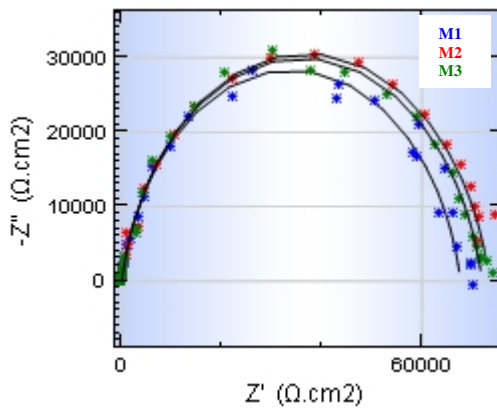
Electrochemical impedance spectroscopy (EIS): Nyquist plots of Ni-P and Ni-P-SiC deposits



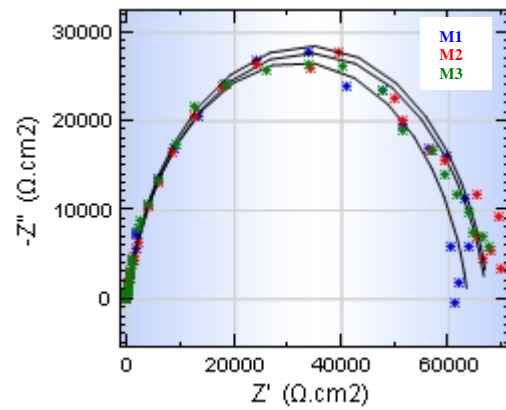
Deposit S1



Deposit S2



Deposit C1



Deposit C2

M1: Measurement 1  
 M2: Measurement 2  
 M3: Measurement 3

APPENDIX 15 (2/2)

Calculation of electrochemical parameters from EIS data of Ni-P and Ni-P-SiC deposits

Deposit S1

Measurement	OCP vs. SCE (V)	R <sub>s</sub> (W.cm <sup>2</sup> )	R <sub>ct</sub> (W.cm <sup>2</sup> )	Y <sub>0</sub> (mMho)	a	W <sub>max</sub> (Hz)	C <sub>dl</sub> (mF/cm <sup>2</sup> )
1	-0,25	11,24	50 002	2,32	0,89	0,27	13,40
2	-0,281	12,88	45 790	3,5	0,91	0,19	20,32
3	-0,243	11,04	47 270	3,58	0,91	0,27	20,14
<b>Average</b>	<b>-0,258</b>	<b>11,72</b>	<b>47 687</b>	<b>3,13</b>	<b>0,90</b>	<b>0,24</b>	<b>17,95</b>
<b>%RSD</b>	<b>8</b>	<b>9</b>	<b>4</b>	<b>23</b>	<b>1</b>	<b>19</b>	<b>22</b>

Deposit S2

Measurement	OCP vs. SCE (V)	R <sub>s</sub> (W.cm <sup>2</sup> )	R <sub>ct</sub> (W.cm <sup>2</sup> )	Y <sub>0</sub> (mMho)	a	W <sub>max</sub> (Hz)	C <sub>dl</sub> (mF/cm <sup>2</sup> )
1	-0,273	9,6	48 959	3,79	0,95	0,19	20,59
2	-0,278	12,18	46 233	3,88	0,95	0,14	21,40
3	-0,282	12,38	44 994	4,02	0,95	0,14	22,18
<b>Average</b>	<b>-0,278</b>	<b>11,39</b>	<b>46 729</b>	<b>3,90</b>	<b>0,95</b>	<b>0,16</b>	<b>21,39</b>
<b>%RSD</b>	<b>2</b>	<b>14</b>	<b>4</b>	<b>3</b>	<b>0</b>	<b>18</b>	<b>4</b>

Deposit C1

Measurement	OCP vs. SCE (V)	R <sub>s</sub> (W.cm <sup>2</sup> )	R <sub>ct</sub> (W.cm <sup>2</sup> )	Y <sub>0</sub> (mMho)	a	W <sub>max</sub> (Hz)	C <sub>dl</sub> (mF/cm <sup>2</sup> )
1	-0,258	10,84	67 651	3,9	0,89	0,14	24,21
2	-0,278	14,22	73 421	3,7	0,88	0,1	24,39
3	-0,276	13,32	71 930	3,8	0,89	0,14	23,59
<b>Average</b>	<b>-0,271</b>	<b>12,79</b>	<b>71 001</b>	<b>3,80</b>	<b>0,89</b>	<b>0,13</b>	<b>24,06</b>
<b>%RSD</b>	<b>4</b>	<b>14</b>	<b>4</b>	<b>3</b>	<b>1</b>	<b>18</b>	<b>2</b>

Deposit C2

Measurement	OCP vs. SCE (V)	R <sub>s</sub> (W.cm <sup>2</sup> )	R <sub>ct</sub> (W.cm <sup>2</sup> )	Y <sub>0</sub> (mMho)	a	W <sub>max</sub> (Hz)	C <sub>dl</sub> (mF/cm <sup>2</sup> )
1	-0,244	12,6	63 521	4,24	0,89	0,1	27,31
2	-0,237	12,16	67 125	4,32	0,88	0,07	29,72
3	-0,256	12,6	67 495	4,31	0,89	0,1	27,76
<b>Average</b>	<b>-0,246</b>	<b>12,45</b>	<b>66 047</b>	<b>4,29</b>	<b>0,89</b>	<b>0,09</b>	<b>28,26</b>
<b>%RSD</b>	<b>4</b>	<b>2</b>	<b>3</b>	<b>1</b>	<b>1</b>	<b>19</b>	<b>5</b>

$$C_{dl} = Y_0 (\omega_{max})^{\alpha-1}$$

